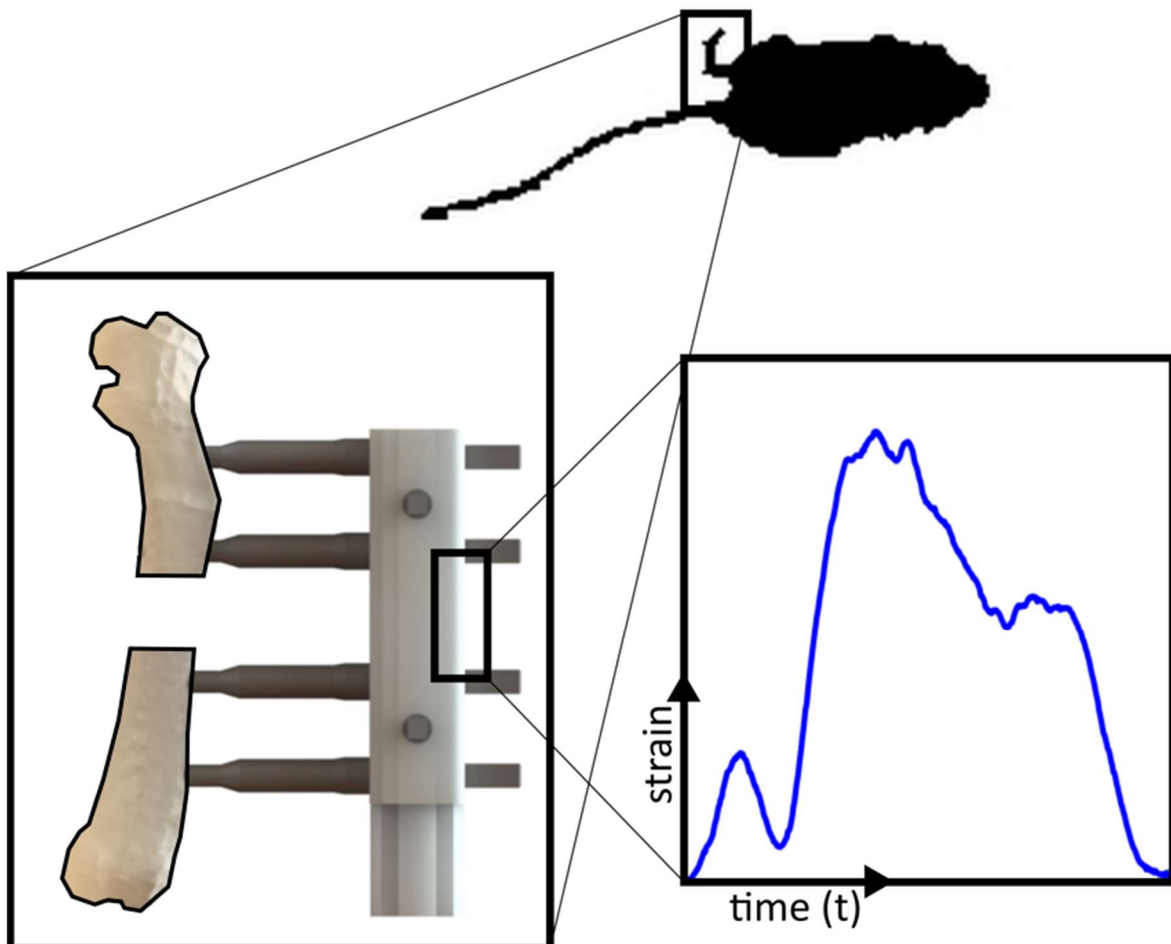


# Individualised multiscale mechanoregulation of fracture healing in mice

Graeme R. Paul





Diss. ETH No. 27097

# **Individualised multiscale mechanoregulation of fracture healing in mice**

A thesis submitted to attain the degree of

DOCTOR OF SCIENCES of ETH ZURICH

(Dr. sc. ETH Zurich)

presented by

**Graeme R. Paul**

M.Sc. Mechanical Engineering, University of Cape Town

born on 07.11.1989

citizen of Great Britain and South Africa

accepted on the recommendation of

Prof. Dr. Ralph Müller, examiner

Prof. Dr. Anita Ignatius, co-examiner

2020





*It is difficult to say what is impossible, for the dream of yesterday is the hope of today and the reality of tomorrow.*

*- Robert H. Goddard*

# Table of Contents

<b>Table of Contents</b> .....	<b>i</b>
<b>Acknowledgements</b> .....	<b>ii</b>
<b>Summary</b> .....	<b>iii</b>
<b>Zusammenfassung</b> .....	<b>vi</b>
<b>Notes on text</b> .....	<b>ix</b>
<b>Chapter 1 : Introduction</b> .....	<b>1</b>
<b>Chapter 2 : Background</b> .....	<b>11</b>
<i>Mechanical Stimuli in the Local In Vivo Environment in Bone: Computational Approaches Linking Organ-Scale Loads to Cellular Signals</i> .....	<i>12</i>
<b>Chapter 3 : Approaches to determine organ-scale individualised physiological and extra-physiological loading in mice</b> .....	<b>35</b>
<i>Determination of organ-scale boundary conditions in bones of individual mice in a fracture-healing model</i>	<i>36</i>
<i>Development of an approach to control and homogenize tissue scale strains in a mouse fracture healing model</i> .....	<i>60</i>
<b>Chapter 4 : Investigation of multiscale mechanoregulation in fracture healing in mice</b> .....	<b>83</b>
<i>Mechanoregulation of bone healing and remodelling at tissue and cell scale in a femur defect healing model in mice</i> .....	<i>84</i>
<i>Tissue level regeneration and remodelling dynamics are driven by local mechanical stimuli in a post-bridging loaded femur defect healing model in mice</i> .....	<i>115</i>
<b>Chapter 5 : Synthesis</b> .....	<b>137</b>
<b>Curriculum Vitae</b> .....	<b>149</b>

# Acknowledgements

This work would not have been possible without the support of several individuals, whose help I would like to acknowledge.

Firstly, I would like to thank Prof. Dr. Ralph Müller for providing the environment at the Laboratory for Bone Biomechanics for me to follow my interests and pursue my curiosity. In particular, I am grateful for his scientific vision, ideas and guidance, which were always available when I needed them.

I would like to thank Prof. Dr. Anita Ignatius for co-examining this thesis.

Over the last five years I have shared many memorable experiences with my colleagues at the Laboratory for Bone Mechanics, and I would like to mention some of them in particular. I would like to thank Dr Duncan Tourolle not only for his friendship, but also for his willingness and enthusiasm to provide insight and ideas whenever they were needed. I am thankful to Dr Angad Malhotra for showing me how to write a scientific paper. I would like to thank Dr Ariane Scheuren for years' worth of collaboration and enthusiasm to engage in projects that should have failed (but didn't). I would like to thank Nicholas Ohs for his readiness to provide technical help and decadent culinary adventures throughout this journey that we started, and will finish, at the same time. I would like to thank Elliot Goff, who shared an office with me for almost four years, for being an excellent sounding board, and for tolerating old sports clothes, climbing shoes and mountain bikes lying around the office.

I have had the privilege of working with excellent students over the last four years, in particular Paul, Nicole, Michelle and Basil. Your work allowed this thesis to be more than it could have been by my efforts alone.

I would like to thank Birte Toussaint for triggering the start of my PhD journey, and supporting me every moment along the way. This thesis simply would not have happened without her. I would also like to thank my parents, Brian and Belinda, who encouraged and supported my curiosity from a young age.

Finally, I would like to thank the European Union (ERC Advanced MechAGE ERC-2016-ADG-741883) for providing funding, which enabled almost all of this work to be achieved.

# Summary

As bone diseases, such as osteoporosis, and trauma events, such as hip fractures, significantly impact the health and well-being of aging populations, our understanding of their causes and progressions is essential for the development of new treatments and prophylactics. Bone is a dynamic material that constantly adapts and renews itself in a process known as bone remodeling, and is able to repair itself completely upon injury. Bone remodelling and healing are driven by mechanical loading of bone and its surrounding tissue. However, bone is a multiscale, hierarchical material and its response and transmission of mechanical loading is complex. Physiological or extra-physiological organ-scale loading is transmitted heterogeneously to the tissue scale. The strains at tissue scale stimulate sensing cells known as osteocytes, which reside within the bone tissue. This stimulation leads to the release of proteins, which instruct osteoblasts to lay down bone or osteoclasts to remove bone. Parts of this mechanical signal transmission throughout bone, and the resultant biological changes within fracture healing, are well understood. However, the linking of organ-scale mechanical loading to osteocyte-specific protein expression and formation, quiescence or resorption has not yet been achieved.

Therefore, in this thesis, we attempted to reconcile these aspects via three aims: (i) to determine organ-scale boundary conditions in bones of individual mice, ii) to determine tissue-scale mechanoregulation in physiologically and extra-physiologically loaded mice, and iii) to apply a combined computational and experimental framework for multiscale investigation of mechanoregulation in a model of fracture healing in mice. To achieve these aims, we employed a mouse model of fracture healing with a surgically induced femoral defect. We investigated the effects of organ-scale loading during the inflammation and early reparative phases, tissue-scale mechanoregulation during the late reparative and remodelling phases, and cell-scale mechanoregulation in the remodelling phase.

To address the first aim, we modified the external fixation system for a femur model of fracture healing. An instrumented side bar for the external fixation system, with which deformations could be captured during mouse locomotion, was created and applied in a study assessing the fracture healing progression in twelve mice. Habitual loading measurements were taken weekly and coupled with weekly micro-computed tomography (micro-CT) imaging. Using the micro-CT data, micro-finite element (micro-FE) simulations were run to determine the fracture

stiffness at each time point. This fracture stiffness was used as a proxy for healing progression. It was observed that organ-scale loading in the inflammation phase (i.e. before the fracture started displaying signs of healing) was predictive of the outcome of the fracture. Mice with lower levels of habitual loading displayed poor healing progressions, or did not heal at all. To address the first aim completely, we developed an approach termed real time finite element (rtFE) analysis. This method allowed the specification of organ-scale loading parameters to target a particular “mechanical dose” of strain within the bone tissue post bridging in our fracture-healing model. We demonstrated, via the use of rtFE to control loading parameters, that variance could be reduced in loaded models of fracture healing. We further demonstrated that the model could be expanded to an extra-physiologically loaded model.

In the second part, we aimed to reconcile the effects of and changes within the multiple scales of bone. A combination of measured boundary conditions, micro-CT imaging, micro-FE simulation and immunohistochemistry was used. This allowed tissue-scale and cell-scale mechanical environments to be simulated from organ-scale loading parameters.

At the tissue scale, mechanoregulatory patterns of both physiologically loaded mice and extra-physiologically loaded mice were analysed over the late reparative and remodelling phases of fracture healing. rtFE was used to specify the organ-scale loads of extra-physiologically loaded mice, allowing a specific strain distribution to be targeted. Mechanical signal was found to be predictive of changes in bone at tissue scale. Regions of high strain displayed an increased probability of bone formation while regions of low strain displayed an increased probability of bone resorption. The results suggest that the late reparative and remodelling phases in fracture healing share similar mechanoregulatory relationships to those in bone adaptation, further supporting the theory that these processes are governed by similar mechanisms.

For cell-scale investigations, the locations of osteocytes within the bone tissue were identified via stained sections. The simulated mechanical environments were then linked to each osteocyte’s local in vivo environment (LiveE) via the registration of 2D sections within the appropriate 3D micro-CT image. From this information, it was determined that highly strained cells were more likely to be associated with sites of formation, while lowly strained cells were more likely to be associated with sites of resorption. The osteocytic expression of two proteins relevant to bone formation and resorption and the mechanical signal in each osteocyte’s LiveE were assessed. Sclerostin, a bone formation inhibitor, was found to be significantly downregulated in osteocytes under high levels of mechanical stimulation. RANKL, an

osteoclast progenitor associated with bone resorption, did not display a clear relationship between mechanical strain and expression by osteocytes. Future studies should aim to increase the sample size of this investigation to clarify the relationship between RANKL, bone adaptation, healing and mechanics.

In summary, measurement and design of organ-scale physiological and extra-physiological loading of mice allowed us to simulate and couple the mechanical environment at tissue scale and cell scale with tissue-scale changes and protein expression. This demonstrated, for the first time, mechanoregulatory relationships during fracture healing at organ, tissue, cell and molecular scales within the same mice. The combination of strain gauge measurement, micro-CT imaging, micro-FE simulation and immunohistochemistry allows the comprehensive investigation of mechanoregulation within bone. The biologically relevant results presented in this thesis indicate that these technologies enable investigation into many open questions regarding the multiscale mechanoregulation of bone during fracture healing. In the future, expansion of such studies to include cell-scale observations during the pre-bridging period would allow a full unravelling of the fracture healing process.

# Zusammenfassung

Knochenerkrankungen, wie Osteoporose, und Traumaereignisse, wie Hüftbrüche, beeinträchtigen die Gesundheit und das Wohlbefinden alternder Bevölkerungen erheblich. Daher ist die Erforschung ihrer Ursachen und Verläufe zur Entwicklung neuer Therapien und Prophylaktika unerlässlich. Knochen ist ein dynamisches Material, das sich in einem Prozess, der als Knochenumbau bezeichnet wird, ständig anpasst und erneuert und sich bei Verletzungen selbstständig regenerieren kann. Knochenumbau und -heilung werden durch die mechanische Belastung des Knochens und des umgebenden Gewebes angetrieben. Da Knochen aus mehreren hierarchischen Schichten besteht, ist die Übertragung mechanischer Belastungen komplex. Physiologische oder extraphysiologische Belastungen auf Organebene werden heterogen auf das Knochengewebe übertragen. Auf Gewebeebene stimulieren diese Belastungen Zellen im Knochengewebe, die Osteozyten genannt werden. Durch diese Stimulation werden Proteine freigesetzt, die Osteoblasten und Osteoklasten instruieren, Knochen niederzulegen, beziehungsweise zu abzubauen. Gewisse Aspekte der mechanischen Signalübertragung in Knochen und die daraus resultierenden biologischen Veränderungen während der Knochenheilung sind gut verstanden. Die Beziehung zwischen organspezifischer mechanischer Belastung und zellspezifischer Proteinexpression ist jedoch noch nicht bekannt.

Daher war das Ziel dieser Arbeit, diese Beziehung zu untersuchen. Dazu wurden drei Zwischenziele definiert: (i) die Bestimmung der Randbedingungen in den Knochen einzelner Mäuse auf Organebene, (ii) die Bestimmung der Mechanoregulation in physiologisch und extraphysiologisch belasteten Mäusen auf Gewebeebene und (iii) die Kombination rechnerischer und experimenteller Ansätze zur Untersuchung der Mechanoregulation auf mehreren Ebenen. Dazu verwendeten wir ein Mäusemodell der Knochenheilung mit einem chirurgisch induzierten Femurdefekt. Wir beobachteten die Auswirkungen einer Belastung auf Organebene während der Entzündungs- und der frühen Reparaturphase. Auf Gewebeebene untersuchten wir die Mechanoregulation während der späten Reparatur- und der Umbauphase und auf der Zellebene die Mechanoregulation in der Umbauphase.

Zum Erreichen des ersten Zwischenziels wurde das externe Fixationssystem für ein Femurmodell zur Knochenheilung modifiziert. Dazu wurde ein instrumentierter Seitensteg für das externe Fixationssystem angefertigt, mit dem die Deformation während Bewegung der Maus gemessen werden konnte. Dieses System wurde in einer Studie zum

Knochenheilungsverlauf an zwölf Mäusen angewandt. Messungen der gewöhnlichen Belastung wurden wöchentlich durchgeführt und mit einer wöchentlichen Mikro-Computertomographie-Bildgebung (Mikro-CT) gekoppelt. Die Mikro-CT-Daten wurden in Mikro-Finite-Elemente-Simulationen (Mikro-FE) verwendet, um die Bruchsteifigkeit zu jedem Messpunkt zu bestimmen. Diese Bruchsteifigkeit wurde als Proxy für den Heilungsverlauf verwendet. Wir beobachteten, dass eine Belastung auf Organebene in der Entzündungsphase (d.h. bevor die Fraktur Anzeichen einer Heilung aufwies), den Ausgang der Fraktur vorhersagte. Mäuse mit geringeren Belastungen zeigten einen schlechten bis gar keinen Heilungsverlauf. Ferner entwickelten wir im Rahmen dieses Zwischenziels einen Ansatz, den wir als Echtzeit--Finite-Elemente-Analyse (englisch: real time finite element analysis, rtFE) bezeichnen. Dieser Ansatz ermöglichte es uns, Belastungsparameter auf Organebene so zu definieren, dass das Knochengewebe in unserem Mäusemodell nach der Überbrückung mit einer gezielten "mechanischen Dosis" belastet werden konnte. Wir konnten zeigen, dass die Verwendung von rtFE zur Steuerung von Belastungsparametern die Varianz im Ausgang der Frakturheilung reduzierte.

Zum Erreichen des zweiten Zwischenziels entwickelten wir einen Ansatz, in dem wir gemessene Randbedingungen, Mikro-CT, Mikro-FE-Simulation und Immunhistochemie kombinierten. Dies ermöglichte die Simulation der mechanischen Umgebung auf Gewebe- und Zellebene anhand von Belastungsparametern auf Organebene.

Auf Gewebeebene analysierten wir mechanoregulatorische Muster sowohl von physiologisch belasteten Mäusen, als auch von extraphysiologisch belasteten Mäusen, in der späten Reparatur- und Umbauphase der Frakturheilung. Mittels rtFE bestimmten wir die Belastungen von extraphysiologisch belasteten Mäusen auf Organebene, sodass eine spezifische Belastungsverteilung angestrebt werden konnte. Wir zeigten, dass das mechanische Signal Veränderungen im Knochen auf Gewebeebene vorhersagt. Regionen mit hoher Belastung wiesen eine erhöhte Wahrscheinlichkeit für Knochenbildung auf, während Regionen mit geringer Belastung eine erhöhte Wahrscheinlichkeit für Knochenresorption zeigten. Unsere Ergebnisse deuten darauf hin, dass die späte Reparaturphase und die Umbauphase in der Frakturheilung ähnliche mechanoregulatorische Beziehungen wie in der Knochenanpassung aufweisen. Diese Ergebnisse stehen im Einklang mit der Theorie, dass diese Prozesse von ähnlichen Mechanismen gesteuert werden.



Zur Analyse auf Zellebene identifizierten wir die Positionen der Osteozyten innerhalb des Knochengewebes anhand von gefärbten Schnitten. Die simulierten mechanischen Umgebungen wurden dann über die Registrierung von 2D-Schnitten innerhalb des 3D-Mikro-CT-Bildes mit der lokalen *in vivo* Umgebung (englisch: local *in vivo* environment, *LivE*) jedes Osteozyten verknüpft. Anhand davon stellten wir fest, dass hoch belastete Zellen mit Orten der Knochenneubildung assoziiert waren, während weniger belastete Zellen mit Resorptionsstellen assoziiert waren. Wir analysierten die osteozytäre Expression von zwei Proteinen, die für die Knochenbildung und -resorption relevant sind, und das mechanische Signal in der *LivE* jedes Osteozyten. Sclerostin, ein Knochenbildungshemmer, wird in Osteozyten unter hoher mechanischer Stimulation signifikant herunterreguliert. RANKL, ein Osteoklastenvorläufer, der mit der Knochenresorption assoziiert ist, wies keine klare Beziehung zwischen mechanischer Belastung und Expression durch Osteozyten auf. Weitere Studien mit höheren Stichprobengrößen sind notwendig, um die Beziehung zwischen RANKL, Knochenanpassung, Heilung und Mechanik genauer zu verstehen.

Zusammenfassend lässt sich sagen, dass die Messung und gezielte Bestimmung der physiologischen und extra-physiologischen Belastung von Mäusen auf Organebene es uns ermöglichte, die mechanische Umgebung auf Gewebe- und Zellebene zu simulieren und mit Veränderungen auf Gewebeebene und Proteinexpression zu koppeln. Auf diese Weise konnten mechanoregulatorische Beziehungen auf Organ-, Gewebe-, Zell- und molekularer Ebene während der Frakturheilung zum ersten Mal in denselben Mäusen nachgewiesen werden. Die Kombination von Dehnungsmessstreifen-Messungen, Mikro-CT, Mikro-FE-Simulation und Immunhistochemie ermöglicht die umfassende Untersuchung der Mechanoregulation im Knochen. Die biologisch relevanten Erkenntnisse in dieser Arbeit deuten darauf hin, dass diese Technologien die Untersuchung vieler offener Fragen bezüglich der Multiskalen-Mechanoregulation in Knochen während der Frakturheilung ermöglichen. In Zukunft sollten Studien auf Beobachtungen im Zellmaßstab während der Vorbrückungszeit eine vollständige Aufklärung des Frakturheilungsprozesses ermöglichen. Zukünftige Erweiterungen dieser Studien, insbesondere mit Bezug auf Beobachtungen auf der Zellebene vor der Überbrückungsphase, werden eine vollständige Aufklärung über den Frakturheilungsprozess ermöglichen.

## Notes on text

In this thesis, Nature-style referencing has been used. However, in Chapter 2: Background, the referencing style of the journal *Current Osteoporosis Reports* has been used. This is due to pre-publication.

Throughout this text the terms formation, resorption and quiescence are used. For those not familiar with the last term, it refers to regions of bone which have not changed over the time interval.

# **Chapter 1 :**

## **Introduction**

## Thesis motivation

To the uninitiated eye, bone appears to be an inert tissue. On the contrary, it is a complex, hierarchical material, in which new bone tissue is constantly laid down and old tissue resorbed in a process known as bone remodelling<sup>1</sup>. This state of flux is driven primarily by mechanical loads experienced by the tissue. A state of higher than normal mechanical loading leads to bone formation, while a state of lower than normal mechanical loading leads to resorption<sup>2</sup>. Mechanical loads are a critical component in the process of healing within bone tissue, with the amount of deformation experienced by the bone defect influencing tissue type and rate of formation during the healing process<sup>3,4</sup>. As diseases, such as osteoporosis, and trauma events, such as hip fractures, significantly impact the health and well-being of aging populations, understanding these remodelling and healing processes is essential<sup>5</sup>. The development of new treatments presupposes an understanding of the physiological pathways and molecular mechanisms governing these processes.

A key aspect of bone is its multiscale, hierarchical nature. At cell scale, it has been established that osteocytes reside in lacunae, structures roughly 10 microns in diameter<sup>6</sup>, and act as molecular sensors. As such, they inhibit or promote molecular pathways that regulate the formation of new bone via the stimulation of osteoblasts, and the resorption of bone via the stimulation of osteoclasts<sup>7,8</sup>. This process<sup>3,4</sup> happens on scales less than  $10^{-6}$  m, yet the dimensions of mechanical forces exerted on the cortical or trabecular bone are three to four orders of magnitude greater<sup>6</sup>. Loads placed at organ scale distribute themselves heterogeneously throughout the bone<sup>9-11</sup>. This leads to points of higher strain and lower strain, which activate the aforementioned pathways as the bone attempts to minimise the distribution of strains higher or lower than particular thresholds<sup>12</sup>.

Identifying the exact strain sensed by osteocytes is challenging, but key for the accurate quantification of genetic and molecular responses to mechanical loads placed on the greater organ. In this regard, experimental and computational techniques developed at the Laboratory of Bone Biomechanics in recent years have led to predictive capacity of bone tissue formation and resorption. These techniques are based on the Strain Energy Density (SED) calculated through micro-Finite Element (micro-FE) analysis<sup>9,13,14</sup> and focus on the mouse as a model system. Loading models, in which a known cyclical load is applied to the caudal vertebrae of mice, were developed and coupled with a longitudinal imaging approach using *in vivo* micro-computed tomography (micro-CT) to track the formation and resorption of bone tissue<sup>9</sup>. This

experimental approach informs micro-FE-based analyses to correlate areas of bone formation and resorption with areas of high and low SED, respectively. Further developments have combined these models with protein expression and single cell mechanomic profiling<sup>15</sup>. This has fostered the development of increasingly detailed models of the bone remodelling process. These models, however, have yet been expanded to bone healing.

At organ scale, numerous approaches have been used to assess the strain in bone. These have ranged from invasive *in vivo* methods such as strain gauging<sup>16-18</sup>, to *ex vivo* techniques such as optical measurement<sup>17,19,20</sup>. Additionally, computational techniques based on bone structure have been used to back-calculate the load history experienced by the bone tissue<sup>4,21</sup>. Stepping down from organ scale to tissue scale, several techniques have been applied to assess microstructural strain in bone. These include the use of machine vision photogrammetry to measure strain gradients<sup>22</sup> and Synchrotron micro-CT imaging to measure propagation of microcracks<sup>23</sup>. However, these techniques are only suitable for *ex vivo* measurements. *In vivo*, spatial resolution often comes at a cost of temporal resolution, while techniques with good spatial and temporal resolution are limited to 2D imaging<sup>6</sup>. As dimensions shrink, the impact of micro-features on the distribution of strain within the microstructure increases<sup>23</sup>. Micro-FE has proved a reliable technique<sup>24</sup> for calculating tissue-scale strains, and provides an excellent bases for simulating mechanical signals within bone healing or remodelling studies<sup>13,14,25,26</sup>.

When comparing *ex vivo* and *in vivo* data on the effect of strain on osteocytes, contrasting results are seen. Areas of bone expressing significant remodelling activity often experience substantially less strain than *in vitro* experiments outline as is necessary for cellular response<sup>27-29</sup>. Using FE analysis to calculate stains within the lacunae-canalliculi structures in which osteocytes reside, several authors have shown stain amplification to occur<sup>30-32</sup>, resulting in strains far greater than those displayed at tissue scale. However, whether or not these observation limit the ability of tissue-scale simulation, such as micro-FE, to estimate the mechanical signal experience by cells has not been established.

Given the complex relationship between organ-scale loads and cell-scale strains, a well-structured framework is required to reconcile the mechanical signal with the biological changes at each scale. At cell scale, the immediate mechanical environment, which has been termed the Local *in vivo* Environment (*LivE*), represents the most important region of understanding in the development of a multiscale framework. Structural changes occur over the course of many weeks as a defect heals or the bone tissue itself remodels<sup>9,11,26,33</sup>. This remodelling influences

the strain experienced by the cells, which in turn causes further structural changes. Hence, a simple snapshot of protein expression in the *LivE* at a study endpoint paints an incomplete picture of the mechanoregulated behaviour. A combination of tools and techniques is therefore required to reconcile the temporal and spatial changes within the bone healing and remodelling environment.

We propose to develop a technology to facilitate the capture of organ-scale boundary conditions, and apply these to simulate the mechanical environment at the various scales of bone within a mouse femur defect model. Using these simulations, we aim to improve knowledge of the strain and strain history experienced by individual cells, and the resultant tissue-scale changes and cell-scale protein expression. This combined computational and experimental approach will enable the investigation of mechanobiology at organ, tissue and cell scales within a femur defect mouse model.

## Specific aims

The goal of this thesis was to develop a framework to link organ-scale boundary conditions to cell-scale stimuli within a femur defect model in mice. To this end, the following three aims were developed:

**Aim 1:** Determination of organ-scale boundary conditions in bones of individual mice.

**Aim 2:** Determination of tissue-scale mechanoregulation in physiologically and extra-physiologically loaded mice.

**Aim 3:** Application of a combined computational and experimental framework for multiscale investigation of mechanoregulation in a model of fracture healing in mice.

## Thesis outline

This thesis consists of five chapters. The first and current chapter outlines the motivation for the following four chapters.

**Chapter 2** discusses techniques used to determine the cell environment in mouse models.

In **Chapter 3** we apply deformation measurement techniques to longitudinally track the organ-scale boundary conditions in an externally fixated femur defect model. We then demonstrate the importance of these measurements in the outcome of the fracture healing process. Further, we propose a solution to specify the level of mechanical strain within the defect healing model. We also discuss an optimisation approach to design the mechanical stimulus at tissue scale in a defect model. This approach allows the knowledge displayed in the first part of this chapter to be utilised to design a “mechanical dose” for interventions.

In Part 1 of **Chapter 4** we apply the methods we developed in Chapter 3 to investigate 1) the mechanoregulation at the tissue and cell scales in the habitually loaded study (described in Chapter 3.1) and 2) the organ-to-tissue-scale healing and remodelling dynamics under extra-physiological loading. Combining organ-to-tissue and tissue-to-cell approaches in our model, we investigate the relationship between measured boundary conditions and the expression of two key mechanoregulated bone remodelling cytokines, Sclerostin and RANKL, to create a link from organ-scale mechanical loading to cell-scale responses. This is achieved by combining micro-CT imaging, registered histologies and micro-FE simulations to calculate the mechanical

environment of cells. In Part 2, a range of analytical methods is applied to a femur defect model under both loading and sham loading to demonstrate mechanical regulation at the tissue scale.

Finally, **Chapter 5** synthesises the major developments and findings of this thesis. Limitations of the work are outlined and directions for future research are suggested.



---

## References

- 1 Rho, J. Y., Kuhn-Spearing, L. & Zioupos, P. Mechanical properties and the hierarchical structure of bone. *Med Eng Phys* **20**, 92-102, doi:Doi 10.1016/S1350-4533(98)00007-1 (1998).
- 2 Huiskes, R., Ruimerman, R., van Lenthe, G. H. & Janssen, J. D. Effects of mechanical forces on maintenance and adaptation of form in trabecular bone. *Nature* **405**, 704-706, doi:Doi 10.1038/35015116 (2000).
- 3 Rontgen, V. *et al.* Fracture Healing in Mice under Controlled Rigid and Flexible Conditions Using an Adjustable External Fixator. *J Orthop Res* **28**, 1456-1462, doi:10.1002/jor.21148 (2010).
- 4 Isaksson, H. *et al.* Remodeling of Fracture Callus in Mice Is Consistent with Mechanical Loading and Bone Remodeling Theory. *J Orthop Res* **27**, 664-672, doi:10.1002/jor.20725 (2009).
- 5 Cooper, C., Campion, G. & Melton, L. J. Hip-Fractures in the Elderly - a Worldwide Projection. *Osteoporosis Int* **2**, 285-289, doi:Doi 10.1007/Bf01623184 (1992).
- 6 Goggin, P. M., Zygalkakis, K. C., Oreffo, R. O. C. & Schneider, P. High-Resolution 3d Imaging of Osteocytes and Computational Modelling in Mechanobiology: Insights on Bone Development, Ageing, Health and Disease. *Eur Cells Mater* **31**, 264-295, doi:10.22203/eCM.v031a18 (2016).
- 7 Bonewald, L. F. The Amazing Osteocyte. *J Bone Miner Res* **26**, 229-238, doi:10.1002/jbmr.320 (2011).
- 8 Tan, S. D. *et al.* Osteocytes subjected to fluid flow inhibit osteoclast formation and bone resorption. *Bone* **41**, 745-751, doi:10.1016/j.bone.2007.07.019 (2007).
- 9 Webster, D. J., Morley, P. L., van Lenthe, G. H. & Muller, R. A novel in vivo mouse model for mechanically stimulated bone adaptation - a combined experimental and computational validation study. *Comput Method Biomec* **11**, 435-441, doi:10.1080/10255840802078014 (2008).
- 10 Lambers, F. M., Schulte, F. A., Kuhn, G., Webster, D. J. & Müller, R. Mouse tail vertebrae adapt to cyclic mechanical loading by increasing bone formation rate and decreasing bone resorption rate as shown by time-lapsed in vivo imaging of dynamic bone morphometry. *Bone* **49**, 1340-1350, doi:10.1016/j.bone.2011.08.035 (2011).
- 11 Webster, D., Wirth, A., van Lenthe, G. H. & Müller, R. Experimental and finite element analysis of the mouse caudal vertebrae loading model: prediction of cortical and

- trabecular bone adaptation. *Biomech Model Mechan* **11**, 221-230, doi:10.1007/s10237-011-0305-3 (2012).
- 12 Christen, P. *et al.* Bone remodelling in humans is load-driven but not lazy. *Nat Commun* **5**, doi:10.1038/ncomms5855 (2014).
- 13 Webster, D., Schulte, F. A., Lambers, F. M., Kuhn, G. & Muller, R. Strain energy density gradients in bone marrow predict osteoblast and osteoclast activity: A finite element study. *J Biomech* **48**, 866-874, doi:10.1016/j.jbiomech.2014.12.009 (2015).
- 14 Schulte, F. A. *et al.* Local Mechanical Stimuli Regulate Bone Formation and Resorption in Mice at the Tissue Level. *Plos One* **8**, doi:ARTN e62172 10.1371/journal.pone.0062172 (2013).
- 15 Trüssel, A., Müller, R. & Webster, D. Toward Mechanical Systems Biology in Bone. *Ann Biomed Eng* **40**, 2475-2487, doi:10.1007/s10439-012-0594-4 (2012).
- 16 Milgrom, C. *et al.* A comparison of bone strain measurements at anatomically relevant sites using surface gauges versus strain gauged bone staples. *J Biomech* **37**, 947-952, doi:10.1016/j.jbiomech.2003.10.008 (2004).
- 17 Roriz, P., Carvalho, L., Frazao, O., Santos, J. L. & Simoes, J. A. From conventional sensors to fibre optic sensors for strain and force measurements in biomechanics applications: A review. *J Biomech* **47**, 1251-1261, doi:10.1016/j.jbiomech.2014.01.054 (2014).
- 18 Lanyon, L. E., Hampson, W. G. J., Goodship, A. E. & Shah, J. S. Bone Deformation Recorded In vivo from Strain Gauges Attached to Human Tibial Shaft. *Acta Orthop Scand* **46**, 256-268 (1975).
- 19 Carvalho, L. *et al.* In the trail of a new bio-sensor for measuring strain in bone: Osteoblastic biocompatibility. *Biosens Bioelectron* **26**, 4046-4052, doi:10.1016/j.bios.2011.03.028 (2011).
- 20 Alvarez, A. S., Ibarra, M. H. D., Santoyo, F. M. & Anaya, T. S. Strain determination in bone sections with simultaneous 3D digital holographic interferometry. *Opt Laser Eng* **57**, 101-108, doi:10.1016/j.optlaseng.2014.01.022 (2014).
- 21 Christen, P., van Rietbergen, B., Lambers, F. M., Muller, R. & Ito, K. Bone morphology allows estimation of loading history in a murine model of bone adaptation. *Biomech Model Mechan* **11**, 483-492, doi:10.1007/s10237-011-0327-x (2012).

- 
- 22 Nicolella, D. P., Nicholls, A. E., Lankford, J. & Davy, D. T. Machine vision photogrammetry: a technique for measurement of microstructural strain in cortical bone. *J Biomech* **34**, 135-139, doi:Doi 10.1016/S0021-9290(00)00163-9 (2001).
- 23 Donaldson, F. *et al.* Modeling microdamage behavior of cortical bone. *Biomech Model Mechan* **13**, 1227-1242, doi:10.1007/s10237-014-0568-6 (2014).
- 24 Chen, Y. *et al.* Micro-CT based finite element models of cancellous bone predict accurately displacement once the boundary condition is well replicated: A validation study. *J Mech Behav Biomed* **65**, 644-651, doi:10.1016/j.jmbbm.2016.09.014 (2017).
- 25 Tourolle né Betts, D. C. *et al.* The association between mineralised tissue formation and the mechanical local *in vivo* environment: Time-lapsed quantification of a mouse defect healing model. *Sci Rep-Uk* **10**, 1-10, doi:10.1038/s41598-020-57461-5 (2020).
- 26 Webster, D., Schulte, F., Lambers, F., Kuhn, G. & Muller, R. The mechanical environment in bone marrow predicts osteoblast and osteoclast activities. *Bone* **50**, S73-S73, doi:10.1016/j.bone.2012.02.208 (2012).
- 27 Owan, I. *et al.* Mechanotransduction in bone: Osteoblasts are more responsive to fluid forces than mechanical strain. *Am J Physiol-Cell Ph* **273**, C810-C815 (1997).
- 28 Paul, G. R., Malhotra, A. & Muller, R. Mechanical Stimuli in the Local In Vivo Environment in Bone: Computational Approaches Linking Organ-Scale Loads to Cellular Signals. *Curr Osteoporos Rep* **16**, 395-403, doi:10.1007/s11914-018-0448-6 (2018).
- 29 Bonewald, L. F. Mechanosensation and Transduction in Osteocytes. *Bonekey Osteovision* **3**, 7-15, doi:10.1138/20060233 (2006).
- 30 Verbruggen, S. W., Vaughan, T. J. & McNamara, L. M. Strain amplification in bone mechanobiology: a computational investigation of the *in vivo* mechanics of osteocytes. *J R Soc Interface* **9**, 2735-2744, doi:10.1098/rsif.2012.0286 (2012).
- 31 Bonivitch, A. R., Bonewald, L. F. & Nicolella, D. P. Tissue strain amplification at the osteocyte lacuna: A microstructural finite element analysis. *J Biomech* **40**, 2199-2206, doi:10.1016/j.jbiomech.2006.10.040 (2007).
- 32 Wang, Y., McNamara, L. M., Schaffler, M. B. & Weinbaum, S. Strain amplification and integrin based signaling in osteocytes. *J Musculoskelet Neuronal Interact* **8**, 332-334 (2008).

- 33 Webster, D. *et al.* Mechanical loading of mouse caudal vertebrae increases trabecular and cortical bone mass-dependence on dose and genotype. *Biomechanics and Modeling in Mechanobiology* **9**, 737-747, doi:10.1007/s10237-010-0210-1 (2010).

# **Chapter 2 :**

# **Background**

---

# Mechanical Stimuli in the Local In Vivo Environment in Bone: Computational Approaches Linking Organ-Scale Loads to Cellular Signals

Graeme R Paul<sup>1</sup>, Angad Malhotra<sup>1</sup> & Ralph Müller<sup>1</sup>

Institute for Biomechanics, ETH Zurich, Leopold-Ruzicka-Weg 4, 8093 Zürich, Switzerland

Reprinted with permission from Springer Nature.

Material from: Paul, G.R., Malhotra, A. & Müller, R. Mechanical Stimuli in the Local In Vivo Environment in Bone: Computational Approaches Linking Organ-Scale Loads to Cellular Signals. *Current Osteoporosis Reports*, 2018, Springer Nature.

## Abstract

### *Purpose of Review*

Connecting organ-scale loads to cellular signals in their local in vivo environment is a current challenge in the field of bone (re)modelling. Understanding this critical missing link would greatly improve our ability to anticipate mechanotransduction during different modes of stimuli and the resultant cellular responses. This review characterises computational approaches that could enable coupling links across the multiple scales of bone.

### *Recent Findings*

Current approaches using strain and fluid shear stress concepts have begun to link organ-scale loads to cellular signals; however, these approaches fail to capture localised micro-structural heterogeneities. Furthermore, models that incorporate downstream communication from osteocytes to osteoclasts, bone-lining cells and osteoblasts, will help improve the understanding of (re)modelling activities. Incorporating this potentially key information in the local in vivo environment will aid in developing multiscale models of mechanotransduction that can predict or help describe resultant biological events related to bone (re)modelling.

*Summary*

Progress towards multiscale determination of the cell mechanical environment from organ-scale loads remains elusive. Construction of organ-, tissue- and cell-scale computational models that include localised environmental variation, strain amplification and intercellular communication mechanisms will ultimately help couple the hierarchal levels of bone.

**Keywords:**

Mechanical stimulation, Osteocytes, Computational systems biomechanics, Local in vivo environment, Bone (re)modelling

## Introduction

Within the last few decades, significant advances in imaging and computational technologies have allowed new insights into biomedical phenomena. However, our ability to utilise these tools has struggled to keep pace with their rapidly expanding capabilities. In the field of bone biomechanics, this is evident in our lack of understanding how organ-scale loads translate to biochemical responses via cellular mechanotransduction. Such information would help to gain deeper insight into how cells respond to loading modalities, leading to computationally driven understanding of, and therapies for, skeletal diseases such as osteoporosis [1]. This review discusses how the transmission of in vivo mechanical stimuli across multiple scales can be greatly improved by using computational methods, often in conjunction with other well-established approaches. The aim is to define a computationally driven framework for translating organ-scale loads into relevant cell-scale responses, which would ultimately increase our understanding of the in vivo mechanosensitive aspects and mechanisms of bone (re)modelling, and its importance in the pathophysiology of bone.

## Existing Tools, Techniques and Concepts

The knowledge of bone systems biomechanics is not new, though translating this into substantial improvements in bone health is yet to be realised. The theory of load driven bone (re)modelling was first postulated over a century ago [2, 3]; however, only with the development of powerful in vivo imaging techniques, such as micro-computed tomography (micro-CT), has detailed time-lapsed micro-scale observation of bone (re)modelling for both formation and resorption been possible [4, 5]. Concurrently, advances in computational power have driven the development of predictive models of mechanical loading within bone tissue [6, 7, 8]. Coupling these technologies has revealed great insights into dynamic bone (re)modelling via comparisons between mechanical loading and structural changes in bone tissue [6, 9,10,11]. As these imaging and computational modelling methods have matured, they have become accurate enough to inform techniques such as laser capture micro-dissection to investigate individual cells within the bone tissue and to perform “mechanomic” analysis, reconciling genetic responses to mechanical stimuli [12, 13] of the acquired cells [14, 15]. The extraction of small populations of cells [16] and the assessment of their molecular and genetic profiles [17] has been combined with computational predictions of mechanical loads within the local in vivo environment (LivE) of these cells [17], advancing our understanding of how organ-



scale loads influence individual cells and the resultant (re)modelling behaviour. Understanding the mechanical environment in which these cell populations reside is a key link in the chain towards understanding the governing mechanisms between mechanical loads and (re)modelling of bone.

Within bone, the organ, tissue and cell scales are linked via complex macro- and micro-structural geometries. The hierarchical structure of bone can be subdivided into four scales: the organ scale, comprising the whole bone; the tissue scale, consisting of cortical and trabecular structures; the cell scale, which also includes micro-structural features such as osteons, lamellae plates, lacunae and canaliculi [18]; and the molecular scale, consisting of ions [19] and proteins such as signalling molecules, receptor and ligands [20]. At the larger scales, mechanical supporting roles are evident from the flaring of proximal condyles in bone, to the changing density and thickness of trabecular struts. However, at the cell scale and beyond, the functionality is less obvious. These scales and their respective computational approaches can be seen in Fig. 1. This environment extends into the bone marrow, where many of the mechanosensitive cells reside, such as osteoblasts, osteoclasts, bone-lining cells and mesenchymal and hemapoetic stem cells. Accurately imaging and modelling the multiscale structures of bone is fundamental to predicting multiscale mechanotransduction. Capturing these features using *in vivo* imaging and converting the organ- and tissue-scale geometries into a computational model is well established [4, 5••]. However, *in vivo* imaging beyond the cell-scale poses a significant challenge. Technologies such as confocal microscopy [27], synchrotron radiation computed tomography [28] and ultra-high-resolution computed tomography [29] have been applied *ex vivo* to attempt to capture the micro-structural geometry. With these methods, several authors [28, 30] have performed comprehensive analyses of osteocyte networks and individual lacunae, assessing typical densities and distributions [28, 29], as well as studies on strain amplification on individual lacunae-caliculi structures [27]. Even with the multitude of tools and techniques available to gather information, they are often single scale focused and seem to struggle coupling the hierarchies of bone.

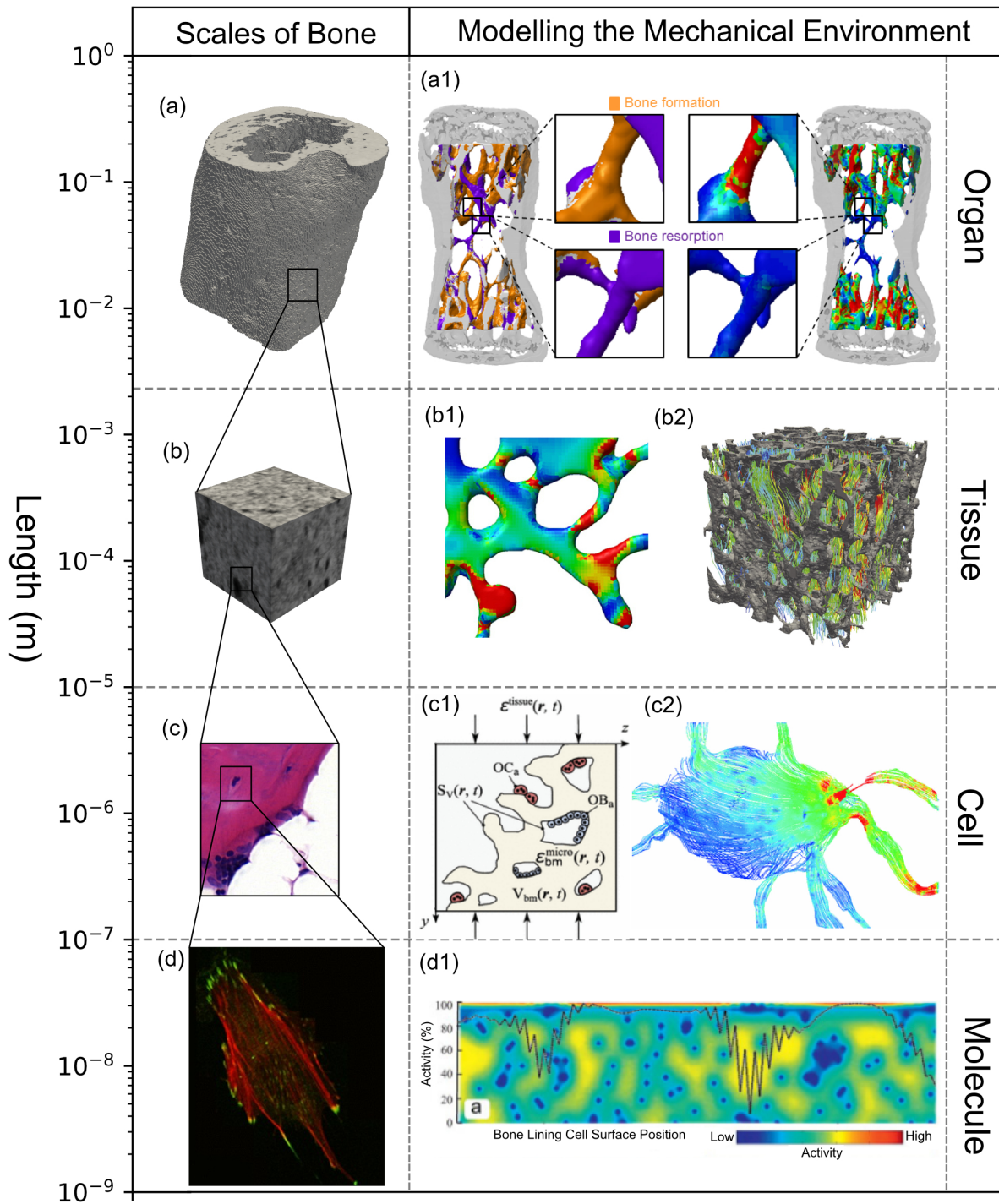


**Figure 2.1:** *Capturing the mechanical environment over different scales has been performed using many approaches. (a) Organ scale, (b) tissue scale, (c) cell scale, and (d) molecular scale [21] have been captured by (a1–c2). Micro-FE models such as (a1) Schulte et al. [10] and (b1) Lambers et al. [22] have been applied at organ level to calculate the tissue level mechanical environment. Within the tissue level, localised tissue boundary conditions can be used to calculate a reduced tissue-scale bone marrow environment, such as (b2) investigated by Metzger et al. [23]. The RVE (c1) concept can be applied to link organ-scale loads to a BMU type environment such as that by Lerebours et al. [24•]. Boundary conditions from the lower end of the tissue scale can be applied to determine fluid flow stresses on the cell, as seen by Verbruggen et al. [25••] in (c2). In the molecular scale, stretch, primary cilia deformation and signalling between osteocytes and other mechanosensitive cells can be simulated; an example of this is the model by Jahani et al. [26] studying the osteocyte—bone-lining cell signalling pathways (d1). a1 reproduced in adherence with the CC BY licence applied by PLOS One, b1, b2, d1 reproduced with permission from Elsevier and c1, c2, d reproduced with permission from Springer*

## Organ- and Tissue-Scale Load Determination

Micro-finite element analysis (micro-FE) has become a standard for organ- and tissue-scale load calculations in bone. It has been extensively used for in vivo studies to compare and correlate strain with bone resorption, formation and quiescence [10, 22, 31, 32, 33, 34]. Such models are created with a mesh generated by direct conversion of micro-CT voxels into hexahedral elements, and solved using well-established micro-FE principles [35]. In contrast to traditional FE approaches, this micro-FE approach provides simple meshing, and a unified approach to solving large-scale problems. The resolution of these models is governed by the resolution of the scanner settings, which typically ranges from 10 to 80  $\mu\text{m}$  in vivo [4], where the very high-resolution images provide voxels in the same size range as osteocytes and osteoblasts, but substantially less than osteoclasts. Primarily, these models are elastic, isotropic and homogenous, omitting ultrastructural details. Further simplification includes modelling of cyclic and dynamic organ-scale boundary conditions as static loads [10, 34], shown still capable of capturing (re)modelling behaviour [36]. Schulte et al. [10] and Lambers et al. [22] applied the micro-CT to micro-FE approach to determine the mechanical environment and its effect on bone (re)modelling in mouse tail vertebrae under normal [10, 22], ovariectomised [10] and ageing conditions [22]. For both studies, strain energy density (SED) was calculated for each

voxel in the vertebrae, with this SED-voxel value representing the mechanical stimuli present at the bone surface. This allowed for correlation of SED values to in vivo formation or resorption at that same voxel. Cresswell et al. [29, 34] applied a similar approach to calculate the mechanical in vivo environment during (re)modelling in rat vertebrae. Micro-CT images of rat vertebrae were converted to micro-FE appropriate hexahedral element using custom software and solved using ABAQUS [34] or a custom solver [29]. Similarly, the SED, maximum principle strain and von Mises stress for each element represented the local mechanical in vivo environment. Using florescent markers of bone formation, they correlated high bone formation with high SED values. In a study in which young and adult mouse tibia were subjected to extra-physiological loads, Willie et al. [9] converted micro-CT images to tetrahedral elements which were then solved using ABAQUS via conventional finite element analysis (FEA). Age-related and location-related material properties were implemented, and maximum and minimum strains were used to assess the local mechanical in vivo environment. Here, both groups had increased anabolic response, though they observed a delayed and reduced response to stimuli in the aged mice versus the young mice. Such studies demonstrate that these computational models can provide a mechanical context for complimentary experimental data.

Another common approach is the use of poroelastic models, instead of linear elastic models, to calculate the mechanical environment. Kameo et al. [6•, 37] applied a voxel-based micro-FE poroelastic model for a fluid shear stress based approach to predict (re)modelling of trabeculae under both bending and uniaxial loads. A uniform and isotropic poroelastic model was used on a cube of randomly arranged trabeculae with a bone volume ratio of 0.4. Over a simulation period of 30 days, an increasing load was used to induce fluid shear stress, which was used as a measure of the local mechanical environment. The initially randomly arranged trabeculae rearranged in the loading direction, with an increase in mean equivalent stress and SED observed from the initial state to the end state of the (re)modelling simulation. However, a significant reduction in the standard deviation of the SED and mean equivalent stress was also observed, confirming their hypothesis that (re)modelling leads to homogenisation of tissue strains. Conventional FEA has also been used to provide a mechanical environment for (re)modelling. Pereira et al. [38] also applied a poroelastic model to simulate (re)modelling in a loaded mouse tibia, in which micro-CT images were acquired from mouse tibia and then converted to a tetrahedral volume mesh, and solved dynamically using a commercial solver. The bone was modelled as a poroelastic material, with isotropic elastic parameters and an anisotropic permeability, where the highest permeability was assumed to lie in line with the

primary direction of the lacuna-canalicular structures. The combination of both fluid and solid phases into a single non-poroelastic model was investigated by Tiwari et al. [39], where a (re)modelling simulation was driven by a combination of both strain based measures (compressive and tensile strain and tensile shear) as well as fluid shear stresses. The mechanical environment was calculated via FEA, and this prediction accuracy of (re)modelling was assessed based on six variations of mechanical parameters in a mouse tibia. Strains were calculated with FEA and the tibia was idealised as a homogeneous, isotropic cantilevered beam. Their model showed that the highest prediction accuracy occurred upon a combination of all types of strain and fluid shear stress.

When approaching the mechanical environment outside the mineralised bone tissue, the bone marrow and the fluid-structure interface pose a challenge in determining the mechanical environment surrounding non-osteocyte cells. Webster et al. [40] applied voxel-based micro-FE to determine SED within the bone marrow of a murine vertebrae, illustrating the importance of the mechanical environment of bone marrow on osteoblast and osteoclast activity. In this study, bone marrow was modelled as a linear elastic solid, and they reported that newly formed bone correlated best with the SED gradient of the marrow. Metzger et al. [41, 42•] investigated the mechanical environment of bone marrow using conventional FEA and fluid-structure interaction. Within a region of  $3 \times 3 \times 3$  mm cubic regions of human trabecular bone, they investigated the effect of constitutive model choice on the mechanical environment within the bone marrow, comparing linear elastic solid, neo-hookean solid, viscoelastic solid and a power law fluid constitutive models. They observed differences of up to 25% in mean shear stress between the constitutive models, indicating the importance of constitutive model selection. Additionally, significant heterogeneities in spatial shear stress distributions were noted.

Approaches other than FEA have also been applied to determine the mechanical environment on a tissue scale. In studies working towards coupling (re)modelling biology with mechanics, Lerebours et al. [24•] and Scheiner et al. [11, 43] applied representative volume element (RVE) concepts, beam theory and continuum micro-mechanics theory, under assumptions of pure normal and bending force, to a femur mid-shaft. Both studies argue that this analytical approach, adopted from Hellmich et al. [44], provides a preferable alternative to the conventional micro-FE approach. With this approach, Lerebours et al. [24•] investigated site-specific bone loss due to mechanical disuse in a multiscale model combining organ, tissue and cell-scale simulation. This approach allowed the combination of tissue and vascular phases into

a single model with an analytical solution and predicted SED for a given RVE, which was coupled with a bone-(re)modelling algorithm. Within the beam theory assumptions lies a challenge for this type of approach. It is assumed that no shear forces or torsional loads are present, and the material cross-section needs to remain plane and un-deflected relative to the bone's neutral axis. Lerebours et al. [24•] claim these assumptions hold true primarily at the femur mid-shaft under small deformations; however, expanding this model to other sections, geometries or anatomical locations would require validation that these assumptions hold true for each location.

Due to the scale and availability of techniques to gather information at the organ and tissue scale, bridging of these levels using fundamental concepts has been demonstrated. Expanding and integrating this with smaller scales becomes the next challenge.

## **Tissue to Cell**

One aspect that would help linking these hierarchical scales is differentiating between the modes of cellular mechanotransduction. Strain experienced by a cell arises primarily from matrix deformation strain and fluid flow strain [20]. However, at least with osteocytes, these mechanisms are coupled to some degree [40]; volumetric tissue deformation surrounding an osteocyte causes interstitial fluid flow, inducing a pressure gradient within the lacunar-canalicular network [45]. Correctly capturing the mechanical environment at a cellular level requires incorporating ultrastructural features and their relation to the mechanisms of cell mechanotransduction. In the immediate cell environment, the effect of the extracellular matrix (ECM), the pericellular matrix (PCM) and micro-structural features such as Volkmann canals and lamellar layers influences strain transmission from tissue level to the cell. This was first shown by Anderson and Tate [46], who modelled fluid flow on osteocytes processes. Using computational fluid dynamics, localised stress spikes of up to  $5\times$  were found on geometries constructed from transmitted electron micrographs (TEM), compared with idealised geometries. Investigating localised structural deformation, Verbruggen et al. [27] constructed geometries of osteocytes and their ECM and PCM from confocal microscopic images, comparing this to FE-based strain results based on idealised geometries. For simulations of physiological tissues strains of 500 to 3000 microstrain, they reported that both the ECM and PCM increased strain transfer to the osteocyte. Specifically, the PCM decreased peak strain transferred but increased the overall transmission of strain to the osteocyte. This suggests that real geometries, consisting of an osteocyte surrounded by ECM and PCM, amplify average

strain by 3–4 times that of idealised geometries without an ECM or PCM network, reaching maximum strains of more than 10,000 microstrain. In a further extension of this work using fluid-structure interaction modelling, Verbruggen et al. [25••] introduced fluid in the PCM, between the ECM and the cell. This fluid-structural coupling was analysed using ANSYS CFX and structural finite element solver, and solved using a staggered iteration approach. All solid structures were linear, elastic and isotropic, while the interstitial fluid was modelled as a laminar flow, with fluid properties of salt water. They reported that the highest stress levels occurred not in the cell body itself, but within the surrounding canaliculi. As such, compared with idealised canaliculi, real canaliculi caused an amplification of stimuli by 2–3 times. Vaughan et al. [7] also showed similar strain amplification when modelling inhomogeneities in the microstructure around osteocytes, by incorporating Volkmann and Haversian canals into an osteon. Osteocytes around the Volkmann canals experienced strain up to 9 times the generalised applied strain, while osteocytes in the region of lamella rings around the osteon experienced greater strain amplification as their primary axis angle relative to the rings increased. This amplification aligns well with several in vitro studies, which report that osteocytes require a stimulation of 5,000 to 10,000 microstrain to elicit a biological response [21], as well as similar results from computational approaches performed by Bonivitch et al. [47], Wang et al. [48] and Kamioka et al. [49]. Estimating the mechanical loads transferred from the tissue scale to the cell scale is achievable with such computational approaches, albeit without in vivo reference, and becomes even more challenging beyond this scale.

## Cell and Beyond

While intracellular mechanics models exist, it is questionable whether multiscale models incorporating intracellular complexity would increase accuracy, or only increase computational burden. Hence, at this stage, it may be more beneficial to incorporate these mechanisms outside of the models. Indeed, several mechanisms transduce mechanical stimuli that ultimately lead to the production of molecules orchestrating the (re)modelling behaviour between all involved cells. Actin filaments within cells are anchored to the ECM via integrins and linker proteins, essentially connecting the ECM and the cell's cytoskeleton [50, 51]. Since cells must be anchored to sense shear stress [52], the adhesion to the ECM is a requirement; as such, there is a dependence on integrin function in transducing strain and fluid shear stresses to cell deformations [53], even if integrins do not sense the strain themselves. Proteins, including myosin II motors, actin filaments and actin crosslinkers, link the cell's membrane via anchoring

proteins such as  $\alpha$ -actinin or filamin, that sense dilation versus shear cell deformations, respectively [54]. Fluid flow is also sensed by primary cilium that extend from the cell surface, whose deformation leads to the opening of ion channels resulting in the internalisation or release of ions [55], though its exact role is debated [56]. Other mechanisms include glycocalyx, and membrane-bound proteins such as connexions, or stretch-activated channels [57]. It is yet to be ascertained whether detailed modelling of the cellular mechanisms that transduce the cell mechanical environment to the cell signals is even necessary; simply treating the region as a ‘black box’ while experimentally quantifying the inputs and outputs may be sufficient for tissue (re)modelling research, at least at this relatively early stage of computational prowess. Such computational biophysical simulations that explore and understand molecular dynamics are under development [58]; however, incorporating such simulations into multiscale approaches in bone biomechanics would pose a challenge.

For now, one accessible building block could be the lacuna-canalicular system, which acts as a communication pathway, chemically, as shown by osteocyte calcium signalling correlations to dynamic loading magnitude [59] and frequency [60], and physically, via gap junctions. Ridha et al. [61] captured elements of these features by applying FEA to simulate rupturing of osteocyte cell connections, showing how the loss of connection leads to bone resorption, while Jahani et al. [26] used network simulations to model osteocyte apoptosis and its effect on bone-lining cells, showing that only a 3% decrease in osteocytes was needed to have a significant reduction in peak signal to the bone-lining cells. These types of studies begin to shed light on the interlinked, mechanosensitive biochemical relationship between osteocytes, osteoclasts and osteoblasts which collectively governs bone (re)modelling. The vast majority of these inter- and intracellular pathways, molecules and signals have been discovered *in vitro*, where creation of an artificial mechanical environment is relatively simple. Contrastingly, it is only *in vivo*, where the mechanical environment is inhomogeneous and substantially harder to measure, that such cell-specific information can be validated in the context of bone (re)modelling. Here, quantitative computational tools may be key to estimate and appreciate *in vivo* cell-scale loads and responses.

## **Towards Multiscale Approaches**

Several approaches have attempted to aggregate the influence of mechanics over the range of scales required to investigate biological processes such as bone remodelling. Frost [62] proposed the concept of the bone multicellular unit (BMU), a unit in which the relevant cell



populations establish a localised mechanically driven homeostasis via (re)modelling. This concept allows the behaviour of this unit to be modelled without taking into account individualised cell behaviour, addressing the behaviour of cell populations within this BMU instead. Several authors [11, 24•, 63] have adopted this approach and made use of an RVE of cortical bone to attempt to aggregate mechanics and capture the combined behaviour of the bone (re)modelling cells. The RVE approach claims to be large enough to account for all the micro-structural heterogeneities, yet small enough to allow averaging of material behaviour over the region [64], hence predicting a relevant mechanical stimuli [11], especially if RVE convergence is considered [65]. Further, the interconnectedness of the lacunar-canalicular network integrates extracellular matrix strain as well as fluid shear stress and provides adequate connection between individual osteocytes that can sense mechanical stimuli on a larger scale, rather solely in the immediate dimensions surrounding a single cell [30]. This results in the averaging of tissue level strain over a particular volume, and the conversion of these stimuli into a set of biochemical responses [24•]. Such approaches could argue that cellular stimuli can be captured by a volume substantially larger than an individual cell. Conversely, it can be argued that to sufficiently capture the intricate details that could affect the translation of mechanical loads to cells, such as strain amplification behaviour [7] or fluid-structure interaction within the lacunae [25••], the RVE, in principle, would need to be smaller than the cell-scale; hence the appropriateness of the use of an RVE in both trabecular and cortical bone is debated [66]. However, it is important to note that it is unknown what scale of detail is required to quantify the mechanotransduction from tissue to cell and determine a complete mechanical environment. As such, depending on the model, the RVE approach may be sufficient.

In contrast to the RVE approach, in vitro investigations have shown that osteocytes require substantially greater levels of strain to display a biological response than that measured in the tissue-scale mechanical environment, established and termed as strain amplification [47]. As known, complex interactions between solid and fluid states [25••] and the micro-structural geometries of the tissue [7, 27] lead to significant amplification factors. These can occur between the average tissue strain and the deformation of osteocytes, or the fluid shear stress either on the cell itself or on its processes [67]. Currently, representative systems have begun to approach multiscale bridging. Whether full multiscale approaches, comprising of the organ to molecular scale, will provide insights that are more relevant over representative systems, is yet unclear.

## Validation of Computational Approaches

While the use of computational bone-based biomechanical models consistently increases, validation of the mechanical signals used is in general very much lacking. Ascertaining whether mechanical signal inputs into (re)modelling models are truly representative of the *in vivo* mechanical signals is very difficult, with increasing ambiguity at smaller scales. At larger scales, the validation of models is somewhat achievable [65]; historically, strain gauges have helped validate surface strains of finite element simulations [33]. Other approaches, such as digital image correlation, have also been implemented as validation tools with varying degrees of success [68]. A limitation of these techniques is that they are only appropriate for surface strains, they stiffen the bone surface, or only capture in plane movement of 2D sections [69].

Beyond the organ-scale, experimental *in vivo* validation of mechanical signals poses the greatest challenges. Cell amplification concepts, as discussed by Vaughan et al. [7] and Verbruggen et al. [25•, 27], begin to address this with models that converge on results observed in experimental studies, generating results that align well with *in vitro* experimentation. Such indirect validation, with experimental observation within the mechanical local *in vivo* environment, has been performed with varying degrees of success. Several decades ago, Weinans et al. [70] proposed a feedback driven mechanical loading approach to bone remodelling, in which FEA calculated the mechanical environment, which was used as a remodelling stimulus in the simulation, leading to bone architecture changes. Over the years, more detailed and modern approaches have built on this. Recently, Schulte et al. [8] extended their own prior model [10], applying SED as a (re)modelling stimulus to predict local spatial patterns of formation and resorption. Here, an osteocyte density distribution of  $1/10.5 \mu\text{m}^3$  was combined with (re)modelling stimuli approximated by Gaussian smoothing of the mechanical environment. Using the same micro-FE methods [10], measured by SED value in the region, they could predict changes in bone volume fraction (BV/TV) with a maximum prediction error of 2.4%. However, this approach did not predict dynamics rates of bone formation/resorption effectively, with significant differences between the simulated data and experimental data. This approach was implemented by Levchuk et al. [71•] in a large scale validation study of feedback controlled bone remodelling. The *in silico* model was used to predict bone (re)modelling behaviour in osteopenic mice under mechanical loading with treatments of bisphosphonates or parathyroid hormone. SED was once again used to describe the local mechanical environment and BV/TV was used as the assessment variable for simulation to experimental comparison.

Similarly to Schulte et al. [8], overall errors for BV/TV prediction were low, ranging from 0.1% (combined mechanical loading and bisphosphonate treatment) to 4.5%, (control group), though again, they could not predict dynamic parameters well. Both these studies indicate the effectiveness of SED as a predictor of mechanical environment, primarily for static parameters. This “soft validation” approach of mechanical signals has provided an acceptable approach for assessing the local mechanical environment. Similar validation approaches have been used in other *in silico* models [6••], such as model behaviour aligning to fundamental (re)modelling theories of bone. Despite the progress, what remains sorely lacking, is the *in vivo* validation by direct comparison of predicted (re)modelling patterns to *in vivo* outcomes. As computational methods gain complexity and incorporate multiple scales, the fundamental challenge of aligning and validating these models becomes even more demanding.

At the organ scale, material models are usually isotropic and purely elastic; inclusion of the viscous effects [72, 73] and anisotropic effects [74] found in bone could improve such models. This can be extended to bone marrow, where comparisons between highly viscous fluid, viscoelastic solid and soft elastic solid constitutive models display different results [41]. Therefore, the correct choice of model is essential, and parameters require a comprehensive and application specific database. Of further benefit would be an ability to quantify the differences between mechanical environments determined under varying model parameters and solving approaches, i.e. linear versus non-linear solvers.

While tissue-averaged strain approaches have shown success in predicting (re)modelling, it is clear that strain and fluid stresses are amplified within the canaliculi-lacunae network, causing cells to receive stimulation in the range found to cause a biological response in *in vitro* experiments. Hence, multiscale models incorporating strains and fluid stresses on the cells themselves, based on tissues strains, could help explain the role of single cells on the (re)modelling process. These models would provide cell-specific mechanical stimuli boundary conditions to inform experimental techniques heading towards single cell analysis. However, many challenges remain. Firstly, accurate mapping of the osteocyte lacunae system, or the location of osteoblasts or osteoclasts on the bone surface, is needed for (re)modelling experiments. Secondly, coupling detailed imaging techniques with *in vivo* experiments represents a significant challenge due to destructive doses of radiation, or long imaging times [28], and a lack of techniques linking the two realms. Regardless, validation of input signals, and the model themselves, appear the biggest hurdle towards accuracy and confidence.

## Conclusion

Over the last few decades in bone systems biomechanics, substantial progress has begun to elucidate the mechanosensitive mechanisms of bone (re)modelling. Complete multiscale modelling of the mechanical environment has significant application towards understanding cellular mechanotransduction, and the resultant processes in bone. In particular, the knowledge of the exact forces and strain experienced by an individual cell, or small populations of cells can be leveraged by rapidly maturing experimental techniques. Techniques, such as laser capture micro-dissection, or imaging mass spectroscopy, that can gather molecular information from small populations of cells, can be coupled with inter- and intracellular downstream simulations converting the mechanical local in vivo environment to direct mechanical transduction within the cell. Combining multiscale models, from organ level to protein and molecular responses, with experimental data, will allow the establishment of a continuum of knowledge from organ-scale to protein expression. This will foster progress towards understanding of the effects mechanics has on bone tissue, allowing accurate characterisation of the molecular pathways and processes involved in (re)modelling, repair and growth.

## References

Papers of particular interest, published recently, have been highlighted as: • Of importance ••

Of major importance

1. Yuan Y, Chen X, Zhang L, Wu J, Guo J, Zou D, et al. The roles of exercise in bone remodeling and in prevention and treatment of osteoporosis. *Prog Biophys Mol Biol.* 2016;122(2):122–30.
2. Roux W. *Der Kampf der Theile im Oranismus: Ein Beitrag zur verollständigung der mechanischen Zweckmässigkeitstheorie.* Leipzig: W. Engelmann; 1881.
3. Wolff J. *Das Gesetz der Transformation der Knochen.* Hirschwald. 1893 Nov;19(47):1222–4.
4. Christen P, Müller R. In vivo visualisation and quantification of bone resorption and bone formation from time-lapse imaging. *Curr Osteoporos Rep.* 2017;15(4):311–7.
5. •• Birkhold AI, Razi H, Weinkamer R, Duda GN, Checa S, Willie BM. Monitoring in vivo (re)modeling: a computational approach using 4D microCT data to quantify bone surface movements. *Bone.* 2015;75:210–21. **This paper covers the key tools for providing temporal and spatial information essential for development of geometries for computational models at the organ to tissue scale and longitudinal analysis for validation of remodelling simulations.**
6. •• Kameo Y, Adachi T. Interstitial fluid flow in canaliculi as a mechanical stimulus for cancellous bone remodeling: in silico validation. *Biomech Model Mechanobiol.* 2014;13(4):851–60. **This paper provides a good example of an implementation of a poroelastic micro-FE simulation used to model the remodelling process coupled with an in silico validation.**
7. Vaughan TJ, Verbruggen SW, McNamara LM. Are all osteocytes equal? Multiscale modelling of cortical bone to characterise the mechanical stimulation of osteocytes. *Int J Numer Method Biomed Eng.* 2013;29(12):1361–72.
8. Schulte FA, Zwahlen A, Lambers FM, Kuhn G, Ruffoni D, Betts D, et al. Strain-adaptive in silico modeling of bone adaptation—a computer simulation validated by in vivo micro-computed tomography data. *Bone.* 2013;52(1):485–92.
9. Willie BM, Birkhold AI, Razi H, Thiele T, Aido M, Kruck B, et al. Diminished response to in vivo mechanical loading in trabecular and not cortical bone in adulthood of female

- C57Bl/6 mice coincides with a reduction in deformation to load. *Bone*. 2013;55(2):335–46.
10. Schulte FA, Ruffoni D, Lambers FM, Christen D, Webster DJ, Kuhn G, et al. Local mechanical stimuli regulate bone formation and resorption in mice at the tissue level. *PLoS One*. 2013;8(4):e62172.
  11. Scheiner S, Pivonka P, Hellmich C. Coupling systems biology with multiscale mechanics, for computer simulations of bone remodeling. *Comput Methods Appl Mech Eng*. 2013;254:181–96.
  12. Knothe Tate ML, Gunning PW, Sansalone V. Emergence of form from function – mechanical engineering approaches to probe the role of stem cell mechanoadaptation in sealing cell fate. *BioArchitecture*. 2016 Sep 2;6(5):85–103.
  13. Wang JW, Lu DY, Mao DB, Long M. Mechanomics: an emerging field between biology and biomechanics. *Protein Cell*. 2014;5(7):518–31.
  14. Trussel A, Müller R, Webster D. Toward mechanical systems biology in bone. *Ann Biomed Eng*. 2012;40(11):2475–87.
  15. Scheuren A, Wehrle E, Flohr F, Müller R. Bone mechanobiology in mice: toward single-cell in vivo mechanomics. *Biomech Model Mechanobiol*. 2017 Dec 1;16(6).
  16. Nichterwitz S, Chen G, Benitez JA, Yilmaz M, Storrval H, Cao M, et al. Laser capture microscopy coupled with smart-seq2 for precise spatial transcriptomic profiling. *Nat Commun*. 2016 Jul 8;7:12139.
  17. Trüssel AJ. Spatial mapping and high throughput microfluidic gene expression analysis of osteocytes in mechanically controlled bone remodeling. 2015 (Doctoral dissertation, ETH Zurich).
  18. Rho JY, Kuhn-Spearing L, Zioupos P. Mechanical properties and the hierarchical structure of bone. *Med Eng Phys*. 1998;20(2):92–102.
  19. Dermience M, Lognay G, Mathieu F, Goyens P. Effects of thirty elements on bone metabolism. *J Trace Elem Med Biol*. 2015;32:86–106.
  20. Bonewald LF. The amazing osteocyte. *J Bone Miner Res*. 2011;26(2):229–38.
  21. Vaughan T, Haugh M, McNamara L. A fluid-structure interaction model to characterize bone cell stimulation in parallel-plate flow chamber systems. *J R Soc Interface*. 2013;10(81):20120900.

22. Lambers FM, Kuhn G, Weigt C, Koch KM, Schulte FA, Müller R. Bone adaptation to cyclic loading in murine caudal vertebrae is maintained with age and directly correlated to the local micromechanical environment. *J Biomech.* 2015;48(6):1179–87.
23. Metzger TA, Schwaner SA, LaNeve AJ, Kreipke TC, Niebur GL. Pressure and shear stress in trabecular bone marrow during whole bone loading. *J Biomech.* 2015;48(12):3035–43.
24. • Lerebours C, Buenzli PR, Scheiner S, Pivonka P. A multiscale mechanobiological model of bone remodelling predicts site-specific bone loss in the femur during osteoporosis and mechanical disuse. *Biomech Model Mechanobiol.* 2016;15(1):43–67. This paper provides an alternative approach to the standard finite element approach for calculating the mechanical environment, using analytical or semi-analytical methods to model the local mechanical environment.
25. •• Verbruggen SW, Vaughan TJ, McNamara LM. Fluid flow in the osteocyte mechanical environment: a fluid-structure interaction approach. *Biomech Model Mechanobiol.* 2014;13(1):85–97. This paper provides an excellent example of coupling fluid and structural mechanics within the cell scale, indicating the importance of a combined structural/fluid approach within bone tissue.
26. Jahani M, Genever PG, Patton RJ, Ahwal F, Fagan MJ. The effect of osteocyte apoptosis on signalling in the osteocyte and bone lining cell network: a computer simulation. *J Biomech.* 2012;45(16):2876–83.
27. Verbruggen SW, Vaughan TJ, McNamara LM. Strain amplification in bone mechanobiology: a computational investigation of the in vivo mechanics of osteocytes. *J R Soc Interface.* 2012;9(75):2735–44.
28. Mader KS, Schneider P, Müller R, Stambanoni M. A quantitative framework for the 3D characterization of the osteocyte lacunar system. *Bone.* 2013;57(1):142–54.
29. Cresswell EN, Nguyen TM, Horsfield MW, Alepuz AJ, Metzger TA, Niebur GL, et al. Mechanically induced bone formation is not sensitive to local osteocyte density in rat vertebral cancellous bone. *J Orthop Res.* 2018 Feb;36(2):672–81.
30. Buenzli PR, Sims NA. Quantifying the osteocyte network in the human skeleton. *Bone.* 2015;75:144–50.
31. Webster DJ, Morley PL, van Lenthe GH, Müller R. A novel in vivo mouse model for mechanically stimulated bone adaptation—a combined experimental and computational validation study. *Comput Methods Biomech Biomed Engin.* 2008;11(5):435–41.

- 
32. Lambers FM, Koch K, Kuhn G, Ruffoni D, Weigt C, Schulte FA, et al. Trabecular bone adapts to long-term cyclic loading by increasing stiffness and normalization of dynamic morphometric rates. *Bone*. 2013;55(2):325–34.
  33. Lambers FM, Stuker F, Weigt C, Kuhn G, Koch K, Schulte FA, et al. Longitudinal in vivo imaging of bone formation and resorption using fluorescence molecular tomography. *Bone*. 2013;52(2):587–95.
  34. Cresswell E, Goff M, Nguyen T, Lee W, Hernandez C. Spatial relationships between bone formation and mechanical stress within cancellous bone. Elsevier; 2016 Jan 25;49(2):222–8.
  35. Vanrietbergen B, Weinans H, Huiskes R, Odgaard A. A new method to determine trabecular bone elastic properties and loading using micromechanical finite-element models. *J Biomech*. 1995;28(1):69–81.
  36. Huiskes R. If bone is the answer, then what is the question? *J Anat*. 2000;197:145–56.
  37. Kameo Y, Adachi T. Modeling trabecular bone adaptation to local bending load regulated by mechanosensing osteocytes. *Acta Mech*. 2014;225(10):2833–40.
  38. Pereira AF, Javaheri B, Pitsillides AA, Shefelbine SJ. Predicting cortical bone adaptation to axial loading in the mouse tibia. *J R Soc Interface*. 2015 Sep 6;12(110):20150590.
  39. Tiwari AK, Prasad J. Computer modelling of bone's adaptation: the role of normal strain, shear strain and fluid flow. *Biomech Model Mechanobiol*. 2017;16(2):395–410.
  40. Webster D, Schulte FA, Lambers FM, Kuhn G, Wuller R. Strain energy density gradients in bone marrow predict osteoblast and osteoclast activity: a finite element study. *J Biomech*. 2015;48(5):866–74.
  41. Metzger TA, Niebur GL. Comparison of solid and fluid constitutive models of bone marrow during trabecular bone compression. *J Biomech*. 2016;49(14):3596–601.
  42. • Metzger TA, Kreipke TC, Vaughan TJ, McNamara LM, Niebur GL. The in situ mechanics of trabecular bone marrow: the potential for mechanobiological response. *J Biomech Eng*. 2015 Jan 1;137(1):011006. **This paper provides thorough investigation into the mechanics of bone marrow, providing an approach for the investigation into the mechano-response of cells on the surface of the bone tissue and within the marrow.**



43. Scheiner S, Pivonka P, Hellmich C. Poromechanical stimulation of bone remodeling: a continuum micromechanics-based mathematical model and experimental validation. *Fifth Biot Conference on Poromechanics 2013*. p. 1867–76.
44. Hellmich C, Kober C, Erdmann B. Micromechanics-based conversion of CT data into anisotropic elasticity tensors, applied to FE simulations of a mandible. *Ann Biomed Eng*. 2008;36(1):108–22.
45. You LD, Weinbaum S, Cowin SC, Schaffler MB. Ultrastructure of the osteocyte process and its pericellular matrix. *Anat Rec A Discov Mol Cell Evol Biol*. 2004;278a(2):505–13.
46. Anderson EJ, Tate MLK. Idealization of pericellular fluid space geometry and dimension results in a profound underprediction of nano-microscale stresses imparted by fluid drag on osteocytes. *J Biomech*. 2008;41(8):1736–46.
47. Bonivitch AR, Bonewald LF, Nicoletta DP. Tissue strain amplification at the osteocyte lacuna: a microstructural finite element analysis. *J Biomech*. 2007;40(10):2199–206.
48. Wang LP, Dong JH, Xian CJ. Strain amplification analysis of an osteocyte under static and cyclic loading: a finite element study. *Biomed Res Int*. 2015;2015.
49. Kamioka H, Kameo Y, Imai Y, Bakker AD, Bacabac RG, Yamada N, et al. Microscale fluid flow analysis in a human osteocyte canaliculus using a realistic high-resolution image-based three-dimensional model. *Integr Biol*. 2012;4(10):1198–206.
50. Schwartz MA. Integrins and extracellular matrix in mechanotransduction. *Cold Spring Harb Perspect Biol*. 2010 Dec 1;2(12):a005066.
51. Campbell ID, Humphries MJ. Integrin structure, activation, and interactions. *Cold Spring Harb Perspect Biol*. 2011 Mar 1;3(3):a004994.
52. Tzima E, del Pozo MA, Shattil SJ, Chien S, Schwartz MA. Activation of integrins in endothelial cells by fluid shear stress mediates Rho-dependent cytoskeletal alignment. *EMBO J*. 2001;20(17):4639–47.
53. Geiger B, Spatz JP, Bershadsky AD. Environmental sensing through focal adhesions. *Nat Rev Mol Cell Biol*. 2009;10(1):21–33.
54. Luo TZ, Mohan K, Iglesias PA, Robinson DN. Molecular mechanisms of cellular mechanosensing. *Nat Mater*. 2013;12(11):1063–70.
55. Nguyen AM, Jacobs CR. Emerging role of primary cilia as mechanosensors in osteocytes. *Bone*. 2013;54(2):196–204.

56. Delling M, Indzhykulian AA, Liu X, Li Y, Xie T, Corey DP, et al. Primary cilia are not calcium-responsive mechanosensors. *Nature*. 2016;531(7596):656–60.
57. Walker LM, Publicover SJ, Preston MR, Ahmed MAAS, El Haj AJ. Calcium-channel activation and matrix protein upregulation in bone cells in response to mechanical strain. *J Cell Biochem*. 2000;79(4):648–61.
58. Dror RO, Dirks RM, Grossman JP, Xu HF, Shaw DE. Biomolecular simulation: a computational microscope for molecular biology. *Annu Rev Biophys*. 2012;41:429–52.
59. Jing D, Baik AD, Lu XL, Zhou B, Lai XH, Wang LY, et al. In situ intracellular calcium oscillations in osteocytes in intact mouse long bones under dynamic mechanical loading. *FASEB J*. 2014;28(4):1582–92.
60. Lewis KJ, Frikha-Benayed D, Louie J, Stephen S, Spray DC, Thi MM, et al. Osteocyte calcium signals encode strain magnitude and loading frequency in vivo. *Proc Natl Acad Sci U S A*. 2017;114(44):11775–80.
61. Ridha H, Almitani KH, Chamekh A, Toumi H, Tavares JMRS. A theory for bone resorption based on the local rupture of osteocytes cells connections: a finite element study. *Math Biosci*. 2015;262:46–55.
62. Frost HM. Bone mass and the mechanostat—a proposal. *Anat Rec*. 1987;219(1):1–9.
63. Pivonka P, Buenzli PR, Scheiner S, Hellmich C, Dunstan CR. The influence of bone surface availability in bone remodelling—a mathematical model including coupled geometrical and biomechanical regulations of bone cells. *Eng Struct*. 2013;47:134–47.
64. Grimal Q, Raum K, Gerisch A, Laugier P. A determination of the minimum sizes of representative volume elements for the prediction of cortical bone elastic properties. *Biomech Model Mechanobiol*. 2011;10(6):925–37.
65. Erdemira A, Guess TM, Halloran J, Tadepalli SC, Morrison TM. Considerations for reporting finite element analysis studies in biomechanics. *J Biomech*. 2012;45(4):625–33.
66. Jasiuk I. Micromechanics of bone modeled as a composite material. In: Meguid SAaW, George J, (Eds.), *Micromechanics and nanomechanics of composite solids*. Springer, Cham. 2018. p. 281–306.
67. Nicolella DP, Moravits DE, Gale AM, Bonewald LF, Lankford J. Osteocyte lacunae tissue strain in cortical bone. *J Biomech*. 2006;39(9):1735–43.

68. Begonia M, Dallas M, Johnson ML, Thiagarajan G. Comparison of strain measurement in the mouse forearm using subject-specific finite element models, strain gaging. *Biomech Model Mechanobiol.* 2017;16(4):1243–53.
69. Begonia MT, Dallas M, Vizcarra B, Liu Y, Johnson ML, Thiagarajan G. Non-contact strain measurement in the mouse forearm loading model using digital image correlation (DIC). *Bone.* 2015;81:593–601.
70. Weinans H, Huiskes R, Grootenboer HJ. The behavior of adaptive bone-remodeling simulation models. *J Biomech.* 1992;25(12):1425–41.
71. • Levchuk A, Zwahlen A, Weigt C, Lambers FM, Badilatti SD, Schulte FA, et al. The clinical biomechanics award 2012—presented by the European Society of Biomechanics: large scale simulations of trabecular bone adaptation to loading and treatment. *Clin Biomech.* 2014;29(4):355–62. **This paper provides an extensive validation of organ and tissue scale models, showing their effectiveness for predictive static parameters and indicating the opportunity for better prediction of dynamic parameters.**
72. Manda K, Wallace RJ, Xie SQ, Levrero-Florencio F, Pankaj P. Nonlinear viscoelastic characterization of bovine trabecular bone. *Biomech Model Mechanobiol.* 2017;16(1):173–89.
73. Xie SQ, Manda K, Wallace RJ, Levrero-Florencio F, Simpson AHRW, Pankaj P. Time dependent behaviour of trabecular bone at multiple load levels. *Ann Biomed Eng.* 2017;45(5):1219–26.
74. Fan Z, Swadener JG, Rho JY, Roy ME, Pharr GM. Anisotropic properties of human tibial cortical bone as measured by nanoindentation. *J Orthop Res.* 2002;20(4):806–10.

## Funding

This work has been supported by the European Union (ERC Advanced MechAGE, ERC-2016-ADG-741883; Marie-Curie-COFUND CaP+MECHLOAD, WHRI-ACADEMY-608765).



## **Chapter 3 :**

# **Approaches to determine organ-scale individualised physiological and extra-physiological loading in mice**

# Determination of organ-scale boundary conditions in bones of individual mice in a fracture-healing model

Graeme R Paul<sup>1</sup>, Esther Wehrle<sup>1</sup>, Jianhua Zhang<sup>1</sup>, Gisela A. Kuhn<sup>1</sup>, Ralph Müller<sup>1</sup>

1. Institute for Biomechanics, ETH Zurich, Zurich, Switzerland

## Abstract

Mechanical loading has been shown to play a significant role in the healing of fractures. However, measuring the exact mechanical loading within a defect is challenging, and has not yet been achieved in mice. We developed an instrumented fixator capable of measuring deformation within the external fixation in a mouse model of defect healing. The measurements obtained with this device allowed us to determine the habitual loading applied by the mouse itself to the defect prior to bridging. Using these measurements, we show that habitual loading in percentage bodyweight is strongly and significantly correlated with the outcome of the fracture healing process, assessed via micro-finite element analysis, in the five weeks post measurement. We further demonstrate that habitual loading alone accounts for 64% of the variance in bone stiffness at week 3, where defects in all but two mice were bridged. These two mice formed non-union fractures and displayed substantially lower and higher mechanical loading than the rest of the group, aligning with current literature on the mechanical causes of non-union fractures.

## Keywords:

Bone, fracture healing, habitual loading, prediction, defect healing

## Introduction

Fracture healing is driven by biological and mechanical factors<sup>1-10</sup>. Mechanical factors arise from several sources, such as habitual loading in combination with fixation stiffness. As a result, many authors have investigated the effects of inter-fragmentary movement within a fracture<sup>11-14</sup>, musculoskeletal loading of a fracture<sup>15,16</sup> and fracture fixation on fracture healing<sup>1,13,16</sup>. These studies have concluded that either too little or too much strain impairs healing, either lengthening the process or leading to the formation of non-unions. Hence, it is clear that a specific “mechanical dose” of strain exists within the defect during the fracture healing process. This mechanical dose allows for optimal fracture healing, leading to reduced healing time and the best outcome in terms of strength and structure<sup>17</sup>.

The fracture healing process can be broken down into three overlapping phases: the inflammation phase begins immediately after fracture with the formation of a haematoma and the laying down of soft granulation tissue. This phase attracts and recruits cells and resources, and gives way to the development of soft bone in the reparative phase. Soft bone eventually forms a bridge across the fracture gap, providing structural support and transferring the mechanical load from highly deformed soft tissue to stiffer bone. The soft, lowly mineralised bony tissue, which has bridged the fracture gap, usually occupies a far greater volume than what is mechanically required of the bone once healing is complete. As the tissue mineralises, excess bone tissue is resorbed in the final remodelling phase. This process has been extensively assessed using micro-computed tomography (micro-CT) in mice<sup>18,19</sup> or rats<sup>20,21</sup>. Micro-CT imaging allows for longitudinal *in vivo* scanning of the fracture region and can hence be used to assess the full fracture healing process. Many attempts have been made to control the level of strain within the tissue throughout all phases of healing. These methods range from direct, such as direct actuation via implants (see chapter 3.2 and 4.2), to indirect loading, such as vibration<sup>22,23</sup> or changing the fixation stiffness<sup>4,12,13,16</sup>. Understanding the habitual mechanical stimulation during the fracture healing process has the potential to guide such approaches and lead to the development of mechanical dosing protocols for optimal healing. Of particular clinical interest is the effect of mechanical stimulation on non-union fractures, which are characterised by maladaptive healing and insufficient structural integrity of the bone. Comprising roughly 5% of cases<sup>24</sup>, these fractures largely result from too much inter-fragmentary movement within the defect<sup>25</sup> and pose a substantial clinical challenge. Timely

interventions to correct insufficient or excessive mechanical stimulation in non-unions may lead to their prevention and treatment.

Numerous attempts have been made to infer habitual loading in mice or rats *in vivo*. Force plates<sup>26-30</sup>, instrumented fixation<sup>15,16,31</sup> and musculoskeletal modelling<sup>32,33</sup> have been used to calculate loading in the hind limb during locomotion. In particular, Wehner et al.<sup>16</sup> and Klosterhoff et al.<sup>15</sup> both applied deformation measurement technologies, in the form of strain gauges on external fixators, to measure the habitually induced loading on the femur during locomotion in rats. By observing changes in fixator loading, Wehner et al.<sup>16</sup> tracked the healing progression of the fracture and quantified the changes in healing time and reparative phase duration. Klosterhoff et al.<sup>15</sup> observed that strain amplitude was predictive of bone volume both three and seven weeks after measurement. Additionally, strain amplitudes measured at week 1 were predictive of failure torques at the end of the of the eight-week study. While the conclusions of these studies focused on two different outcomes, both indicate that habitual loading is an important component in understanding the fracture healing progression.

In this study, we implemented an instrumented external fixation in a femoral defect mouse model and tracked habitual loading throughout the study duration. By combining this information with longitudinal micro-CT tracking of the fracture healing progression, we linked habitual loading behaviour prior to bone formation with healing outcome. Additionally, we investigated whether the mechanical environment explains the variance within the fracture healing progression. Specifically, we hypothesised that pre-bridging loading would predict the healing outcome.



## Materials and Methods

### *Study Design*

To investigate the effect of self-induced mechanical loading on fracture healing, twelve mice were osteotomised. The osteotomy was fixated using an external fixator. To measure strains within the external fixator, the side bars were swapped out with custom-made strain-gauged side bars. Force and displacement values in the defect region of the femur could be inferred via calibration. These values were correlated with fracture progression, assessed by the stiffness of a micro-finite element (micro-FE) simulation derived from weekly micro-CT measurements. Using these displacement values as boundary conditions, the mechanical environment within the soft tissue of the osteotomy was inferred.

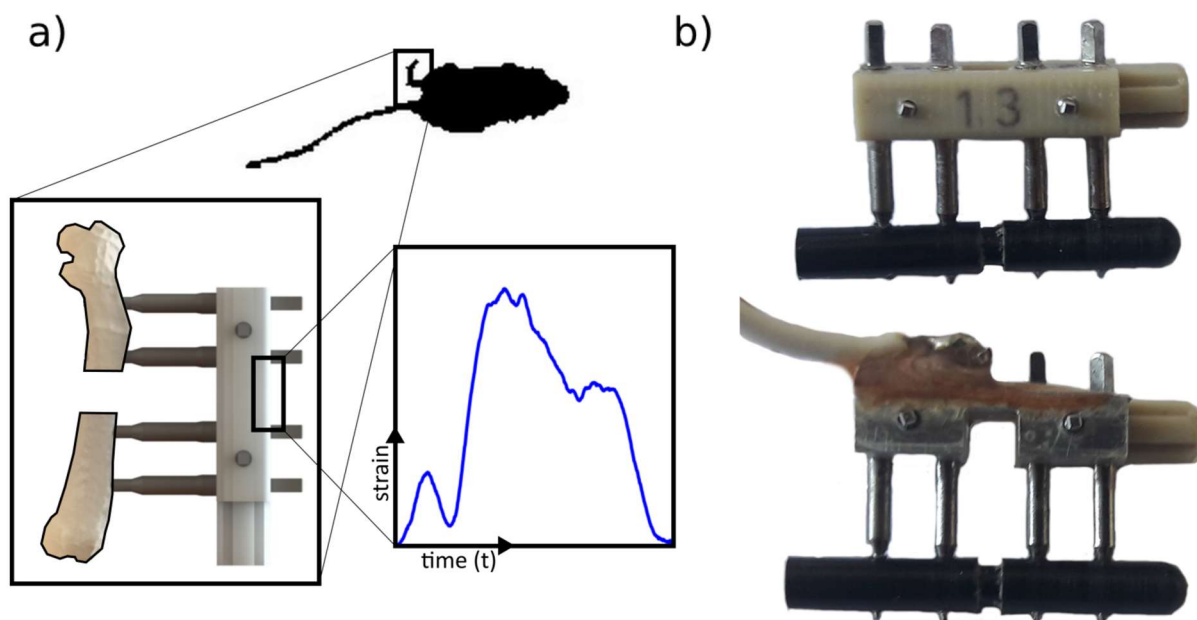


**Figure 3.1:** Example and locations of a strain-gauged instrumented fixator. a) The right femur of the mouse was stabilised with an external fixator with removable side bars. Upon deformation, the strains within the external fixator were recorded. b) The removable PEEK side bars were replaced with aluminium side bars, one of which was strain-gauged and tethered to the data acquisition system.

### *Animals*

All animal procedures were approved by the local authorities (licence number: 181/2015 Kantonales Veterinäramt Zürich, Zurich, Switzerland) and all methods were carried out in accordance with the relevant regulations and guidelines (ARRIVE guidelines and Swiss Animal

Welfare Act and Ordinance (TSchG, TSchV)). The study group consisted of twelve female C57BL/6L (JANVIER, Saint Berthevin Cedex, France) mice, which were acquired at 12 weeks of age and underwent surgery at 20 weeks. The mice were housed in the ETH Phenomics Centre (EPIC; 12h:12h light-dark cycle, maintenance feed (3437, KLIBA NAFAG, Kaiseraugst, Switzerland), 5 animals/cage prior to surgery, 2-3 animals/cage after surgery) for 8 weeks prior to surgery. Perioperative analgesia (25 mg/L, Tramal®, Gruenthal GmbH, Aachen, Germany) was provided via the drinking water from two days before surgery until the third day after surgery. All surgery and scanning occurred under anaesthesia (initiation 5%, continuous 2% isoflurane/oxygen). All animals were osteotomised on the right femur with a 0.66mm Gigli wire and were fixated using an external fixator (Mouse ExFix, RISystem, Davos, Switzerland; stiffness  $13.7 \pm 2.4$  N/mm) by the same veterinarian. A detailed description of the surgery process is provided elsewhere<sup>18</sup>.

To measure strain in the defect during locomotion, a mouse was anaesthetised (initiation 5%, continuous 2% isoflurane/oxygen), the lateral fixator side bar was replaced with the instrumented side bar, and the medial side bar was replaced with a blank aluminium bar. The mouse was taken to the CatWalk (Noldus, Wageningen, the Netherlands) and, once awake, placed on the walkway. Mice were allowed to move freely along the length of the CatWalk (~1 m) until three good runs were recorded. This was performed under direct supervision, with researchers ensuring that the tether did not affect the mouse gait or obstruct the mouse's movement. Once sufficient data was acquired, the mouse was anaesthetised and the PEEK side bars were replaced on the fixator. The mouse was then micro-CT scanned.

#### *Measurement of strain in the defect*

Strain gauges (L2A-13-015LW-120, Vishay-Micromeritics, Wendell, USA) were attached to aluminium side bars with epoxy (M-BOND AE-10, Vishay-Micromeritics, Wendell, USA). Strains within the tethered aluminium side bar were captured during mouse locomotion along a CatWalk. A National Instruments cDAQ (NI-9235, 8 ch, 120 ohm quarter-bridge, 24-bit, 10 kS/s/ch C Series Bridge/Strain Input Module and cDAQ-9171 chassis, National Instruments, Austin, Texas, USA) was used to power the strain gauge in a Wheatstone bridge configuration with dummy resistors. Custom LabVIEW software was used to run the NI cDAQ instrumentation, capture the resultant signal from the strain gauge, and read out files. Further signal processing was performed in Python<sup>34</sup>. Each run was manually assessed (aided by time-stamped video recordings) and the most consistent run (i.e. the run in which the mouse

paused the least and ran continuously from one side of the CatWalk to the other) was selected and extracted. Signal peaks and troughs were identified automatically. Peaks with a prominence of less than half the maximum signal height were discarded to ensure capture of a full foot strike movement. The relative strain amplitude was calculated from the difference between each peak-trough pair and the median of the set was used in further analysis. The strain-gauged aluminium bars were calibrated for both force in an empty defect region and displacement in the defect region. Calibration was performed by uniaxial tests on a Zwick compression tester (ZwickRoell, Ulm, Germany) from 0 N to 1 N using a 10 N load cell. The force-calibrated foot strike amplitude was normalised by mouse body weight to obtain a percentage body weight measurement. Measurement began at week 1 and continued weekly until week 7 on the same day as the micro-CT scanning.

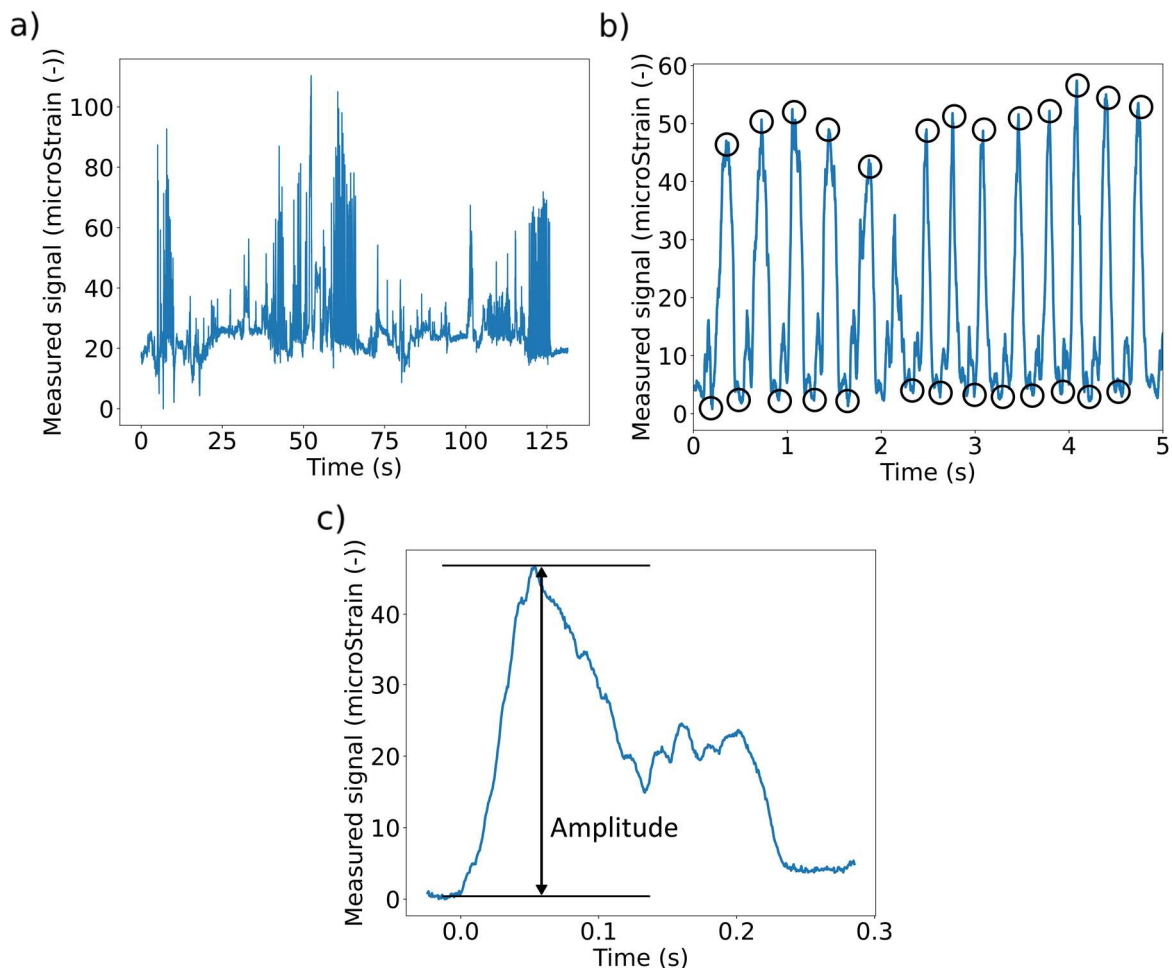


**Figure 3.2:** Signal processing. a) The raw signal, which contained many non-locomotion specific artefacts, was time-stamped to a video feed to ensure that locomotion across the CatWalk was correctly identified. b) The most consistent burst was chosen for analysis. Peak-

*trough pairs were identified algorithmically and required peak prominence of at least half the maximum height of the largest peak-trough difference. c) The peak-to-peak amplitude of each foot strike was analysed.*

#### *Imaging, pre-processing and multi-density finite element analysis*

Imaging was performed on a vivaCT 40 micro-CT scanner (Scanco Medical, Brüttisellen, Switzerland) with a nominal resolution of 10.5  $\mu\text{m}$ . The scanned region required two stacks of 211 voxels each, and had an imaging time of 15 minutes (55 kVp, 145  $\mu\text{A}$ , 350 ms integration time, 500 projections per 180°, 21 mm field of view (FOV), aluminium filter to prevent beam hardening). All animals were scanned weekly from day 0 (post operation) until week 7. Pre-processing entailed the extraction of the relevant subvolume (to a dimension of 180 voxels), Gaussian filtering ( $\sigma = 1.2$ , support = 1) and binning grey values using a multi-density approach<sup>35</sup>. The binned greyscale values were converted from density ( $\text{mg HA}/\text{cm}^3$ ) to Young's moduli (GPa), on a per voxel basis, from 395  $\text{mg HA}/\text{cm}^3$  to 720  $\text{mg HA}/\text{cm}^3$  in steps of 25  $\text{mg HA}/\text{cm}^3$ , corresponding to 4.045 GPa to 12.170 GPa with steps of 0.626 GPa, respectively. Regions of soft tissue were set to a Young's modulus of 0.003 GPa<sup>6</sup> and the marrow cavity of the femur was capped with a plate of 20 GPa, preventing edge effects due to the soft tissue found lying on the top slice of the finite element mesh. To ensure that boundary conditions were consistently applied, longitudinal images were registered to one another prior to the multi-density conversion process. A linear micro-FE solver, ParOSol<sup>36</sup>, was used to simulate the stiffness of the volume of interest by applying 1% uniaxial compression to the top slice of the volume while fixing the bottom slice. The stiffness of the fracture callus was determined by dividing the sum of the vertical resultant force from each node of the uppermost plane of the mesh with the displacement boundary condition distance, giving a stiffness value for the region of interest (in N/mm). Mouse 4 was excluded from correlations and statistical models due to substantial bone fragments within the defect, leading to abnormal stiffness results. To determine the mechanical environment, similar simulation were run using the displacement values of measured boundary conditions (see supplementary material, table 3) on the top slice instead of a 1% uniaxial compression. The strains within the soft tissue of the osteotomy gap were then extracted using the masking approach outlined by Tourolle et al.<sup>35</sup> and all zero strains were removed.

*Statistics*

A Schapiro-Wilk test indicated that both the stiffness progression data and the mechanical loading data were not normally distributed. Therefore, we computed the relationship between these two variables using Spearman's correlation. We performed a linear regression of habitual loading at week 1 against fracture stiffness at week 2 to week 7. All tests were performed using SciPy Stats<sup>34</sup>.

## Results

We combined weekly habitual loading measurements using an instrumented fixator (**Figure 3.1a and b, Figure 3.2**) with weekly micro-CT measurements (**Figure 3.3**) to track the relationship between habitual loading and fracture progression in twelve mice in a femoral defect model. Micro-FE analysis was performed based on micro-CT images to calculate the stiffness of the volume of interest throughout the duration of the study (seven weeks). We assessed correlations and predictive relationships between pre-bone formation loading and the longitudinal progression of the fracture healing process. Additionally, we used the measured displacements as boundary conditions to simulate the soft tissue strains within the osteotomy at week 1.

Example of a union fracture's healing progression



Example of a non-union fracture's healing progression

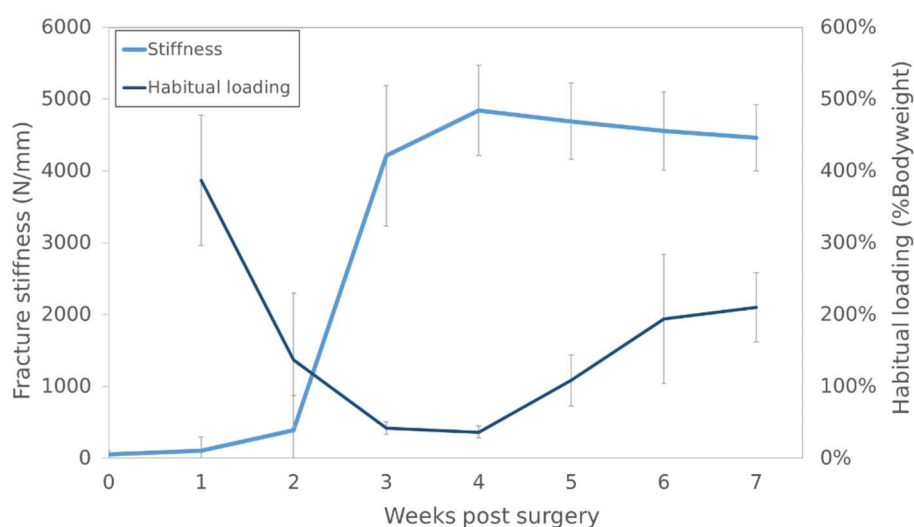


**Figure 3.3:** Examples of union and non-union healing progression up to seven weeks post surgery. Bridging occurred at week 3 for all but the two non-union mice.

### *Fracture healing and habitual loading progression*

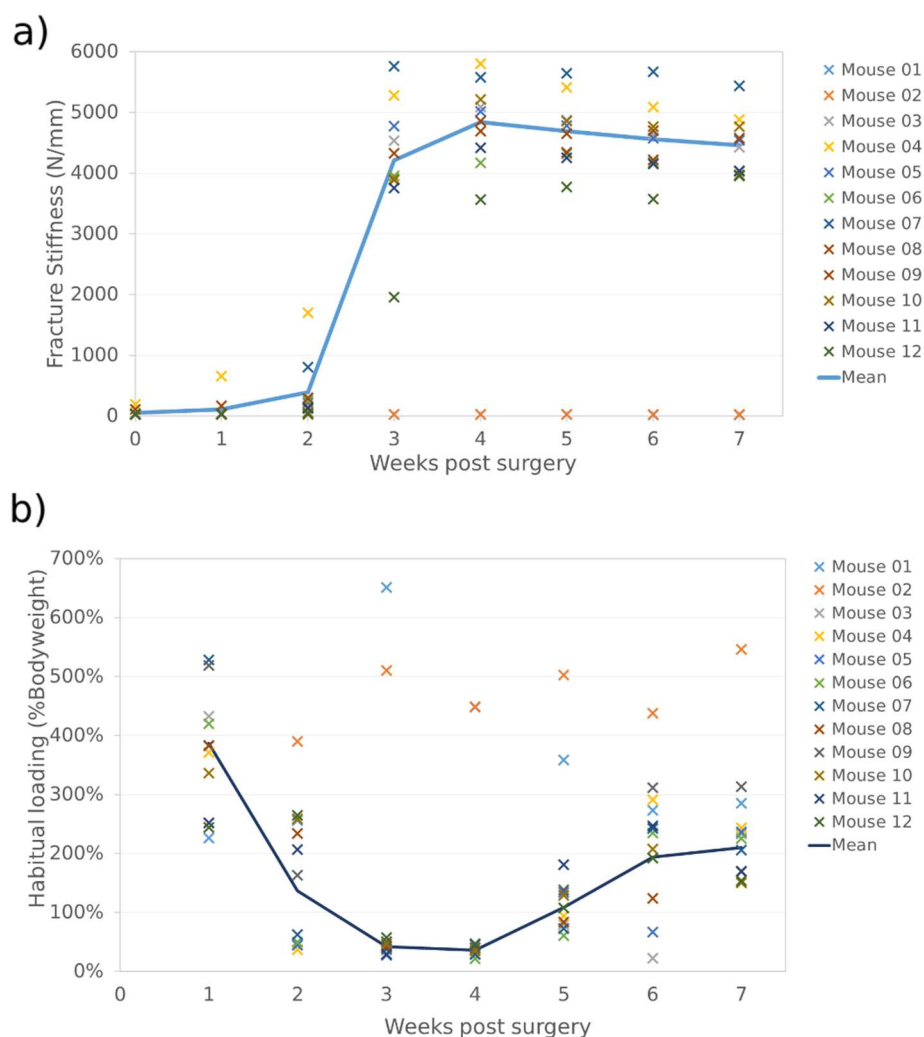
The results of the micro-FE simulation displayed a stiffness progression (**Figure 3.4**) typical of fracture healing for ten of the twelve mice. Specifically, callous stiffness rose quickly between weeks 2 (group mean  $395 \pm 481$  N/mm) and 3 (group mean  $4213 \pm 976$  N/mm) to a peak stiffness at week 4 (group mean  $4842 \pm 631$  N/mm), indicating that new bone tissue was laid down and the fracture had bridged. After week 4, a slight decrease was observed until the end of the experiment at week 7 (group mean  $4463 \pm 458$  N/mm); this corresponds to the removal of structurally unnecessary bone tissue, converging on an optimised structure. In turn, the habitual loading followed an inverted pattern, with measurements decreasing from weeks 1 to 21 (group mean  $387 \pm 91\%$  to  $137 \pm 93\%$ ), corresponding to bone formation observed in the micro-CT

images (as demonstrated in **Figure 3.3**). The lowest level of habitual loading was observed at week 4, corresponding to the highest stiffness.



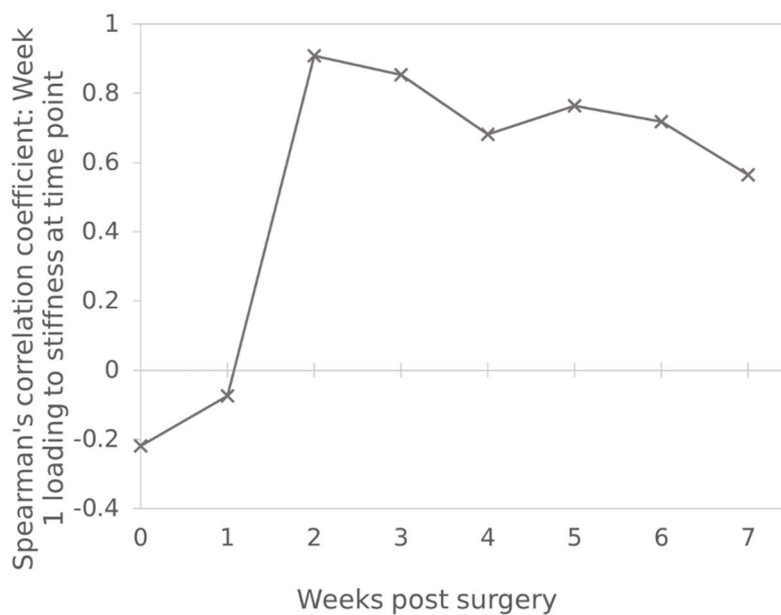
**Figure 3.4:** Group habitual loading and fracture stiffness over seven weeks. Fracture stiffness followed a sigmoidal shape, with maximum stiffness reached at week 4. Habitual loading, in %bodyweight, followed an inverse pattern. As fracture stiffness increased, more force was transferred through the stiff bone and less through the fixator. Post week 4, the mice applied greater loading to the system as a whole and fracture stiffness decreased, with more force being transferred through the fixator.

On an individualised basis (**Figure 3.5**) a large range of values was observed at week 1. However, amongst the mice that bridged, the range of habitual loading values was small once bridging occurred. As the remodelling of the callus was underway, the habitual loading levels diverged, such that at week 7 several mice applied a load of roughly half their habitual load at week 1.



**Figure 3.5:** Individualised fracture stiffness and habitual loading progressions. *a)* Most mice display a sigmoidal healing progression. Mouse 04 and mouse 07 display better healing results than the rest of the group, while mouse 01 and mouse 02 did not bridge and displayed the stiffness progression typical of non-union fractures. *b)* These results are mimicked (but inverted) in habitual loading. Note the great range of habitual loading values displayed by mouse 01 and mouse 02, which differs from that in the union mice.



*Correlation and prediction of healing progression from habitual loading*

**Figure 3.6:** Correlations between habitual loading at week 1 and fracture stiffness at week 0 to week 7.

Habitual loading at week one displayed a significant correlation with stiffness from week 2 until week 6 (week 2:  $\text{corr} = 0.91$ ,  $p = 0.00013$ ; week 3:  $\text{corr} = 0.85$ ,  $p = 0.00081$ ; week 4:  $\text{corr} = 0.68$ ,  $p = 0.021$ ; week 5:  $\text{corr} = 0.76$ ,  $p = 0.006$ ; week 6:  $\text{corr} = 0.72$ ,  $p = 0.013$ ) (**Figure 3.6**). A non-significant relationship was observed between habitual loading at week 1 and stiffness at week 7 ( $\text{corr} = 0.56$ ,  $p = 0.071$ ). Habitual loading at week 1 was neither correlated with stiffness at week 1 ( $\text{corr} = -0.073$ ,  $p = 0.83$ ), nor with stiffness at week 0 ( $\text{corr} = -0.218$ ,  $p = 0.52$ ).

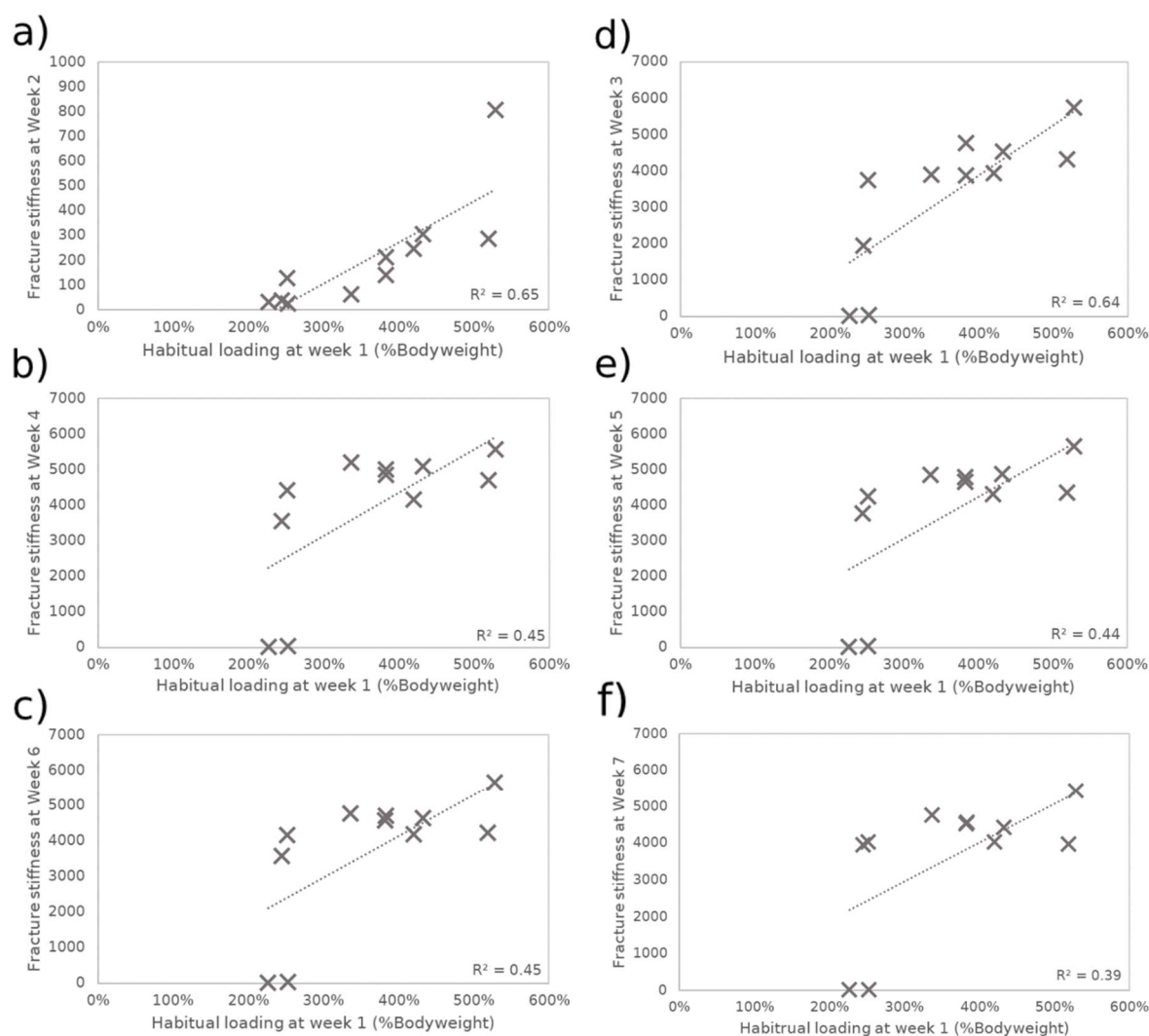


**Figure 3.7:** Habitual loading as a predictive factor in a linear regression model. Habitual loading most strongly predicted fracture stiffness at week 2, with the effect size decreasing as time progressed.

In addition to the significant correlations between fracture stiffness progression and habitual loading, habitual loading at week 1 was a strong predictor of the outcome of the fracture stiffness progression (**Figure 3.7**). Habitual loading at week 1 was a better predictor of the stiffness at week 2 ( $R^2 = 0.65$ ) and week 3 ( $R^2 = 0.64$ ) than at the following time points (weeks 4 and 6:  $R^2 = 0.45$ ; week 5:  $R^2 = 0.44$ ; week 7:  $R^2 = 0.39$ ).

Fracture stiffness progression was not significantly correlated with external fixator stiffness, osteotomy gap volume, lowly mineralised bone volume (threshold of  $395 \text{ mg HA/cm}^3$ ) or highly mineralised bone volume (threshold of  $720 \text{ mg HA/cm}^3$ ) at any time points. Additional

variables, such as fixator stiffness or osteotomy volume, did not increase the adjusted  $R^2$  value when used as predictors in a multivariate regression model.

### *Mechanical Environments*

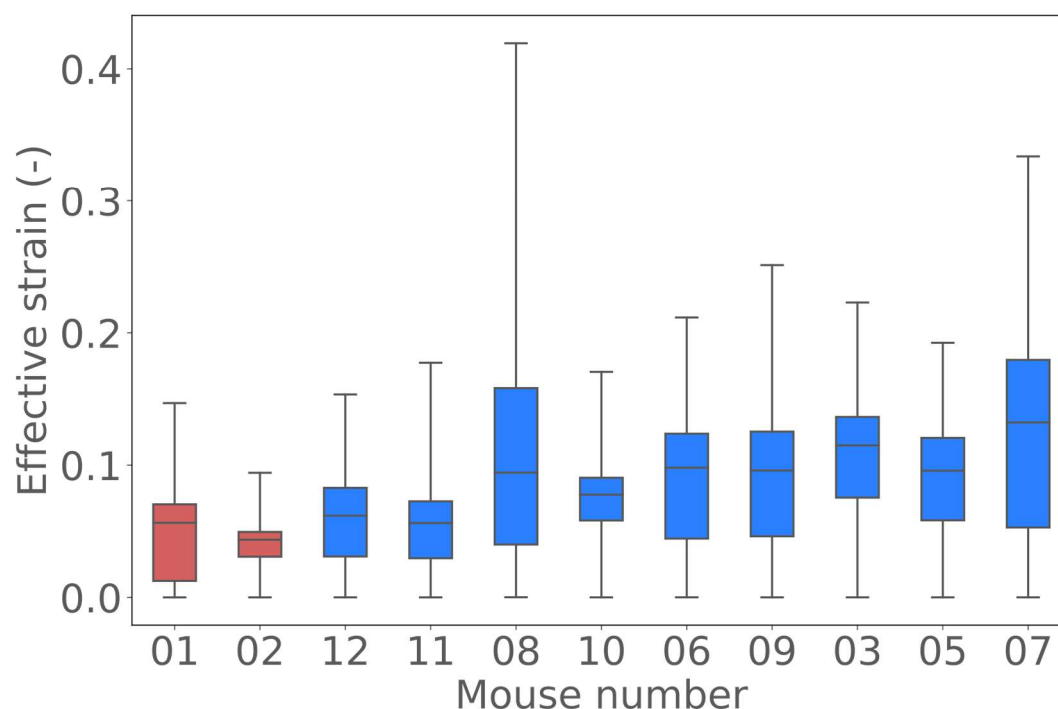


**Figure 3.8:** Mechanical environment inside the osteotomy gap, sorted by fracture stiffness at week 3 from lowest (left) to highest (right). Mouse 01 and mouse 02 displayed the lowest medians and the smallest ranges of effective strain values. Mouse 07 displayed the highest median effective strain and a large range of effective strain values within the osteotomy gap.

The mechanical environment within the osteotomy gap showed similar trends to the organ scale loading. Mice with high median strains displayed a better fracture stiffness progression than those with low median strains (**Figure 3.8**).

### *Mice displaying non-union*

Two mice displayed non-union fracture throughout the duration of the experiment, with a fracture stiffness ranging between 20 and 30 N/mm. These non-unions were clearly visible in the habitual loading measurements, as there was no decrease due to strain shielding from newly formed bone. The loading progression can be seen in **Figure 3.5b**, with a range of values (from 226% to 651% bodyweight loading) greatly exceeding that in the union group.

## Discussion

The purpose of this study was to investigate the relationship between habitual loading in a femoral defect model in mice and healing progression on an organ scale. Our results demonstrate that habitual loading is a significant factor in the progression of fracture healing on an individualised basis. When habitual loading is analysed before any signs of bone healing are observed, a strong correlation with the healing progression (measured by weekly stiffness) is seen for the following five weeks. Importantly, the absence of a correlation between habitual loading at week 1 and fracture stiffness at week 1 indicates that measuring habitual loading via an indirect means (such as an external fixator) prior to bone formation is not merely a reflection of fracture stiffness. Our results show many similarities to those of both Wehner et al.<sup>16</sup> and Klosterhoff et al.<sup>15</sup>, with a clear decrease in signal at the start of bone formation, and an increase towards the end of the healing period during the remodelling phase. This is likely a result of the primary load-bearing structure shifting from the external fixator to the newly bridged bone. Similar to Klosterhoff et al.<sup>15</sup>, we observed a predictive relationship between pre-bone formation habitual loading and the outcome of the healing process. However, we observed this pattern using fracture stiffness as a measure of healing progression, and were unable to replicate the relationship when using bone volume like Klosterhoff et al.<sup>15</sup>. We hypothesise that this may be a function of defect size. In a smaller defect, formation of bone alone is more likely to be a good predictor of healing, as it improves defect stability regardless of its location within the defect. Contrastingly, in our relatively larger defect the location of the newly laid down bone is paramount, and hence stiffness proved a better measurement of defect healing than bone formation. We also observed that mice with a higher median effective strain tended towards improved fracture stiffness at bridging, indicating the need for further investigation into the relationship between soft tissue strains and local formation of bone tissue.

Validation of our measurement poses a challenge, as there is no existing habitual loading data for this particular model. However, comparisons with musculoskeletal modelling of mouse hind limb kinematics during locomotion<sup>32,33</sup> and force plates<sup>26,27,29,37</sup> show similar patterns to our measured loading signal. Equivalent peaks and rises are observed in both ground reaction forces<sup>26,27</sup> and our measurement. However, one key difference is the final peak (**Figure 3.2**), which is not seen in force plate measurements. We hypothesise that this loading occurs from lifting of the foot, a process not captured by force plates. Our %bodyweight loading level also differs substantially from force plate studies. Clarke et al.<sup>26,27</sup>, Fowler et al.<sup>29,30</sup>, and Roach et

al<sup>28</sup>, reported a %bodyweight loading in the range of 50% to 70%, while we observe a mean of 387% in our group. This difference can arise from amplification occurring due to muscle loading of the femur, an effect noted in humans<sup>38</sup>. With regard to musculoskeletal modelling, the amplitude of our measurement is similar to those shown by Charles et al. in hind limb loading<sup>32</sup> (~0.5-1 N versus 0.2 N, see Table 1, Supplementary Material) and muscle forces surrounding the femur<sup>33</sup>. An additional approach to validate our results is the use of the bone microstructure to back-calculate the loading that would have resulted in such a structure<sup>39</sup>. However, the results of this approach differ from our measurement by an order of magnitude<sup>35</sup>.

Two of the twelve mice in this study demonstrated a non-union fracture. Each non-union mouse displayed a habitual loading level of substantially less than one standard deviation of that in the union group. The two non-union mice displayed habitual loading of 226% and 252% bodyweight, compared to the main group with a mean of 387±91% bodyweight. Furthermore, there were two mice within the union group who displayed similar loading levels to the non-union group. Even though these mice bridged, they displayed poor healing progression, providing support for the concept that non-unions are a potential result of several possible causes and not just insufficient mechanical stimulation<sup>9,40,41</sup>. Additionally, one of these mice showed loss of bone during the study, displaying atrophic patterns observed in certain models of non-union fractures<sup>40</sup>.

In this work, several limitations are present. Primarily, our results are a small snapshot of the general habitual loading present throughout the healing process. However, certain technological challenges limit full continuous monitoring of loading within the fracture. Firstly, most commercial device for mice are inappropriately sized for such a measurement. Incorporating wireless communication with appropriate amplification and power sources at such a size is difficult. Secondly, the tether produces signal artefacts, which manifest as a slow (> 5s) linear increase or decrease of the signal. However, since the additional strain induced on the fixator by the attached wire occurred over a duration far greater than a mouse foot strike, this artefact could be removed via linear detrending. Finally, as the measured amplitude of loading was taken as the difference between peak-trough combinations, the recorded deformation was relative and did not account for any pre-loading or pre-conditioning during the loading pattern. An additional limitation is that we only focused on consistent movement bursts on the CatWalk. Often, when the mouse reached the end of the CatWalk and turned around before engaging in another run, there was a substantially high peak force exerted on the fixator. Similar high peaks

were observed during non-walking movements (such as the mouse bobbing slightly up and down) or pre-walking movements (the initiation of the movement sequence). Future studies may benefit from incorporating such low frequency high amplitude loading events into their analyses. Finally, the use of strain gauges on an external fixator provides an indirect measurement. Even with calibration, measured loading is not a completely accurate reflection of the forces and deformations within the defect. Due to this, our method is limited by the compliance of the fixator. If the fixator pins and parts are loose, either within the bone or on the external fixator itself, a certain degree of deformation could occur without the strain gauge deforming. This limitation results in the measured force being a lower bound of loading.

In conclusion, this work experimentally determines individualised loading in a femur defect model in mice. We observed that habitual loading pre bone formation is a key metric in the healing progression of a defect. From this data, we can begin quantifying a mechanical dose, which can be delivered to the defect in the pre-bridging situation. With this knowledge, improved mechanical intervention approaches and studies can be designed. Based on the two mice that formed non-union fractures, more research and an increased sample size are needed to expand upon the observations of insufficient mechanical stimulation and to elucidate the mechanoregulation of non-union cases.

## **Acknowledgements**

The authors would like to acknowledge support from the European Union (ERC Advanced MechAGE, ERC-2016-ADG-741883).

## **Competing Interests**

The authors declare no competing interests

## Supplementary Material

Table 1: Median peak loading amplitude (in N)

	Week 1	Week 2	Week 3	Week 4	Week 5	Week 6	Week 7
Mouse 01	0.49	0.55	1.43	1.01	0.78	0.6	0.62
Mouse 02	0.47	0.74	0.97	0.88	0.96	0.83	1.06
Mouse 03	0.96	0.1	0.08	0.06	0.17	0.05	0.5
Mouse 04	0.73	0.07	0.1	0.06	0.19	0.58	0.48
Mouse 05	0.85	0.1	0.06	0.1	0.29	0.14	0.52
Mouse 06	0.89	0.1	0.08	0.04	0.12	0.46	0.47
Mouse 07	1.15	0.14	0.09	0.07	0.16	0.55	0.47
Mouse 08	0.81	0.49	0.09	0.09	0.18	0.27	0.36
Mouse 09	1.03	0.34	0.11	0.09	0.29	0.66	0.67
Mouse 10	0.77	0.63	0.1	0.08	0.29	0.49	0.35
Mouse 11	0.58	0.48	0.07	0.11	0.42	0.59	0.41
Mouse 12	0.52	0.58	0.13	0.1	0.24	0.43	0.35

Table 2: Bodyweight prior to CatWalk measurement (in g)

	Week 0	Week 1	Week 2	Week 3	Week 4	Week 5	Week 6	Week 7
Mouse 01	22.4	22.1	22	22.4	23	22.1	22.6	22.4
Mouse 02	19.4	18.9	19.3	19.4	20	19.5	19.3	19.7
Mouse 03	22.4	22.7	22.4	22.4	22.5	21.8	22	21.9
Mouse 04	19.8	20	20.2	20.4	20.6	20.4	20.5	20.3
Mouse 05	23	22.7	22.1	22.4	21.9	22.1	22.1	22.2
Mouse 06	21.3	21.5	20	20.4	20	20.1	20	21.2
Mouse 07	23.6	22.2	23.2	23.3	23.7	22.7	23.1	23.5
Mouse 08	22.7	21.5	21.4	21.4	22.3	21.4	22	22
Mouse 09	21.5	20.3	21.3	21.8	21.3	21.4	21.6	21.8
Mouse 10	25.5	23.4	24.9	22.8	24.2	23	24.1	24.1
Mouse 11	24.5	23.6	23.6	23.6	24	23.8	24.5	24.4
Mouse 12	22.4	21.8	22.4	22.2	22.3	22.4	22.6	23.2



*Table 3: Peak deformation during CatWalk measurements (in mm)*

	Week 1	Week 2	Week 3	Week 4	Week 5	Week 6	Week 7
Mouse 01	0.0029	0.0034	0.0085	0.0061	0.0050	0.0036	0.0037
Mouse 02	0.0027	0.0045	0.0056	0.0057	0.0057	0.0049	0.0064
Mouse 03	0.0059	0.0006	0.0005	0.0004	0.0010	0.0003	0.0031
Mouse 04	0.0043	0.0005	0.0006	0.0004	0.0012	0.0035	0.0030
Mouse 05	0.0051	0.0006	0.0004	0.0007	0.0018	0.0009	0.0032
Mouse 06	0.0052	0.0006	0.0005	0.0003	0.0008	0.0029	0.0029
Mouse 07	0.0069	0.0009	0.0005	0.0004	0.0009	0.0032	0.0028
Mouse 08	0.0047	0.0030	0.0005	0.0005	0.0011	0.0016	0.0023
Mouse 09	0.0066	0.0020	0.0007	0.0005	0.0017	0.0039	0.0045
Mouse 10	0.0047	0.0036	0.0006	0.0005	0.0017	0.0029	0.0022
Mouse 11	0.0035	0.0029	0.0004	0.0007	0.0024	0.0039	0.0025
Mouse 12	0.0031	0.0037	0.0008	0.0006	0.0014	0.0026	0.0022

---

## References

- 1 Augat, P. *et al.* Local tissue properties in bone healing: Influence of size and stability of the osteotomy gap. *J Orthop Res* **16**, 475-481, doi:DOI 10.1002/jor.1100160413 (1998).
- 2 Augat, P., Simon, U., Liedert, A. & Claes, L. Mechanics and mechano-biology of fracture healing in normal and osteoporotic bone. *Osteoporosis Int* **16**, S36-S43, doi:10.1007/s00198-004-1728-9 (2005).
- 3 Bailon-Plaza, A. & van der Meulen, M. C. H. Beneficial effects of moderate, early loading and adverse effects of delayed or excessive loading on bone healing. *J Biomech* **36**, 1069-1077, doi:10.1016/S0021-9290(03)00117-9 (2003).
- 4 Boerckel, J. D. *et al.* Effects of in vivo mechanical loading on large bone defect regeneration. *J Orthop Res* **30**, 1067-1075, doi:10.1002/jor.22042 (2012).
- 5 Carter, D. R., Beaupre, G. S., Giori, N. J. & Helms, J. A. Mechanobiology of skeletal regeneration. *Clin Orthop Relat R*, S41-S55 (1998).
- 6 Claes, L. E. & Heigele, C. A. Magnitudes of local stress and strain along bony surfaces predict the course and type of fracture healing. *J Biomech* **32**, 255-266, doi:Doi 10.1016/S0021-9290(98)00153-5 (1999).
- 7 Claes, L. E. *et al.* Effects of mechanical factors on the fracture healing process. *Clin Orthop Relat R*, S132-S147 (1998).
- 8 Einhorn, T. A. & Gerstenfeld, L. C. Fracture healing: mechanisms and interventions. *Nat Rev Rheumatol* **11**, 45-54, doi:10.1038/nrrheum.2014.164 (2015).
- 9 Giannoudis, P. V., Einhorn, T. A. & Marsh, D. Fracture healing: The diamond concept. *Injury* **38**, S3-S6, doi:Doi 10.1016/S0020-1383(08)70003-2 (2007).
- 10 Claes, L., Recknagel, S. & Ignatius, A. Fracture healing under healthy and inflammatory conditions. *Nat Rev Rheumatol* **8**, 133-143, doi:10.1038/nrrheum.2012.1 (2012).
- 11 Claes, L., Augat, P., Suger, G. & Wilke, H. J. Influence of size and stability of the osteotomy gap on the success of fracture healing. *J Orthop Res* **15**, 577-584, doi:DOI 10.1002/jor.1100150414 (1997).
- 12 Augat, P. *et al.* Early, full weightbearing with flexible fixation delays fracture healing. *Clin Orthop Relat R*, 194-202 (1996).
- 13 Rontgen, V. *et al.* Fracture Healing in Mice under Controlled Rigid and Flexible Conditions Using an Adjustable External Fixator. *J Orthop Res* **28**, 1456-1462, doi:10.1002/jor.21148 (2010).

- 14 Duda, G. N. *et al.* Analysis of inter-fragmentary movement as a function of musculoskeletal loading conditions in sheep. *J Biomech* **31**, 201-210 (1998).
- 15 Klosterhoff, B. S. *et al.* Wireless sensor enables longitudinal monitoring of regenerative niche mechanics during rehabilitation that enhance bone repair. *Bone* **135**, doi:10.1016/j.bone.2020.115311 (2020).
- 16 Wehner, T. *et al.* Temporal Delimitation of the Healing Phases Via Monitoring of Fracture Callus Stiffness in Rats. *J Orthop Res* **32**, 1589-1595, doi:10.1002/jor.22721 (2014).
- 17 Mavcic, B. & Antolic, V. Optimal mechanical environment of the healing bone fracture/osteotomy. *Int Orthop* **36**, 689-695, doi:10.1007/s00264-012-1487-8 (2012).
- 18 Wehrle, E. *et al.* Evaluation of longitudinal time-lapsed in vivo micro-CT for monitoring fracture healing in mouse femur defect models. *Sci Rep* **9**, 17445, doi:10.1038/s41598-019-53822-x (2019).
- 19 O'Neill, K. R. *et al.* Micro-computed tomography assessment of the progression of fracture healing in mice. *Bone* **50**, 1357-1367, doi:10.1016/j.bone.2012.03.008 (2012).
- 20 Hao, Y. J. *et al.* Changes of microstructure and mineralized tissue in the middle and late phase of osteoporotic fracture healing in rats. *Bone* **41**, 631-638, doi:10.1016/j.bone.2007.06.006 (2007).
- 21 Nyman, J. S. *et al.* Quantitative measures of femoral fracture repair in rats derived by micro-computed tomography. *J Biomech* **42**, 891-897, doi:10.1016/j.jbiomech.2009.01.016 (2009).
- 22 Wehrle, E. *et al.* The impact of low-magnitude high-frequency vibration on fracture healing is profoundly influenced by the oestrogen status in mice. *Dis Model Mech* **8**, 93-104, doi:10.1242/dmm.018622 (2015).
- 23 Wehrle, E. *et al.* Distinct Frequency Dependent Effects of Whole-Body Vibration on Non-Fractured Bone and Fracture Healing in Mice. *J Orthop Res* **32**, 1006-1013, doi:10.1002/jor.22629 (2014).
- 24 Zura, R. *et al.* Epidemiology of Fracture Nonunion in 18 Human Bones. *Jama Surg* **151**, doi:10.1001/jamasurg.2016.2775 (2016).
- 25 Elliott, D. S. *et al.* A unified theory of bone healing and nonunion. *Bone Joint J* **98b**, 884-891, doi:10.1302/0301-620x.98b7.36061 (2016).

- 
- 26 Clarke, K. A., Smart, L. & Still, J. Ground reaction force and spatiotemporal measurements of the gait of the mouse. *Behav Res Meth Ins C* **33**, 422-426, doi:Doi 10.3758/Bf03195396 (2001).
- 27 Clarke, K. A. & Still, J. Gait analysis in the mouse. *Physiol Behav* **66**, 723-729, doi:Doi 10.1016/S0031-9384(98)00343-6 (1999).
- 28 Roach, G. C., Edke, M. & Griffin, T. M. A novel mouse running wheel that senses individual limb forces: biomechanical validation and in vivo testing. *J Appl Physiol* **113**, 627-635, doi:10.1152/jappphysiol.00272.2012 (2012).
- 29 Fowler, S. C. *et al.* A force-plate actometer for quantitating rodent behaviors: illustrative data on locomotion, rotation, spatial patterning, stereotypies, and tremor. *J Neurosci Meth* **107**, 107-124, doi:Doi 10.1016/S0165-0270(01)00359-4 (2001).
- 30 Fowler, S. C., Miller, B. R., Gaither, T. W., Johnson, M. A. & Rebec, G. V. Force-plate quantification of progressive behavioral deficits in the R6/2 mouse model of Huntington's disease. *Behav Brain Res* **202**, 130-137, doi:10.1016/j.bbr.2009.03.022 (2009).
- 31 Grasa, J. *et al.* Monitoring In Vivo Load Transmission Through an External Fixator. *Ann Biomed Eng* **38**, 605-612, doi:10.1007/s10439-009-9889-5 (2010).
- 32 Charles, J. P., Cappellari, O. & Hutchinson, J. R. A Dynamic Simulation of Musculoskeletal Function in the Mouse Hindlimb During Trotting Locomotion. *Front Bioeng Biotech* **6**, doi:10.3389/fbioe.2018.00061 (2018).
- 33 Charles, J. P., Cappellari, O., Spence, A. J., Wells, D. J. & Hutchinson, J. R. Muscle moment arms and sensitivity analysis of a mouse hindlimb musculoskeletal model. *J Anat* **229**, 514-535, doi:10.1111/joa.12461 (2016).
- 34 Virtanen, P. *et al.* SciPy 1.0: fundamental algorithms for scientific computing in Python. *Nat Methods* **17**, 261-272, doi:10.1038/s41592-019-0686-2 (2020).
- 35 Tourolle né Betts, D. C. *et al.* The association between mineralised tissue formation and the mechanical local *in vivo* environment: Time-lapsed quantification of a mouse defect healing model. *Sci Rep-Uk* **10**, 1-10, doi:10.1038/s41598-020-57461-5 (2020).
- 36 Flaig, C. & Arbenz, P. A scalable memory efficient multigrid solver for micro-finite element analyses based on CT images. *Parallel Comput* **37**, 846-854, doi:10.1016/j.parco.2011.08.001 (2011).

- 
- 37 Schmitt, D., Zumwalt, A. C. & Hamrick, M. W. The relationship between bone mechanical properties and ground reaction forces in normal and hypermuscular mice. *J Exp Zool A Ecol Genet Physiol* **313**, 339-351, doi:10.1002/jez.604 (2010).
- 38 Taylor, W. R., Heller, M. O., Bergmann, G. & Duda, G. N. Tibio-femoral loading during human gait and stair climbing. *J Orthop Res* **22**, 625-632, doi:10.1016/j.orthres.2003.09.003 (2004).
- 39 Christen, P., van Rietbergen, B., Lambers, F. M., Muller, R. & Ito, K. Bone morphology allows estimation of loading history in a murine model of bone adaptation. *Biomech Model Mechan* **11**, 483-492, doi:10.1007/s10237-011-0327-x (2012).
- 40 Giannoudis, P. V. *et al.* Subtrochanteric fracture non-unions with implant failure managed with the "Diamond" concept. *Injury* **44**, S76-S81, doi:Doi 10.1016/S0020-1383(13)70017-2 (2013).
- 41 Andrzejowski, P. & Giannoudis, P. V. The 'diamond concept' for long bone non-union management. *J Orthop Traumatol* **20**, doi:10.1186/s10195-019-0528-0 (2019).

# Development of an approach to control and homogenize tissue scale strains in a mouse fracture healing model

Graeme R. Paul<sup>1</sup>, Esther Wehrle<sup>1</sup>, Duncan C. Tourolle<sup>1</sup>, Gisela Kuhn<sup>1</sup>, Ralph Müller<sup>1</sup>

1. Institute for Biomechanics, ETH Zurich, Zurich, Switzerland

## Abstract

Mechanical loading allows both investigation into the mechanoregulation of fracture healing as well as interventions to improve fracture-healing outcomes. However, loading is seldom individualised or even targeted to an effective mechanical stimulus level within the bone tissue. In this study, we use micro-finite element analysis to demonstrate the result of using a constant loading assumption for all mice in a given group. We then contrast this with the application of an adaptive loading approach, denoted Real Time Finite Element adaptation, in which micro-computer tomography images provide the basis for micro-FE based simulations and the resulting strains are manipulated and targeted to a reference distribution. Using this approach, we demonstrate that individualised loading will lead to a better-specified strain distribution and lower variance across all mice, both longitudinally and cross-sectionally.

## Keywords:

Bone, bone regeneration, fracture healing, bone adaptation, mechanical strain, real time, finite element analysis, individualised

## Introduction

Bone requires mechanical stimulation for fractures to heal. Improved understanding of the mechanical stimulation – fracture-healing relationship will provide substantial benefit in both basic scientific investigation of cell fate and behaviour as well as clinical application. However, the exact mechanical stimulation required to initiate bone formation is still up to debate, with *in vivo*, *in vitro* and *in silico* models showing differing levels of activation strains at different anatomical scales<sup>1-4</sup>. For example, at tissue level, strains of up to 3'000 microstrain occur due to strenuous physiological loading in humans<sup>5</sup>, while at cell level, *in silico* models have shown that micro-architectural variations lead to strain amplifications and strain peaks exceeding 10'000 microstrain in and around osteocytes<sup>6,7</sup>. These levels of strain approach the activation levels seen in single cell *in vitro* investigations on the response of osteocytes to mechanical loading<sup>8</sup>. However, even though mechanical stimulation at each scale differs greatly, our ability to control the mechanical stimuli is most easily performed at organ scale, manipulating the bone via some sort of actuation resulting in a specific strain distribution at each scale. Controlling this “mechanical dose” in the mechanical environment is essential for experimental methods to either optimise or map mechanical stimulation to understand the formation processes underlying bone healing and develop improved interventions. In turn, with the growth of personalised medicine approaches, treatments adjusted towards a patient’s individual anatomy would require mechanical interventions with a specific “mechanical dose” for each patient.

The mechanical environment is greatly dependant on the geometry of bone<sup>9</sup>. Strains propagate differently through each individual bone, providing a variety of mechanical stimuli throughout the tissue<sup>10</sup>. This geometric variance is seen from traumatic fractures in humans<sup>11</sup> to well controlled osteotomies in sheep<sup>12</sup> or murine models<sup>13</sup>. While inbred mouse or rat strains should provide the lowest variance out of all appropriate model animals for fracture healing, often the variance is not as low as expected. For example, even within studies, defect size variance can be large, often displaying a standard deviation of over 10% of the nominal size in osteotomy based experiments<sup>12-14</sup>. In addition, even though it is known that the resulting strain from the initial size of the fracture gap<sup>12,15-18</sup> is influential in the outcome of the healing process, this geometric information is regularly left either unreported, with no size or geometric description of the defect presented<sup>19-21</sup>, or underreported with only the nominal size being presented<sup>22-24</sup>. While such basic geometric conditions are critical for outcome, additional affecters such as activity of the animal<sup>25</sup>, disruption of the periosteum<sup>26,27</sup> and inter-fragmentary movement<sup>28</sup>

provide further biological and mechanical cues. These cues influence the longitudinal progression of bone formation and resorption and hence lead to geometric changes, which in turn further influence the mechanical environment within the tissue and the resultant healing outcome divergence across a group. Additionally, effects attributed to interventions such as pharmacological agents could be obscured due to inconsistent mechanical environments within and between groups. As loading models are often used to study the effects of mechanical stimulation on physiological processes in bone such as remodelling and healing, controlling the local and global stimuli acting on the tissue would improve the validity of such investigations<sup>16</sup>.

Non-individualised loading has been applied during all phases of the fracture healing process. Vibration loading has often been attempted during the inflammation phase with mixed results<sup>20,23,24,29</sup>, while results that are more consistent have been seen with direct mechanical stimulation during the end stages of the reparative phase and the remodelling phase<sup>30,31</sup>. However, while these studies aim at providing some degree of mechanical stimulation to the bone structure, limitations lie in the lack of either targeted mechanical stimulation (i.e. attempting to achieve a certain mechanical strain within the tissue), or application of load regardless of the individual structural and geometric state of the bone<sup>32-34</sup>. Often attempts at targeting strains and the resultant mechanical loads are derived from past studies using bone-surface strain gauge measurements, amalgamating loading-strain relationships throughout the animal group<sup>35,36</sup>. However, strain gauged based mechanical loading values show substantial in-group variance, with values differing by up to 30% in such studies<sup>35,36</sup>.

In this study, we analyse the inter-individual and temporal variance of the mechanical environment using image-based finite element analysis<sup>16</sup> during the bridging and post-bridging phase under a 10 N load and, due to individual differences seen within groups, propose and apply a novel methodology of adapting loading conditions to the individual bone geometry within an *in vivo* mouse femur osteotomy model. We term this method real time Finite Element (rtFE) adaptive loading. Via the incorporation of finite element simulations into the experimental pipeline in real time, we are able to homogenise tissue level strains between each mouse, adapting the experimental load based on these simulations in one imaging and loading session. Additionally, we are able to assess whether a bone has a risk of refracture when under loading, allowing loading on the healing mouse femur to start as soon as it is safe to do so. This



allows complete intervention control throughout the repair and remodelling phases of fracture healing.

## Materials and Methods

### *Study Design*

All animal procedures were approved by the authorities (licence number: 36/2014; Kantonales Veterinäramt Zürich, Zurich, Switzerland). We confirm that all methods were carried out and reported in accordance with relevant guidelines and regulations (Swiss Animal Welfare Act and Ordinance (TSchG, TSchV) and ARRIVE guidelines). In this study, we used 30 sets of micro-CT images (30 animals, 5 time points per set) taken during a defect healing study in an externally fixated mouse osteotomy model (described in Chapter 4.2). Each mouse was scanned weekly over a period of 49 days after surgery. 10 of the mice received mechanical loading starting at week 3 post surgery and the rest were sham loaded at 0 N, (details can be found in Chapter 4.2). We applied micro-FE analysis to simulate the mechanical environment under constant boundary conditions for all mice, and analysed the longitudinal changes in the mechanical environment of bones. We then applied an adaptive loading approach, targeting the loading to an idealised reference strain distribution, and then analysed and compared the longitudinal changes of the mechanical environment between the constant load dataset and the adaptive load dataset.

### *Imaging and pre-processing*

All images were acquired by a vivaCT 40 (Scanco Medical, Brüttsellen, Switzerland) with the following scanner settings: 55 kVp, 145  $\mu$ A, 350 ms integration time, 500 projections per 180°, 21 mm field of view (FOV), aluminium filter. Images were of 10.5  $\mu$ m resolution. All images were assessed to ensure they were free of artefacts and were of sufficient quality. All original images were cropped to a dimension 300x300x210 voxels and were of the same femoral region between the internal screws of the external fixator for each mouse. The longitudinal images were then registered to the week 0 time-point, to ensure boundary conditions were consistently applied. For post registration, each image was cropped to 180 voxels length via the removal of 15 slices on the top and bottom of the volume. This was done to remove empty slices caused by rotation and translation during image registration. This volume was then Gaussian filtered ( $\sigma=1.2$ , support=1) and we applied the multi-density approach proposed by Tourolle et al 16. All greyscale values were binned and then converted from density (mg HA/cm<sup>3</sup>) to Young's moduli (GPa), on a per voxel basis, from 395 mg HA/cm<sup>3</sup> to 720 mg HA/cm<sup>3</sup> in steps of 25 mg

HA/cm<sup>3</sup>, corresponding to 4.045 GPa to 12.170 GPa respectively with steps of 0.626 GPa. Regions of soft tissue were set to a Young's modulus of 0.003 GPa and the marrow cavity of the femur was capped with a plate of 20 GPa, preventing edge effects due to the soft tissue found lying on the top slice of the finite element mesh.

#### *Finite element analysis and scaling of the mechanical environment*

From this mesh, the mechanical environment was determined using a linear micro-finite element (micro-FE) solver, Parasol 42. A compressive displacement of 1% was applied to the top slice in the axial direction while the bottom slice was fixed. The Swiss National Supercomputing Centre (CSCS) was used to solve each finite element simulation, requiring roughly 2 min per image. Effective strain results of the simulation were taken as the mechanical environment of the bone. Two sets of mechanical environments were created from the sets of images (in total 60 mechanical environments per time points (2 per mouse), one at a load of  $F_{applied} = 10$  N as per Tourolle et al.<sup>16</sup> and then one at an adaptive load, which was determined by minimising (via a Nelder-Mead optimiser<sup>37</sup>) the Kolmogorov-Smirnov test result to a reference distribution, determined to be representative of a well-healed mouse with a median strain of 700 microstrain. To align the force on the bone to the constant or calculated values across all mice, the results of the simulations were appropriately scaled based on the assumed loading parameters using the following ratio:

$$\varepsilon_{actual} = \frac{F_{applied}}{F_{resultant}} \varepsilon_{simulation}$$

Where  $\varepsilon_{simulation}$  is the effective strain result of the simulation (based on the 1% displacement),  $F_{resultant}$  is the sum of reaction forces of all the nodes of the uppermost surface,  $F_{applied}$  is the selected force (i.e. a force provided by a mechanical stimulation machine) and  $\varepsilon_{actual}$  is the strains under the applied force. All analysis was performed on strains in the bone tissue only, ignoring both the soft tissue and the marrow cap. This was done by masking out regions of soft tissue and marrow caps and then performing all relevant analysis on the remaining voxels.

#### *Statistics*

For each mechanical environment, the median effective strain value was calculated. For all groups at each time point, means and standard deviations were calculated. All histograms were calculated for the range of 0 to 15 000 microstrain with 250 bins over the range. All statistics were performed using SciPy 1.0<sup>37</sup>.

## Results

In this study, we compared the effect of traditional constant loading (**Figure 3.9a**) with loading, which is adjusted by rtFE adaptive loading, on the mechanical environment in a healing bone defect (**Figure 3.9b, c**). We used longitudinal *in vivo* micro-CT images (5 per animal) taken from 30 mice during healing of a femur osteotomy fixed by an external fixator. Ten of the animals received loading of the defect. Based on the CT images, we calculated the local strain distribution within the callus by micro-FE analysis for a simulated 10 N loading. In a second step, we adapted the applied loading such that the distribution of strains is minimised with reference to a target distribution, derived from a mouse displaying a good healing progression. The whole process was optimized to allow incorporation into a single anaesthesia session, hence the name real time FE. We successfully ran the rtFE adaptive loading process with an increase of less than 5 min, in addition to image reconstruction times, between the end of scanning and the start of loading (**Figure 3.9c**). This is important as it prevents the need to re-anaesthetise the animal, which induces stress and could influence study results.

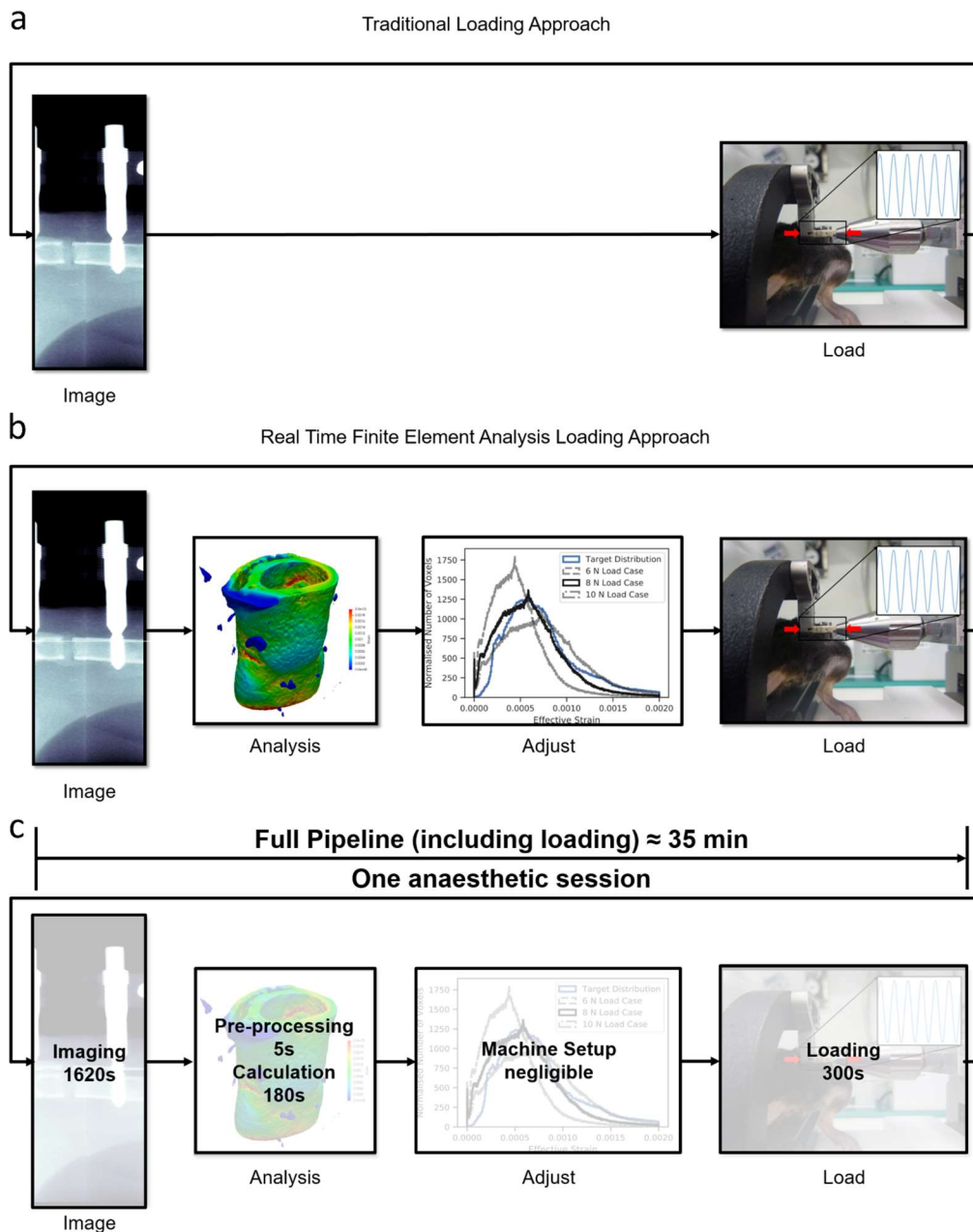


**Figure 3.9:** a) A traditional loading experiment images the animal and uses a loading protocol decided on before the experiment has begun. b) The rtFE approach incorporates the simulation and adjustment of the loading parameters to ensure a targeted mechanical stimulation at each time point for the animal. c) When incorporated within the experimental pipeline, appropriate implementation of the rtFE will allow the imaging to loading process to be incorporated in a single anaesthetic session.

### Longitudinal observations of the bone healing process

Bridging of the fracture defect occurred between week 2 and week 3 post surgery. As seen in **Figure 3.10 a** and **d**, between week 2 and week 3, a considerable amount of bone was formed. The callus structure had many small strut- and truss-like features that transfer the structural load. These can be seen at week 3 (**Figure 3.11 a** and **b**). These small structural elements concentrated mechanical strains into small regions, increasing strain variance, such as seen at week 2, 3 and week 4 in **Figure 3.10 b, c, e** and **f**, where strain standard deviation exceeds future values. Once these small structural elements were absorbed into the new cortical wall, (as can be seen in **Figure 3.10a** and **b**, week 3 to 5), the strain distributions displayed lower standard deviation, as the thicker structure dissipates the load more evenly.

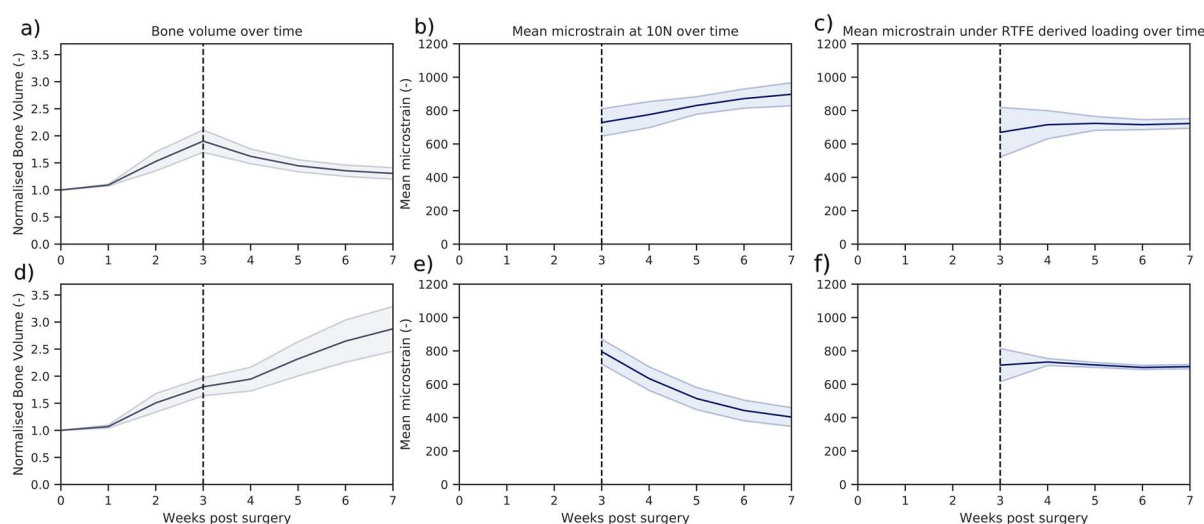


**Figure 3.10:** As bone volume decreases (a), or increases (d), the mechanical strains increase (b) or decrease (e) respectively throughout the duration of the loading period. This causes a changing mechanical environment at each point of time. (c) and (f) display the application of the rtFE approach to ensure this change in the local mechanical environment does not occur. Additionally, comparisons between (b) and (c), and (e) and (f), show the reduction of variance caused by rtFE specifying appropriate loading parameters on an individualised basis. Bone volume is normalised to the amount of bone volume at week 0 post surgery.

### Constant loading and the mechanical environment

At week 3 for the control group, with a load of 10 N, the median strain under constant loading was  $683 \pm 81$  microstrain. With the observed decreasing bone volume (**Figure 3.10a**), the median strain and standard deviation increased throughout the study duration,  $740 \pm 60$

microstrain at week 4,  $818 \pm 61$  at week 5,  $873 \pm 71$  at week 6 and  $905 \pm 86$  at week 7 (**Figure 3.10b**).

Contrastingly, in the loaded group, with an increasing bone volume (**Figure 3.10d**), the median strain decreased throughout the remaining reparative and remodelling phase ( $727 \pm 74$  at week 3,  $582 \pm 77$  at week 4,  $471 \pm 68$  at week 5,  $413 \pm 61$  at week 6 and  $383 \pm 56$  at week 7) (**Figure 3.10e**). For both loading and control group, the standard deviation of strains in the mechanical environment remained high, roughly or greater than 10% of the median strain for all simulated time points.

#### *Real Time Finite Element adaptive loading*

Adaptation of loading parameters to ensure minimisation of strain variance was then performed, in a means that can be incorporated into an experiment; a process we term Real Time Finite Element (rtFE) adaptive loading. In this process, finite element analysis is performed after the animal is imaged and the results are used to change the experiments loading parameters, ensuring similar strain distributions within or across groups. The rtFE adaptation required two stages: a strain distribution matching stage, to minimise variance between longitudinal and cross sectional mechanical environments, and a fracture-risk identification stage; where given the determined loading parameters, the risk of fracture is identified and the load downscaled if required.

A target distribution was developed from a mouse with good healing progression and scaled to be of a median strain of 700 microstrain. This acted as an idealised strain distribution for the application of rtFE. We then minimised the Kolmogorov-Smirnov test statistic (**Figure 3.11a**) between the mechanical environment of each mouse from week 3 to week 7 and this target distribution using a Nedler-Mead optimiser. This ensured minimal differences between the cumulative distribution functions of each distribution. Alternatively, the strain distribution can be plotted with a series of incremental possible loading options governed by whatever mechanical actuator is in use. The researcher can then select the most appropriate distribution (**Figure 3.11b**), where each possible scenario is plotted with regard to the target distribution.

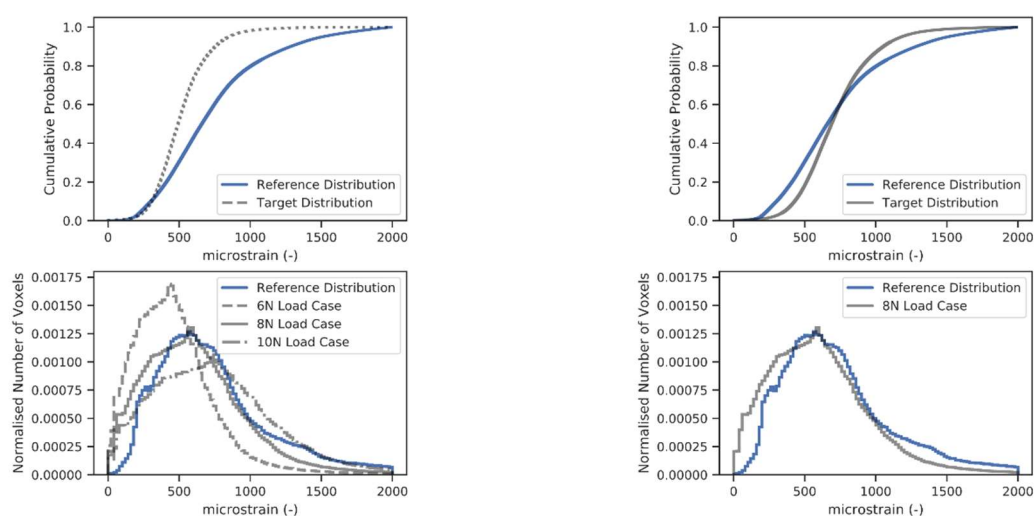


**Figure 3.11:** Longitudinal and cross-sectional strain progression under constant loading and rtFE adaptation simulations results show the progression of strain within the bone tissue. (a) demonstrates how poorly healed bones have less consistent strain distributions throughout the tissue, with regions of dangerously high strain and regions of lower strains. Well-healed bones however show a decrease in the strains throughout the tissue, as is the case in L06. (b) rtFE adapts the loading to ensure no peak strain voxels exist (C10) and maintains consistent strain fields (L06). For mice with smaller changes in bone geometry (C09 and C14), the adaptation is less obvious, but still present.

However, scaling load and matching strain distribution can lead to certain fragile structures within the callus developing dangerously high strain, potentially leading to refracture. After the strain distribution matching is complete, a fracture risk analysis is performed. The aim of this analysis is to determine if the new loading parameters could lead to failure of the bone, and hence such an occurrence can be mitigated. For the selected loading case, the number of voxels of 10 000 microstrain or greater are counted. If this exceeds fifty voxels, the load is downscaled by 2 N and the number of voxels greater than 10 000 microstrain is counted again. This process is repeated until no voxels exceeding 10 000 microstrain remain (as depicted in **Figure 3.12a-f**) and the final loading parameter is selected.

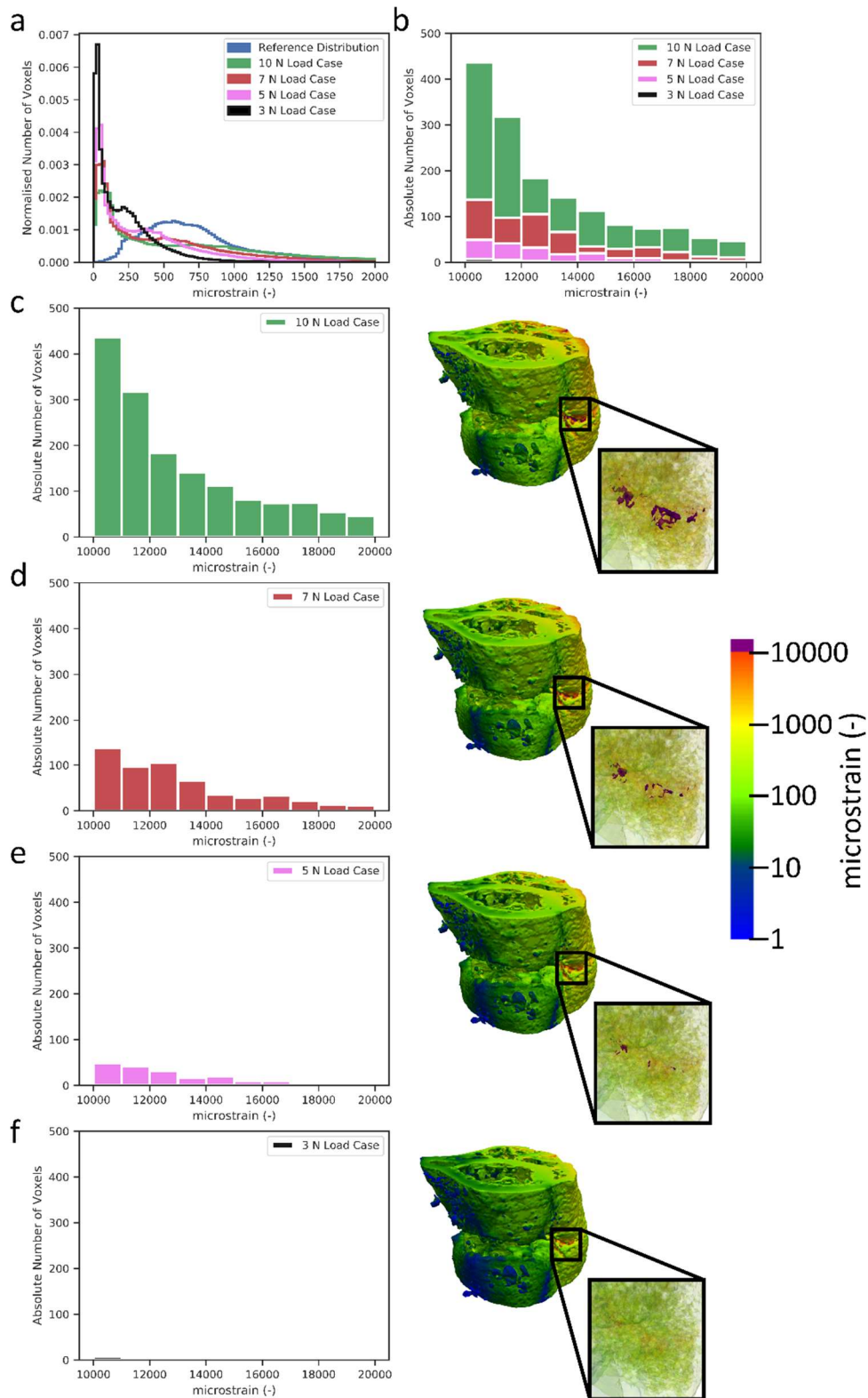


**Figure 3.12:** Fracture risk profiling (a) identifies the number of voxels over 1% strain (B) and down scales the load (c – f) until there are less than 50 voxels in the identified strain risk region.



We successfully ran the rtFE adaptive loading within an appropriate time window to be incorporated into a single anaesthetic session during an experiment. As the simulation time for an image is roughly 2 min, this process can be easily incorporated into the usual imaging and loading pipelines with minimal extra time required (~5 min in addition to image reconstruction times, **Figure 3.9c**).

#### *Adaptive loading and the mechanical environment*

With application of rtFE adaptive loading (**Figure 3.13**, **Figure 3.14**), a set of loading parameters was determined. Control mice required a decreasing load throughout the observation period, while loaded mice required an increasing load. When looking at the mechanical environment, the median strain for the control group remained within narrow bounds (713±33 at week 3, 792±35 microstrain at week 4, 714±38 at week 5, 726±35 at week 6 and 736±30 at week 7) throughout the remaining reparative and remodelling phase. A similar pattern was seen in the loaded group with median strains remaining similar (721±32 at week 3, 712±20 microstrain at week 4, 700±15 at week 5, 681±14 at week 6 and 698±14 at week 7) from week 3 to week 7. As with the control group, upon rtFE application, standard deviation decreased substantially from week 3 to week 4, and further decreased during the remodelling period, remaining 35% and 25% of the constant load case for the control and loaded groups at week 7 respectively.

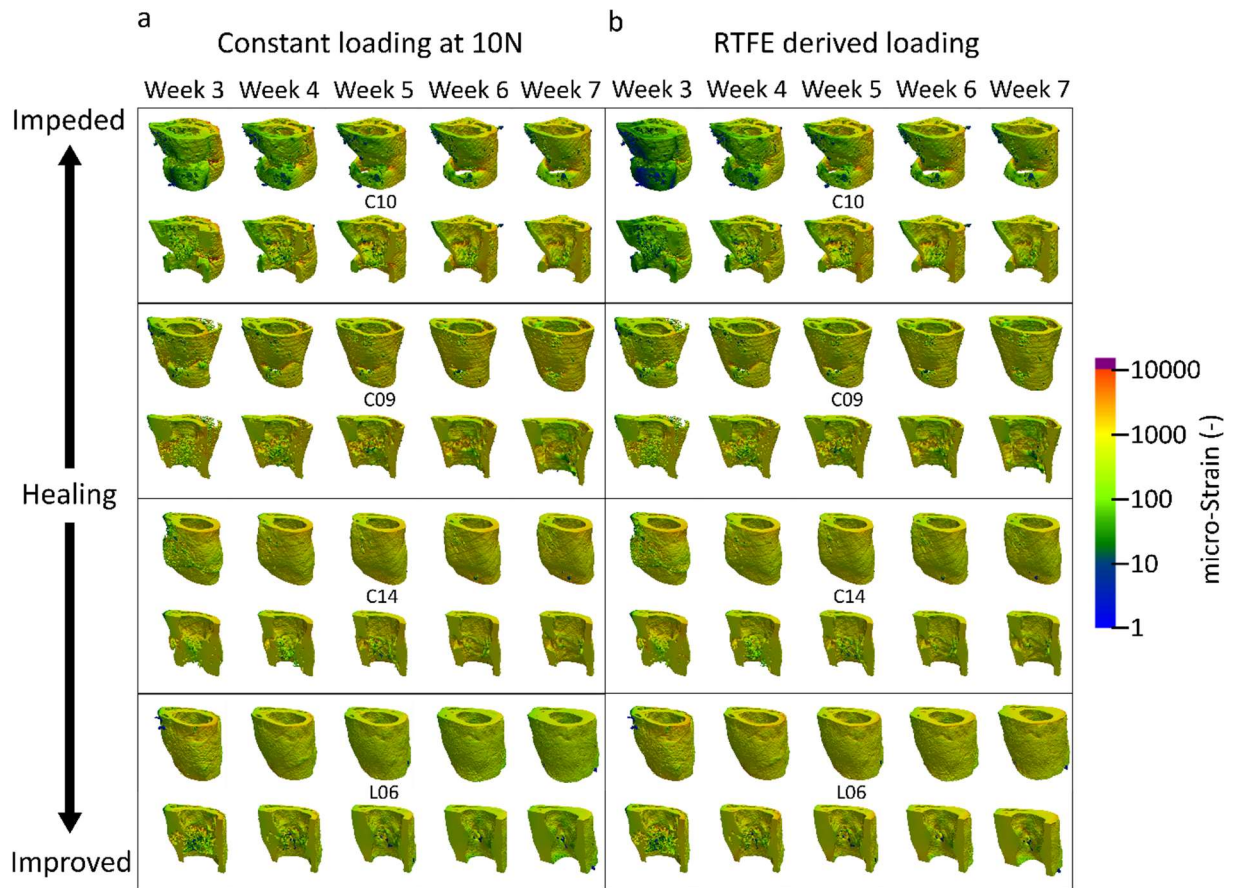


**Figure 3.13:** Two approaches can be implemented for the *rtFE* approach. Optimising via a Kolmogorov–Smirnov test (a) allows an automated process, saving time and giving an exact value, while plotting and selecting (b) from a list of loading options provides the researcher with more understanding of the strain distributions for each loading parameter.

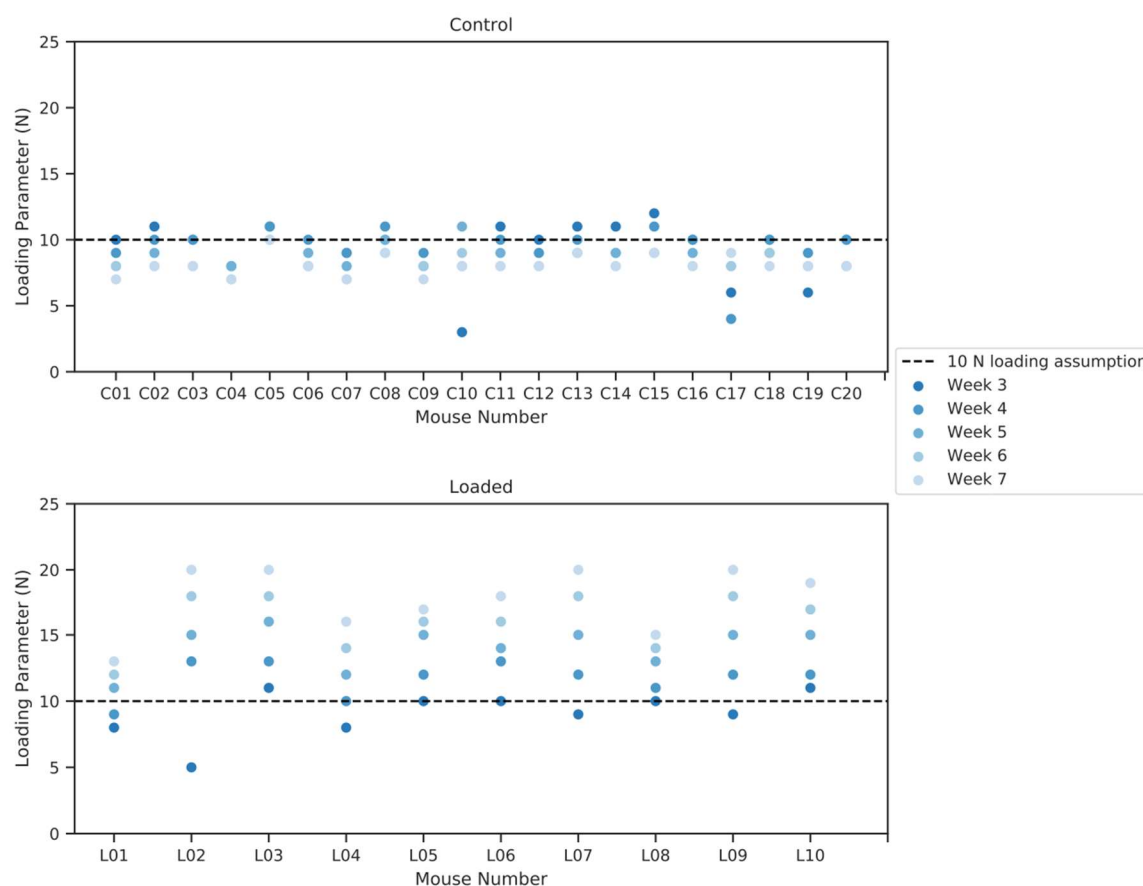


**Figure 3.14:** Loading parameters relative to the 10 N assumption, determined by rtFE. (a) a decreasing load is needed to maintain a consistent mechanical environment in a control group. (b) an increasing load is needed to maintain a consistent mechanical environment in a loaded group.

Upon application of the fracture prevention step, the control group observed a decrease in median strain and an increase in standard deviation ( $691 \pm 158$  at week 3,  $726 \pm 110$  microstrain at week 4,  $714 \pm 47$  at week 5,  $726 \pm 44$  at week 6 and  $736 \pm 30$  at week 7) (**Figure 3.10c**) in comparison with the mechanical environment prior to this step. Likewise, the loaded group also displayed an increase in standard deviation for earlier time points yet a quicker reduction than in the unloaded group ( $721 \pm 122$  at week 3,  $712 \pm 20$  microstrain at week 4,  $700 \pm 15$  at week 5,  $681 \pm 14$  at week 6 and  $698 \pm 14$  at week 7). While the fracture prevention step of the rtFE led to an increase in variation, it still was lower in comparison to all other time points past week 4.

## Discussion

In this study, we demonstrated that the introduction of an adaptive loading approach to individualise load would lead to reduced mechanical environment variance in a femur defect model in mice. Mechanical environments under the assumption of constant loading remain divergent throughout the reparative and remodelling phase of week 3 to week 7. This was more pronounced in the event of substantial bone growth seen in the loaded group, where mechanical stimulation is constantly decreasing under an assumption of constant load for loaded mice. Conversely, a substantial increase in median strain in the control mice is observed with declining bone volume. With the constant loading assumption the lowest variation in median strain is at week 7, where all bones have sufficiently bridged and fragile structures of the callus are being or have been modelled into new cortical bone or have been removed in remodelling processes. This indicates how changes in geometry from loading interventions cause large changes in the mechanical environment, which by the very nature of the fracture-healing environment are present, with or without loading. Contrasting the constant loading assumption, when rFE adaptation is applied, even with fracture prevention screening, we can clearly see that we are able to keep the median strains similar, and reduce group variance, for all mice. The rFE adaptation responds with changes in bone volume, with control mice requiring a decrease in mechanical load throughout the study, i.e. as excess bone tissue is removed via remodelling, a similar mechanical load would produce a greater median strain within the tissue, hence the load needs to be reduced to compensate for these changes. Contrastingly, the loaded mice display an increasing level of loading required to develop a sufficient strain within the tissue, this is due to loading causing greater bone formation and hence more structural regions to support a particular load. From the displayed data, it is quite clear that if one wants a consistent or targetable degree of mechanical stimulation, one needs to counter the changes in geometry during the repair and remodelling phases, and hence adaptation of loading is required to minimise strain variance between mice at the tissue level. On the other hand, it is clear that using a constant load will lead to varying mechanical environments during the course of fracture healing, delivering drastically different mechanical stimulation to each mouse and its bone tissue. rFE adaptation allows the identification of a set of loading parameters (**Figure 3.14**), which would achieve a more consistent mechanical environment both longitudinally, throughout the study, as well as cross sectionally within any group, or across groups.

Even though we selected a target distribution with a median strain of 700 microstrain, this in practice can be any choice of distribution centred on any particular median value. However, it would obviously make sense to select a distribution that one hypothesises would give a particularly effect, such as bone growth. In the event of pharmaceutical intervention, one that could aim to create an environment as close to perfect quiescence as possible, minimising the confounding of the pharmaceutical intervention by a longitudinally or cross sectionally varying mechanical environment. Additionally, this approach has a primary advantage over approaches based on strain gauge measurements on the surface of the bone<sup>35,36,38</sup>. RtFE allows surfaces, which are inaccessible to strain gauges, yet active in formation and resorption events in the callus region, to be included in strain targeting.

While the fracture prevention approach is conservative, it plays a critical role in preventing load adaptation reaching dangerously high strains in the potential fragile environment within the reparative and remodelling phases. Often once the time point has been reached where the experimental design calls for loading to begin, there are several animals with partially or incompletely bridged fractures. In **Figure 3.12** b & c, we can see the difference from delicate truss like structure to a more solidified cortical structure within the same bone via drastic changes in median strain. While the majority of mice for this model heal quickly and well, other models can include larger defects that require more time to bridge<sup>16</sup>, leaving the start date of loading in doubt. Even in the presented data, where the fracture gaps are relatively small, several mice displayed low bone volume at week 3 and hence had less structure to absorb load. This leads to small, fragile structures within the callus being over loaded. This can be clearly seen in **Figure 3.11a** & b, where a very small number of voxels, in comparison to total voxels, exceed the 1% strain margin, yet in **Figure 3.11c**, one can observe that many of these highly strain voxels lie next to one another in the thin structural parts of the callus. This increases the risk of refracture and hence poses a risk to the animal. From this visualisation, it becomes clear why the general strain distribution can be misleading in terms of identifying the appropriate load. Without proper visualisation and screening for the upper limit of strains in the tissue, there a high chance of excessive loading of fragile, small structures within the callus, impairing healing, or at worst threatening the welfare of the animal. While the above mentioned fracture risk approach is conservative and will not provide the same accuracy of a validated failure assessment of the bone tissue, it provides a metric for justification of reducing loading forces in the event that animal welfare may be compromised. Hence, a conservative estimate is appropriate given the experimental situation.

Limitations of the above work are largely related to simulation accuracy and correct description of boundary conditions. Micro-FE has been validated as an approach to simulate strains within normal bone as well as callus<sup>39-42</sup>. However, it has proved challenging to validate micro-FE at a tissue level and well specified boundary conditions are essential for accurate results<sup>42</sup>. Since the core intent of the rtFE adaptation will be implementation in conjunction with a loading machine in an experimental setting, boundary conditions merely need to match such an actuators behaviour. Regardless, this would be a requirement for accurate modelling of the mechanical environment in post-processing and mechanoregulation analysis. This implies that the best use of the concept of adaptive loading is in conjunction with a well-designed and accurate mechanical loading device in defect healing experiments. In this dataset's case, we assumed only uniaxial loads. However, the boundary conditions could be expanded to any set of uniaxial, shear, bending or torsional boundary conditions with the same principle and analysis applied. Additionally, it is important to note that this approach is not limited to mice. Targeted mechanical stimulus would have the potential to allow induction of specific strain distributions within any bone, fracture or mechanically responsive tissue whether it be in mice, rats, sheep or humans.

Here we analysed mice with the same fixation systems, same sex, operated on by the same surgeon in the same environment, ideally leading to a best-case scenario for external factor that could drive healing differences, yet variances remained. Even though it is well established that tissue level strains are the main driver behind remodelling and healing<sup>2,16</sup> the vast majority of mechanical interventions do not aim to target particular strains within the tissue directly. However, it is possible that an individualised adaptive loading approach, derived from longitudinal *in vivo* imaging, targeting a specific strain distribution could lead to improved results, reduced confounds and deliver improved outcomes in studies and approaches that have historically produced mixed results. Finally, with the growth in interest and application of personalised medicine the individualised approaches in mice could possibly be translated to humans. In this case, rtFE adaptation would be applicable for mechanical intervention for fractures in patients.

Mechanical environments differ greatly within defect models, even within a group of mice of identical strain, fixation and surgeon. We have shown the need to reduce the inter-animal variance in tissue scale mechanical strains loaded models of bone healing. We propose to do this via optimising each mechanical environment to achieve as similar tissue level strains as

possible between individuals within each group. Mechanical environment optimisation provides several benefits within loading models: a) it allows targeting of a strain distribution, providing a specific median strain within the bone tissue, b) it reduces in-group mechanical environment variance, both longitudinally and cross-sectionally, and c) it reduces the probability of refracture in the callus region of the animal. We propose incorporating mechanical environment optimisation into the experimental pipeline; a process, which we have named Real Time Finite Element (rtFE) adaptation. This would provide a means of reducing mechanical environment variation throughout the post-bridging phrases. Such an approach can be executed during the conventional imaging-loading pipeline with minimal additional time under anaesthetic for each animal. We believe that when coupled with accurate identification of mechanical dosages required to optimise defect-healing outcome, rtFE adaptive loading can be used to specify and apply these required dosages to homogenise the mechanical environment and reduce variance in both impaired and non-impaired healing cases.

## **Acknowledgements**

The authors would like to acknowledge support from the European Union (ERC Advanced MechAGE, ERC-2016-ADG-741883). E. Wehrle received funding from the ETH Postdoctoral Fellowship Program (MSCA-COFUND, FEL-25\_15-1).

## **Competing Interests**

The authors declare no competing interests



---

## References

- 1 Paul, G. R., Malhotra, A. & Muller, R. Mechanical Stimuli in the Local In Vivo Environment in Bone: Computational Approaches Linking Organ-Scale Loads to Cellular Signals. *Curr Osteoporos Rep* **16**, 395-403, doi:10.1007/s11914-018-0448-6 (2018).
- 2 Schulte, F. A. *et al.* Local Mechanical Stimuli Regulate Bone Formation and Resorption in Mice at the Tissue Level. *Plos One* **8**, doi:ARTN e62172 10.1371/journal.pone.0062172 (2013).
- 3 Goodman, S. & Aspenberg, P. Effects of Mechanical Stimulation on the Differentiation of Hard Tissues. *Biomaterials* **14**, 563-569, doi:Doi 10.1016/0142-9612(93)90171-W (1993).
- 4 Morgan, E. F. *et al.* Correlations between local strains and tissue phenotypes in an experimental model of skeletal healing. *J Biomech* **43**, 2418-2424, doi:10.1016/j.jbiomech.2010.04.019 (2010).
- 5 Burr, D. B. *et al.* In vivo measurement of human tibial strains during vigorous activity. *Bone* **18**, 405-410, doi:Doi 10.1016/8756-3282(96)00028-2 (1996).
- 6 Verbruggen, S. W., Vaughan, T. J. & McNamara, L. M. Strain amplification in bone mechanobiology: a computational investigation of the in vivo mechanics of osteocytes. *J R Soc Interface* **9**, 2735-2744, doi:10.1098/rsif.2012.0286 (2012).
- 7 Vaughan, T. J., Verbruggen, S. W. & McNamara, L. M. Are all osteocytes equal? Multiscale modelling of cortical bone to characterise the mechanical stimulation of osteocytes. *Int J Numer Meth Bio* **29**, 1361-1372, doi:10.1002/cnm.2578 (2013).
- 8 You, J. *et al.* Substrate deformation levels associated with routine physical activity are less stimulatory to bone cells relative to loading-induced oscillatory fluid flow. *J Biomech Eng-T Asme* **122**, 387-393, doi:Doi 10.1115/1.1287161 (2000).
- 9 Fritton, S. P., McLeod, K. J. & Rubin, C. T. Quantifying the strain history of bone: spatial uniformity and self-similarity of low-magnitude strains. *J Biomech* **33**, 317-325, doi:Doi 10.1016/S0021-9290(99)00210-9 (2000).
- 10 Karali, A. *et al.* Full-field strain of regenerated bone tissue in a femoral fracture model. *J Microsc*, doi:10.1111/jmi.12937 (2020).
- 11 Augat, P., Simon, U., Liedert, A. & Claes, L. Mechanics and mechano-biology of fracture healing in normal and osteoporotic bone. *Osteoporosis Int* **16**, S36-S43, doi:10.1007/s00198-004-1728-9 (2005).

- 12 Claes, L., Augat, P., Suger, G. & Wilke, H. J. Influence of size and stability of the osteotomy gap on the success of fracture healing. *J Orthop Res* **15**, 577-584, doi:DOI 10.1002/jor.1100150414 (1997).
- 13 Wehrle, E. *et al.* Evaluation of longitudinal time-lapsed *in vivo* micro-CT for monitoring fracture healing in mouse femur defect models. *Sci Rep* **9**, 17445, doi:10.1038/s41598-019-53822-x (2019).
- 14 Rontgen, V. *et al.* Fracture Healing in Mice under Controlled Rigid and Flexible Conditions Using an Adjustable External Fixator. *J Orthop Res* **28**, 1456-1462, doi:10.1002/jor.21148 (2010).
- 15 Claes, L. E. & Heigele, C. A. Magnitudes of local stress and strain along bony surfaces predict the course and type of fracture healing. *J Biomech* **32**, 255-266, doi:Doi 10.1016/S0021-9290(98)00153-5 (1999).
- 16 Tourolle né Betts, D. C. *et al.* The association between mineralised tissue formation and the mechanical local *in vivo* environment: Time-lapsed quantification of a mouse defect healing model. *Sci Rep-Uk* **10**, 1-10, doi:10.1038/s41598-020-57461-5 (2020).
- 17 Claes, L., Eckert-Hubner, K. & Augat, P. The fracture gap size influences the local vascularization and tissue differentiation in callus healing. *Langenbeck Arch Surg* **388**, 316-322, doi:10.1007/s00423-003-0396-0 (2003).
- 18 Claes, L. E. *et al.* Effects of mechanical factors on the fracture healing process. *Clin Orthop Relat R*, S132-S147 (1998).
- 19 Brady, R. D. *et al.* Closed head experimental traumatic brain injury increases size and bone volume of callus in mice with concomitant tibial fracture. *Sci Rep-Uk* **6**, doi:ARTN 34491 10.1038/srep34491 (2016).
- 20 Shi, H. F., Cheung, W. H., Qin, L., Leung, A. H. C. & Leung, K. S. Low-magnitude high-frequency vibration treatment augments fracture healing in ovariectomy-induced osteoporotic bone. *Bone* **46**, 1299-1305, doi:10.1016/j.bone.2009.11.028 (2010).
- 21 Leung, K. S. *et al.* Low-magnitude high-frequency vibration accelerates callus formation, mineralization, and fracture healing in rats. *J Orthop Res* **27**, 458-465, doi:10.1002/jor.20753 (2009).
- 22 Recknagel, S. *et al.* Experimental blunt chest trauma impairs fracture healing in rats. *J Orthop Res* **29**, 734-739, doi:10.1002/jor.21299 (2011).

- 
- 23 Wehrle, E. *et al.* The impact of low-magnitude high-frequency vibration on fracture healing is profoundly influenced by the oestrogen status in mice. *Dis Model Mech* **8**, 93-104, doi:10.1242/dmm.018622 (2015).
- 24 Wehrle, E. *et al.* Distinct Frequency Dependent Effects of Whole-Body Vibration on Non-Fractured Bone and Fracture Healing in Mice. *J Orthop Res* **32**, 1006-1013, doi:10.1002/jor.22629 (2014).
- 25 Klosterhoff, B. S. *et al.* Wireless sensor enables longitudinal monitoring of regenerative niche mechanics during rehabilitation that enhance bone repair. *Bone* **135**, doi:10.1016/j.bone.2020.115311 (2020).
- 26 Kojimoto, H., Yasui, N., Goto, T., Matsuda, S. & Shimomura, Y. Bone Lengthening in Rabbits by Callus Distraction - the Role of Periosteum and Endosteum. *J Bone Joint Surg Br* **70**, 543-549 (1988).
- 27 Murao, H., Yamamoto, K., Matsuda, S. & Akiyama, H. Periosteal cells are a major source of soft callus in bone fracture. *J Bone Miner Metab* **31**, 390-398, doi:10.1007/s00774-013-0429-x (2013).
- 28 Claes, L., Recknagel, S. & Ignatius, A. Fracture healing under healthy and inflammatory conditions. *Nat Rev Rheumatol* **8**, 133-143, doi:10.1038/nrrheum.2012.1 (2012).
- 29 Wolf, S. *et al.* Effects of high-frequency, low-magnitude mechanical stimulus on bone healing. *Clin Orthop Relat R*, 192-198 (2001).
- 30 Palomares, K. T. S. *et al.* Mechanical Stimulation Alters Tissue Differentiation and Molecular Expression during Bone Healing. *J Orthop Res* **27**, 1123-1132, doi:10.1002/jor.20863 (2009).
- 31 Gardner, M. J. *et al.* In vivo cyclic axial compression affects bone healing in the mouse tibia. *J Orthop Res* **24**, 1679-1686, doi:10.1002/jor.20230 (2006).
- 32 Liu, C. *et al.* Effects of mechanical loading on cortical defect repair using a novel mechanobiological model of bone healing. *Bone* **108**, 145-155, doi:10.1016/j.bone.2017.12.027 (2018).
- 33 Rapp, A. E. *et al.* Systemic Mesenchymal Stem Cell Administration Enhances Bone Formation in Fracture Repair but Not Load-Induced Bone Formation. *Eur Cells Mater* **29**, 22-34, doi:DOI 10.22203/eCM.v029a02 (2015).
- 34 Morse, A. *et al.* Sclerostin Antibody Increases Callus Size and Strength but does not Improve Fracture Union in a Challenged Open Rat Fracture Model. *Calcified Tissue Int* **101**, 217-228, doi:10.1007/s00223-017-0275-2 (2017).

- 
- 35 Birkhold, A. I. *et al.* Mineralizing surface is the main target of mechanical stimulation independent of age: 3D dynamic in vivo morphometry. *Bone* **66**, 15-25, doi:10.1016/j.bone.2014.05.013 (2014).
- 36 Webster, D. J., Morley, P. L., van Lenthe, G. H. & Muller, R. A novel in vivo mouse model for mechanically stimulated bone adaptation - a combined experimental and computational validation study. *Comput Method Biomec* **11**, 435-441, doi:10.1080/10255840802078014 (2008).
- 37 Virtanen, P. *et al.* SciPy 1.0: fundamental algorithms for scientific computing in Python. *Nat Methods* **17**, 261-272, doi:10.1038/s41592-019-0686-2 (2020).
- 38 Razi, H. *et al.* Skeletal maturity leads to a reduction in the strain magnitudes induced within the bone: A murine tibia study. *Acta Biomater* **13**, 301-310, doi:10.1016/j.actbio.2014.11.021 (2015).
- 39 Shefelbine, S. J. *et al.* Prediction of fracture callus mechanical properties using micro-CT images and voxel-based finite element analysis. *Bone* **36**, 480-488, doi:10.1016/j.bone.2004.11.007 (2005).
- 40 Oliviero, S., Giorgi, M. & Dall'Ara, E. Validation of finite element models of the mouse tibia using digital volume correlation. *J Mech Behav Biomed* **86**, 172-184, doi:10.1016/j.jmbbm.2018.06.022 (2018).
- 41 Zysset, P. K., Dall'ara, E., Varga, P. & Pahr, D. H. Finite element analysis for prediction of bone strength. *Bonekey Rep* **2**, 386, doi:10.1038/bonekey.2013.120 (2013).
- 42 Chen, Y. *et al.* Micro-CT based finite element models of cancellous bone predict accurately displacement once the boundary condition is well replicated: A validation study. *J Mech Behav Biomed* **65**, 644-651, doi:10.1016/j.jmbbm.2016.09.014 (2017).

## **Chapter 4 :**

### **Investigation of multiscale**

### **mechanoregulation in fracture healing in**

### **mice**

# Mechanoregulation of bone healing and remodelling at tissue and cell scale in a femur defect healing model in mice

Graeme R Paul<sup>1</sup>, Ariane C. Scheuren<sup>1</sup>, Nicole Grob-Mcdonnald<sup>1</sup>, Bryant Schroeder<sup>1</sup>, Dilara Yilmaz<sup>1</sup>, Ralph Müller<sup>1</sup>

1. Institute for Biomechanics, ETH Zurich, Zurich, Switzerland

## Abstract

Bone is a dynamic material, in which mechanical loading drives healing and remodelling. The four dominant scales within bone – organ, tissue, cell and molecular – display a complex interconnectivity. Mechanical forces at organ scale cause heterogeneous tissue level strains, which stimulate osteocytes to produce proteins. These proteins govern the actions of osteoblasts, leading to bone formation, and osteoclasts, leading to bone resorption. Several aspects of this multiscale process within fracture healing have been extensively researched and are well understood. However, a comprehensive approach that links loads at organ scale to proteins expressed at molecular scale in fracture healing is currently lacking. In this study, we applied individualised organ-scale loads, measured during the fracture healing process, to simulate tissue-scale strains within twelve mice. We analysed the ability of these strains to predict the formation, resorption or quiescence of the tissue, and showed that fracture healing was mechanoregulated at tissue scale. These strains were combined with a local *in vivo* environment (*LivE*) approach, where immunohistochemistry-stained sections from two mice were registered to micro-CT scans. We linked the micro-FE-simulated tissue-scale strains from these micro-CT scans to the locations of cells within these two bones, and hence to sites of formation, resorption and quiescence. We observed that cells under high levels of mechanical stimulation are more likely to be associated with sites of formation, while those under low levels of mechanical stimulation are more likely to be associated with regions of resorption. This indicates that tissue-scale mechanoregulation occurs at cell scale in addition to tissue scale. In addition, we assessed the degree of staining of two relevant proteins, namely Sclerostin, a bone formation inhibitor, and RANKL, an osteocyte progenitor. We observed that Sclerostin

expression was inversely related to mechanical stimulation, where regions of high mechanical stimulation were associated with unstained cells. This study lays the groundwork for full integration of micro-CT, micro-FE and immunohistochemistry, and shows promising preliminary results, which indicate that mechanoregulation of bone is observable *in vivo* from organ to molecular scale.

**Keywords:**

Bone healing, bone remodelling, multiscale, mechanoregulation, immunohistochemistry, micro-CT, micro-FE, Sclerostin, RANKL, osteocytes

## Introduction

Bone is a multiscale and hierarchical material<sup>1,2</sup>, in which mechanical loading regulates adaptation and healing<sup>3</sup>. The multiple scales of bone, which are roughly divided into organ, tissue, cell and molecular scales, govern the transmission of mechanical signals, and thereby influence how bone tissue remodels and heals. At organ scale, bones are loaded i) physiologically, via locomotion of the animal<sup>4-10</sup>, or ii) extra-physiologically<sup>8,11-18</sup>, via interventions such as vibration plates, machines or actuated implants. Organ-scale mechanical loading is transmitted to the bone tissue<sup>19</sup>, where the local microarchitecture of the bone leads to heterogeneous strain fields<sup>20,21</sup>, which drive localised formation and resorption of bone<sup>22,23</sup>. These formation and resorption processes, common to both bone remodelling and bone healing, optimise the bone structure to applied loads<sup>24</sup>, reinforcing regions of high strain, and removing unnecessary tissue, preventing low strains. At the cellular scale, both bone remodelling and fracture healing are regulated by proteins that signal cells to lay down new bone or remove structurally redundant bone. Three cell types are essential in these processes: osteocytes, which are embedded within the bone tissue, and osteoclasts and osteoblasts, which lie on its surface. Osteoblasts lay down packets of lowly mineralised bone tissue<sup>25,26</sup>, which is mineralised over time. Opposing this action, osteoclasts remove bone<sup>26</sup>. The behaviour of these two cell types is coordinated by osteocytes<sup>25,27</sup>, which act as mechanical sensors of tissue deformation<sup>3,28-30</sup> and fluid flow within the canaliculi-lacuna network<sup>3,30-32</sup>. At organ and tissue scale, it is well established that mechanical loading is a key governing factor in the healing of fractures and bone remodelling<sup>23,33-41</sup>; however, the links between mechanics and biological responses over the multiple scales of bone are poorly understood.

Spatial scales within the bone need to be reconciled with temporal changes occurring *in vivo*. Micro-CT allows accurate imaging at organ and tissue scales, but does not provide sufficient spatial resolution to accurately discern small features such as cells *in vivo*. However, micro-CT enables *in vivo* imaging, combining moderate spatial resolution with the capability to repeat measurements over the duration of an experiment. A broad range of microscope technologies offers spatial resolutions sufficient to image cells, and to some extent molecules, within bone tissue<sup>42</sup>. However, these techniques often require extensive pre-processing and are hence limited to study end points. Attempts to reconcile these issues have resulted in a Local *in vivo* Environment (*LivE*) immunohistochemistry approach<sup>43,44</sup>, where 2D histological sections are registered into 3D longitudinal micro-CT images. The registered data is linked to micro-FE



simulations to locate cells within their mechanical environments. Scheuren et al.<sup>45</sup> applied this approach to analyse two specific proteins in a frequency-dependent model of bone adaptation: Sclerostin, an osteocyte-specific bone formation inhibitor<sup>46-49</sup>, and receptor activator of nuclear factor- $\kappa$ B ligand (RANKL), an osteoclast differentiator that promotes resorption<sup>26,47-49</sup>. Each cell was linked to its mechanical environment and assessed for relationships between mechanical stimulation, protein expression, and associations with sites of formation, quiescence and resorption. Scheuren et al.<sup>45</sup> observed a lower level of Sclerostin and RANKL in cyclically loaded mice, compared to sham loaded mice. However, the authors identified limited links between the mechanical stimulation of specific cells and the expression of Sclerostin and RANKL in the *LivE*<sup>45</sup>.

In this study, we investigated the effects of individualised organ-scale habitual loading on the tissue- and cell-scale mechanoregulatory responses in a defect healing model in mice. In particular, we assessed the mechanoregulation of sites of formation, resorption and quiescence with respect to tissue-scale mechanical strains. We also examined these regions with respect to the locations of osteocytes, the mechanical signal in their *LivE*, and their regulation of Sclerostin and RANKL. To achieve this, we applied micro-FE on a longitudinal micro-CT-imaged dataset of twelve mice and analysed mechanoregulated changes at a tissue scale. Using immunohistochemistry, we stained two sectioned femurs from two mice for Sclerostin and RANKL from the study endpoint (seven weeks after surgery). These sections were linked to the simulated mechanical environment, and relationships between cellular expression of Sclerostin and RANKL were investigated. We hypothesised that high tissue-scale strain would lead to bone formation and the downregulation of Sclerostin and RANKL, while low strain would lead to bone resorption and the upregulation of these proteins. The use of measured boundary conditions allowed us to assign specific values of strain to these relationships, and hence to group different animals with physiologically relevant mechanical environments.

## Materials and Methods

### *In vivo data*

Details regarding the *in vivo* experiment, imaging and micro-FE simulations can be found in Chapter 3.1. Effective strain<sup>50</sup> was used as the mechanical environment, aligning with work done by Tourolle et al<sup>41</sup>. Visual examples of the temporal progression of healing can be seen in Chapter 3.1 in **Figure 3.3**.

### *Multi-density analysis*

For all morphological and mechanoregulatory data, multiple thresholds were used to observe patterns in the range of tissue mineralisation that occur within healing bone. Masks were created for thresholds from 395 mg HA/cm<sup>3</sup> to 720 mg HA/cm<sup>3</sup> in steps of 25 mg HA/cm<sup>3</sup>. These masks were applied to bone volume, bone volume rate, mechanical environment, area under the curve, and correct classification rate analyses. This method is described in detail by Tourolle et al.<sup>41</sup>.

### *Analysis of bone volume and formation/quiescence and resorption rates and mechanical environment*

Bone volume was calculated by counting the number of voxels above a certain density threshold. Regions of formation, quiescence and resorption were calculated by the binary difference between an image at a given time point and the image at a preceding time point. Voxels present in both images were labelled quiescent. Voxels present only in the most current time point were labelled formation, while those present only in the preceding time point were labelled resorption. Masks were created to describe these regions. The mechanical stimuli, as calculated above, were mapped to each appropriate voxel. The mean strain at each time point and density was then calculated for each mouse. The data from each mouse was averaged to obtain the group response.

### *Analysis of local mechanoregulation*

The scaled results of the micro-FE simulation in terms of effective strain was used as a measure of mechanical stimuli. The area under the curve (AUC) of a receiver operating characteristic (ROC) curve was used to assess the performance of the particular effective strain value as a predictor of formation and mineralisation. A higher AUC means that the identification of a randomly selected voxel changing, for a given strain value, to a site of formation being a true positive is greater than a negative. Hence, an AUC greater than 0.5 implies that the change in voxel (either formation or increase in mineralisation) was associated with mechanical

stimulation. An AUC of 0.5 indicates no relationship between the mechanical stimuli and the voxel, while an AUC below 0.5 indicates an inverse relationship between mechanical stimuli and the voxel's behaviour.

As prediction of formation, quiescence and resorption from preceding strain is a multi-class classification problem, AUC/ROC approaches could not be used. Hence, the mechanobiology of callus remodelling classification approach developed by Tourolle et al.<sup>41</sup> was applied. This approach uses two thresholds within the effective strain range; a higher one to classify sites of formation, and a lower one to classify sites of resorption. Any value between these thresholds was classified as quiescence. The ground truth was determined by comparing the sequential images. Similar to ROC, the thresholds were then swept through the range of possible effective strain values to derive a matrix encoding whether a voxel was correctly classified based on the two thresholds. The correct classification rate (CCR) was determined for each mouse at each time point and at each tissue density level. As three states are possible (formation, quiescence and resorption), the maximum CCR would need to exceed 33% to indicate mechanoregulation within the tissue.

#### *Histologies and Imaging*

Twelve hours after micro-CT scanning, the right femurs were removed from three mice. These three femurs were fixed in 4% neutrally buffered formalin for 24 hours, dehydrated in increasing levels of alcohol for three days (70%, 80% and 100%), and subsequently stored in 70% alcohol until they were decalcified in 12.5% EDTA for 10 days. Post decalcification, the samples were embedded in paraffin and sectioned into 10 µm thick serial sections. Sections were stained with Haematoxylin and Eosin (H&E) for lacunae and osteocyte detection, or stained using immunohistochemistry for antibodies against Sclerostin or RANKL. This process involved the deparaffinisation of the section with xylene, followed by rehydration with graded ethanol. Primary antibodies were incubated over night at 4 °C, rinsed with TBS-Tween, and blocked at room temperature for ten minutes using peroxidase-blocking buffer solution. RANKL sections were incubated with Evison+ System HRP Labelled Polymer Anti-Rabbit (K4003, DAKO), and Sclerostin sections were stained with anti-goat IgG HRP. Both sections were incubated at room temperature for sixty minutes and counterstained with FastGreen (F7258, Sigma-Aldrich, St Louis, MO). Diaminobenzidine (K3468, Dako) was used as a detection substrate. All sections were imaged with a Panoramic 250 Slide Scanner (3D Histech, Budapest, Hungary) at 20x magnification.

### Linking tissue-scale strain and cell signals

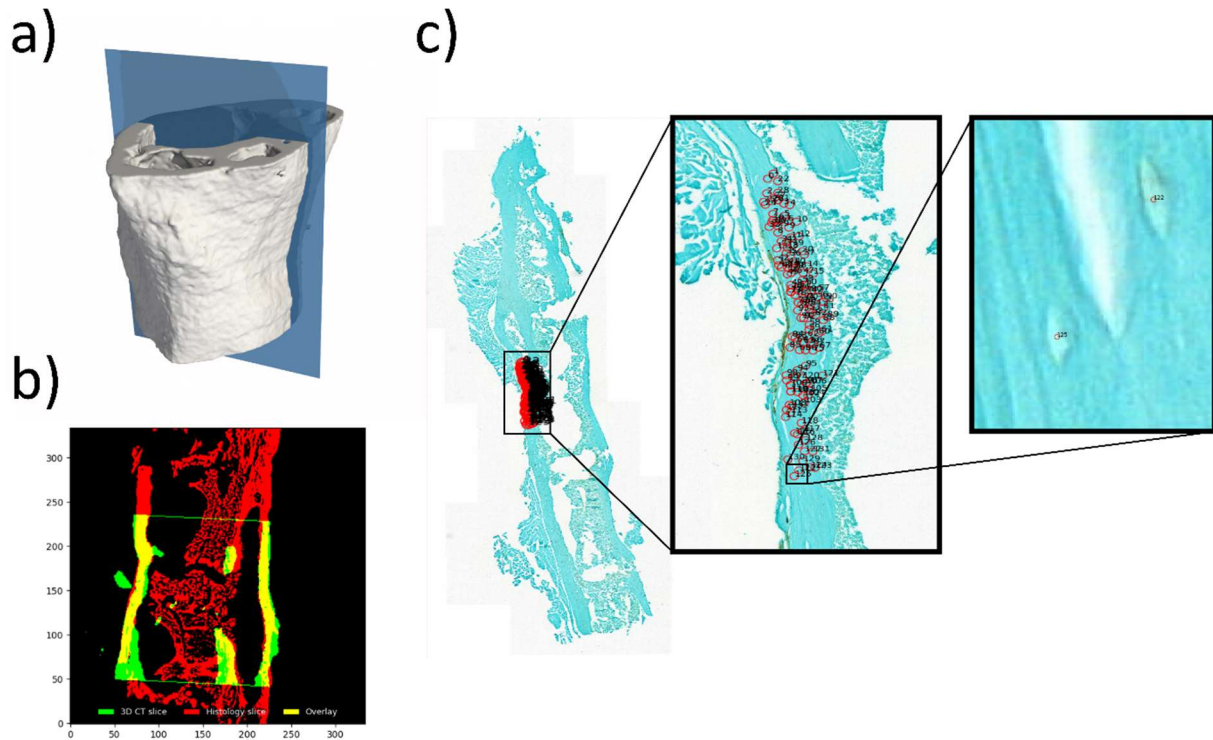


**Figure 4.1:** Localisation of sections and cells. Sections were found within the micro-CT image using custom-built software (a), which allowed overlaying of both images (b). Cells are located within the section (c).

### Section registration

Images of histological sections with no visible artefacts were scaled to a matching resolution of the micro-CT images ( $0.3 \mu\text{m}$  to  $10.5 \mu\text{m}$ ). The images were then binarised and manually registered to the reconstructed 3D volume or the appropriate micro-CT image of the mouse (**Figure 4.1**) at week seven. This registration was performed using an in-house software tool. Each slice was held stationary while a plane was moved through the 3D volume until a solution was found. Due to discrepancies between histological sections and micro-CT images, registration was optimised to relevant local features, as opposed to the whole slice.

### Cell identification and region extraction

Each histology slice was assessed for specific cell locations in each region of interest (**Figure 4.1**). This was performed using in-house software and involved manual selection of each cell. Each cell was assigned a 2D coordinate within the slice, which was then transformed to a 3D coordinate corresponding to a location within the 3D micro-CT image. From the location on the slice, a region representing the *LivE* was extracted. This corresponded to a 50 by 50 pixel

region on the slice, or a 15  $\mu\text{m}$  by 15  $\mu\text{m}$  square. A similar extraction was done in three dimensions (15  $\mu\text{m}$  by 15  $\mu\text{m}$  by 15  $\mu\text{m}$ ) from the result of the micro-FE simulation. The maximum and mean of the effective strain in the extracted region were calculated. Finally, the same three-dimensional region was also extracted from the formation/quiescent/resorption masks to locate remodelling changes within the cellular environment.

#### *Assessment of protein expression*

The extracted regions corresponding to each cell on the histology slice were classified as either unstained or stained. This was done via thresholding ( $\text{threshold}_{\text{Sclerostin}} = 180$ ,  $\text{threshold}_{\text{RANKL}} = 75$ ) of the blue channel of the RGB micrograph to separate stained areas from unstained areas. The number of stained pixels was counted and converted to a  $\mu\text{m}^2$  per osteocyte/cell. A stained region above 15  $\mu\text{m}^2$  for Sclerostin and above 75  $\mu\text{m}^2$  for RANKL, was considered stained. Regions below these thresholds were considered unstained.

#### *Assessment of remodelling association of cells*

Cells were linked to formation, quiescent or resorption sites by calculating the Euclidean distance to surrounding sites and assigning the category of the site with the smallest distance to the cell. If a cell was associated with more than one category, it was excluded from analysis.

#### *Analysis of temporal and spatial strain gradients*

To gain further insight into spatial and temporal links between cell associations with formation, quiescence and resorption and mechanical stimulation, we calculated the spatial and temporal gradients of effective strain. The spatial gradient was calculated as the difference between a voxel and its neighbouring effective strain in the x, y and z directions. The norm of the orthogonal vectors was calculated from these x, y, and z values, and the scalar value of the resultant vector was used. The temporal gradient was calculated as the difference between a voxel's effective strain at the time point of analysis, and the effective strain at the voxel in the same location at the preceding time point. For our analysis, this always refers to the difference between the effective strain at week 7 and week 6.

#### *Statistical analysis*

Unstained and stained cells and their respective mechanical environments were assessed for normality via a Shapiro-Wilks test and compared via either a parametric statistical test (if normal), or a non-parametric statistical test (if non-normal). All parametric comparisons between groups were performed using a two-tailed independent t-test, while a Mann-Whitney

U test was used for non-parametric significance testing. As the dataset was non-normally distributed, a Kruskal-Wallis test was used for comparisons of multiple means. All tests were performed using SciPy 1.0<sup>51</sup>.

## Results

In this study, we analysed the mechanoregulation of the remodelling phase of the fracture healing process. We combined longitudinal micro-CT with micro-FE simulated from measured boundary conditions. We applied classifiers to these two modalities to determine if effective strain is a predictor of sites of formation, resorption or quiescence. For two of the ten mice, we combined micro-CT images and micro-FE simulations with immunohistochemistry. We registered the 2D sections with the 3D micro-CT images, localised the cells observed in the 2D sections with their 3D locations, and determined the mechanical stimulation in each cell's *LivE*. Each cell was associated with the nearest site of formation, resorption or quiescence, and the area of staining for either Sclerostin or RANKL. From these associations, cell-scale relationships between mechanical stimulation, sites of formation, resorption and quiescence, and protein expression were established.

### *Tissue-scale longitudinal healing dynamics*

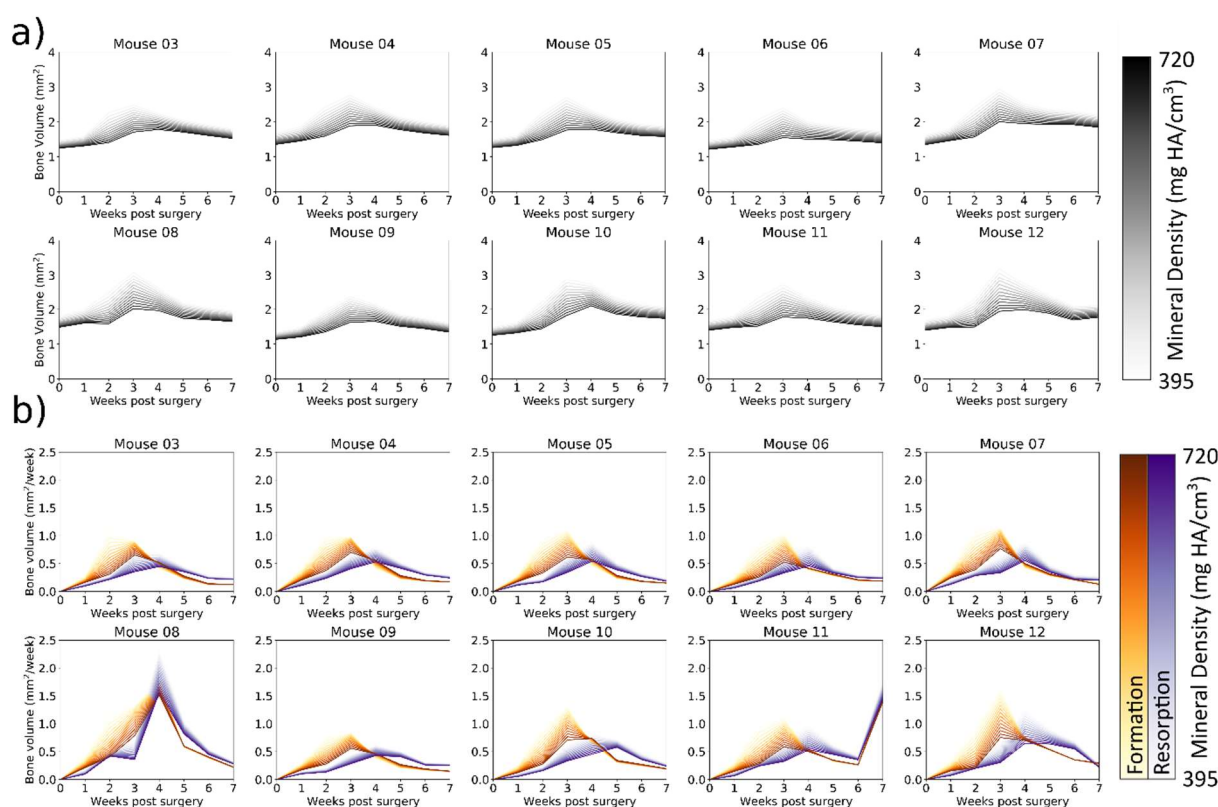


**Figure 4.2:** Individual healing dynamics of mice. a) All mice display a similar healing response. Initially a large amount of lowly mineralised bone tissue is formed, which then mineralises and remodels towards a state of equilibrium. b) Bone formation peaks at week 3, and resorption

peaks at week 4. By week 7, formation and resorption rates are almost equal, indicating that healing has given way to balanced remodelling.

Ten of twelve mice displayed successful healing (**Figure 4.2**), with bridging occurring between week 2 and week 3. Bone volume for all ten mice peaked at about  $2.75 \text{ mm}^3$  (**Figure 4.3**), with large amounts of lowly mineralised bone. This was then remodelled away and mineralised until roughly  $2 \text{ mm}^3$  remained (**Figure 4.3**). Peak bone formation occurred at week 3, with a rate of roughly  $1 \text{ mm}^3$  of bone formed per week in all but two mice. Mouse 08 and mouse 12 showed higher rates of bone formation ( $1.5 \text{ mm}^3$  per week) (**Figure 4.2**). Resorption peaked at roughly  $0.75 \text{ mm}^3$  per week for all mice, with the exception of mouse 09, which had a far higher rate of  $2 \text{ mm}^3$  per week. This counterbalanced the high rate of formation to result in a bone volume of roughly  $2 \text{ mm}^3$  by week 7, close to the average bone volume (**Figure 4.3**) for the ten mice. This indicates that healing was successful by the end of the study.

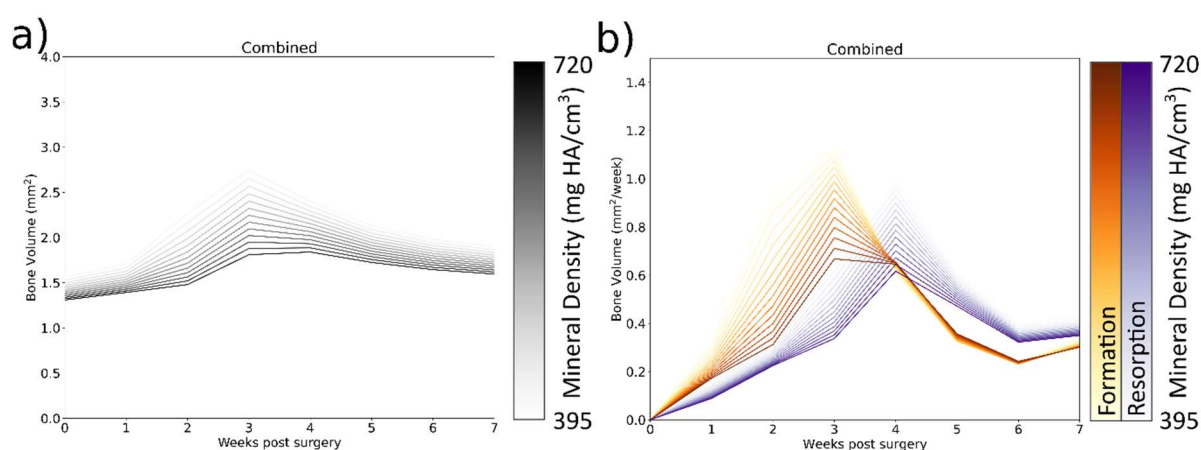


**Figure 4.3:** Group healing dynamics of mice. The average formation and resorption patterns were representative of each individual mouse. Formation peaked one week before resorption, and progressed towards balanced remodelling by week 7.



### Tissue-scale mechanical environment and mechanoregulation

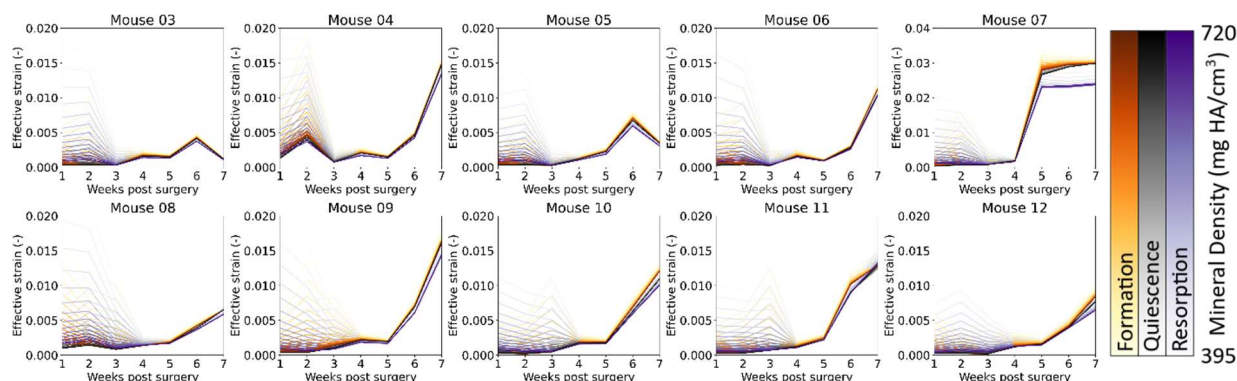


**Figure 4.4:** Individualised mechanical environment for all union mice.

From week 1 to week 3, lowly mineralised tissue showed a greater degree of mechanical stimulation than at later time points in all mice, with an upper bound of 0.013 strain for the lowest density level of bone. For all time points and in all mice, formation voxels experienced a higher level of mechanical stimulation than quiescence and resorption voxels.

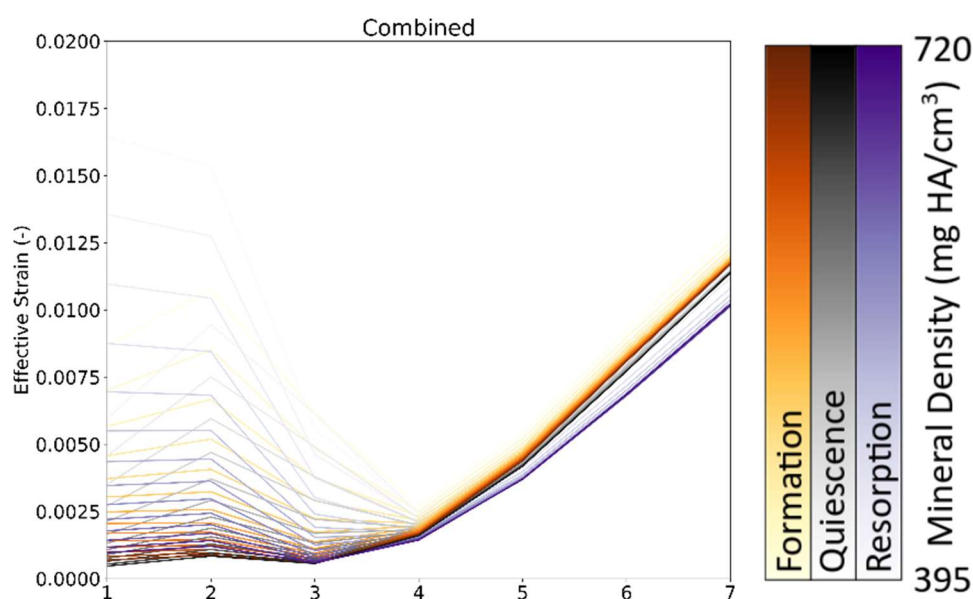


**Figure 4.5:** Average mechanical environment across all union mice.

In all mice, post bridging (week 4 onwards the AUC of the ROC was greater than 0.5 (**Figure 4.6**). This indicated that formation, as well as the mineralisation of those formed voxels, was

under mechanical control. On average, tissue of lower mineralisation displayed a greater degree of mechanical control based on AUC analysis for all time points post week 3 (**Figure 4.7**).

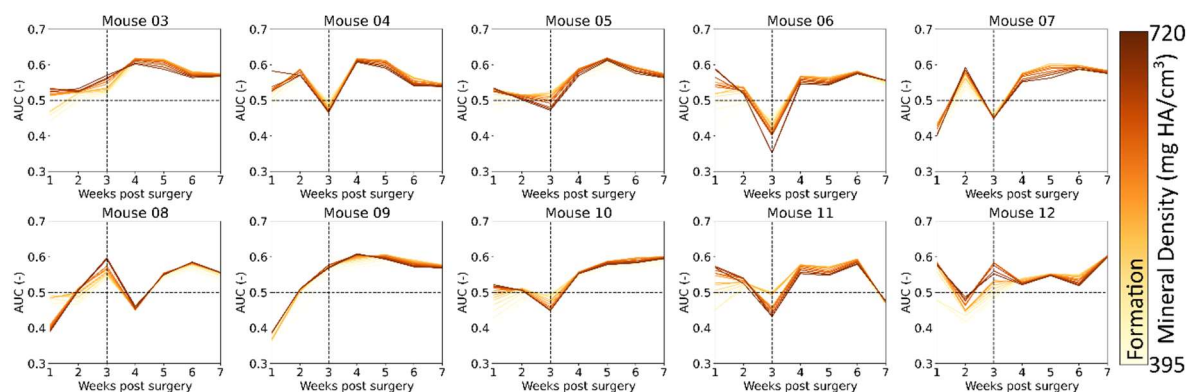


**Figure 4.6:** Area under the curve (AUC) for the receiver operating characteristic (ROC) curve of formation and mineralisation for each mouse.

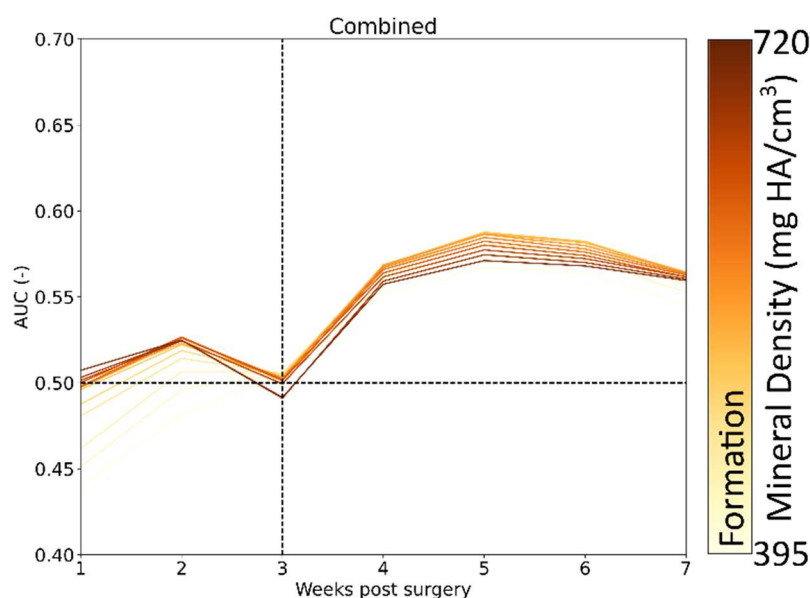


**Figure 4.7:** Average area under the curve (AUC) results for all mice

Similar patterns were seen in the CCR analysis, which was greater than 33% for all mice (**Figure 4.8**) and time points. This indicated that formation, resorption and quiescence were under mechanical control for the study duration. Mice 08, 11 and 12, all of which displayed a poor healing progression (see **Chapter 3.1**), exhibited a high level of CCR (above 48%) from week 3 until week 6. Contrastingly, the CCR of well-healed mice, such as mice 03 and 07, peaked at week 4 and then decreased to 45% or less. On average (**Figure 4.9**), the CCR peak at

week 4 was 48.5%. Formation, quiescence and resorption of lowly mineralised tissue were more likely to be predicted by effective strain for time points before week 4. After week four these differences disappeared, and the CCR was effectively equal for all mineralisation levels.

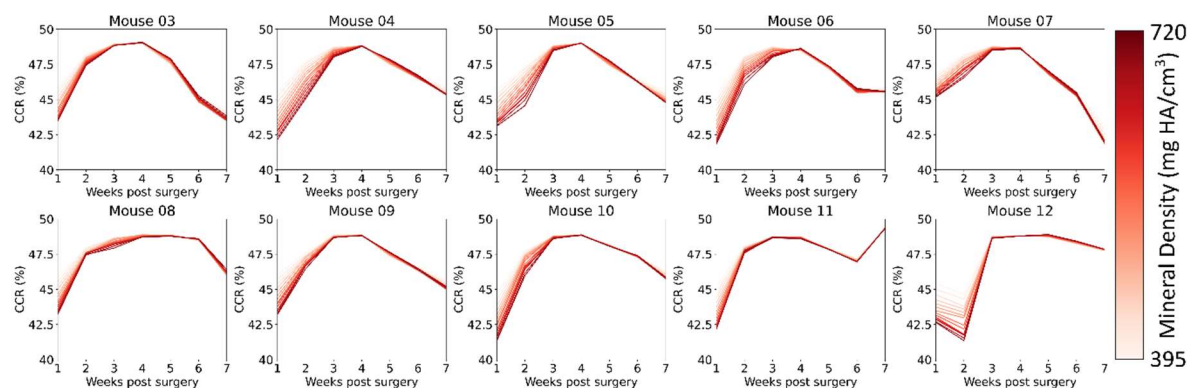


**Figure 4.8:** Correct Classification Rate (CCR) of individual mice.

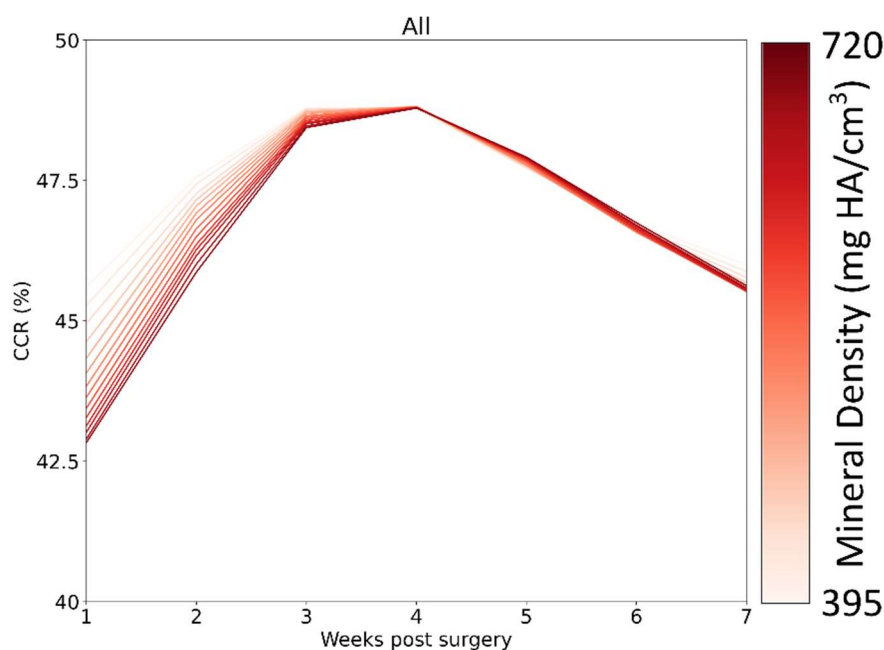


**Figure 4.9:** Group Correct Classification Rate (CCR).

#### *Tissue-scale observations of longitudinal healing dynamics from non-union mice*

Two mice formed non-union fractures during the duration of the study. (**Figure 4.10a and b**) These mice display a lack of either soft bone formation or mineralisation of soft tissue through all observations. In particular, mouse 01 displayed a large peak of resorption of all degrees of

mineralisation one week earlier than seen in other mice. Early formation and resorption rates did not differ greatly from the union mice at week 1 or week 2. However, from week 3 onwards formation rates were substantially lower than in union mice. Additionally, mouse 01 displayed a loss of over 30% of its bone tissue over the seven weeks.

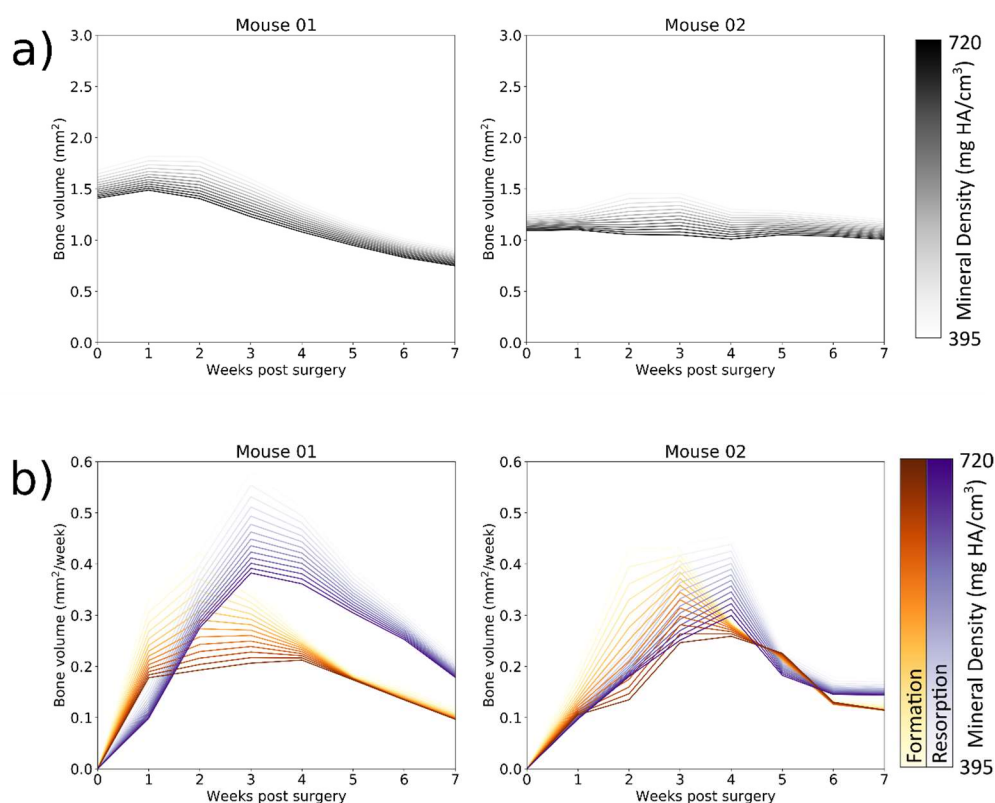


**Figure 4.10:** Bone volume and change in bone volume rates in non-union mice. a) Insufficient bone volume developed to bridge the fracture in both mouse 01 and mouse 02. b) Bone formation rates were substantially less than in union mice. Resorption rates displayed an earlier peak (week 3 instead of week 4) in non-union mice instead of union mice.

#### *Tissue-scale observations of the mechanical environment and mechanoregulation in non-union mice*

Low mechanical stimulation was seen in non-union mice (**Figure 4.11**) in comparison to union mice. Both mouse 01 and mouse 02 displayed bone strains within the region of 0.0025 strain, while union mice displayed strains roughly double that within the bone tissue prior to bridging. The CCR (**Figure 4.12**) of formation, quiescence and resorption was comparable to union mice, and ranged from 45 at week 1 to a peak of 48% at week 4. The CCR showed a greater value for tissue of lower mineralisation at earlier time points (weeks 1 through 4) than at later time points.

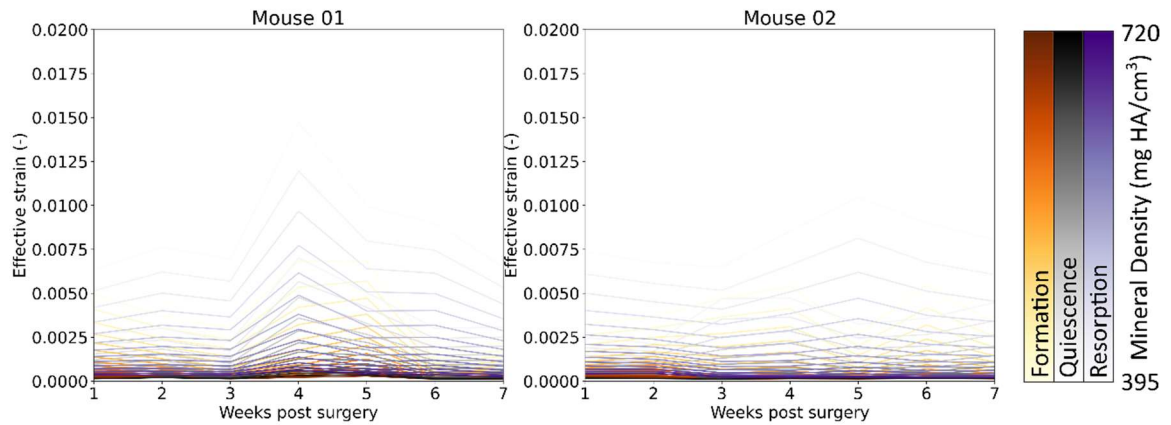


**Figure 4.11:** The mechanical environment of non-union mice. Based on habitual loading parameters, non-union mice displayed less mechanical stimulation than that seen union mice.

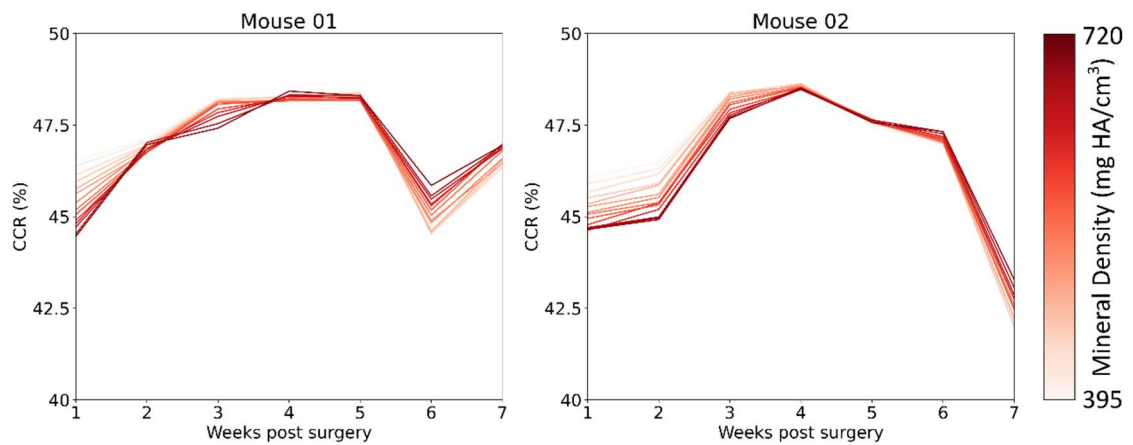


**Figure 4.12:** Correct Classification Rate (CCR) for non-union mice. The CCR for both mouse 01 and mouse 02 was above 33%, indicating that mechanoregulation even occurs even within a non-union fracture.

### Cell-scale mechanical relationships of cell-scale protein expression

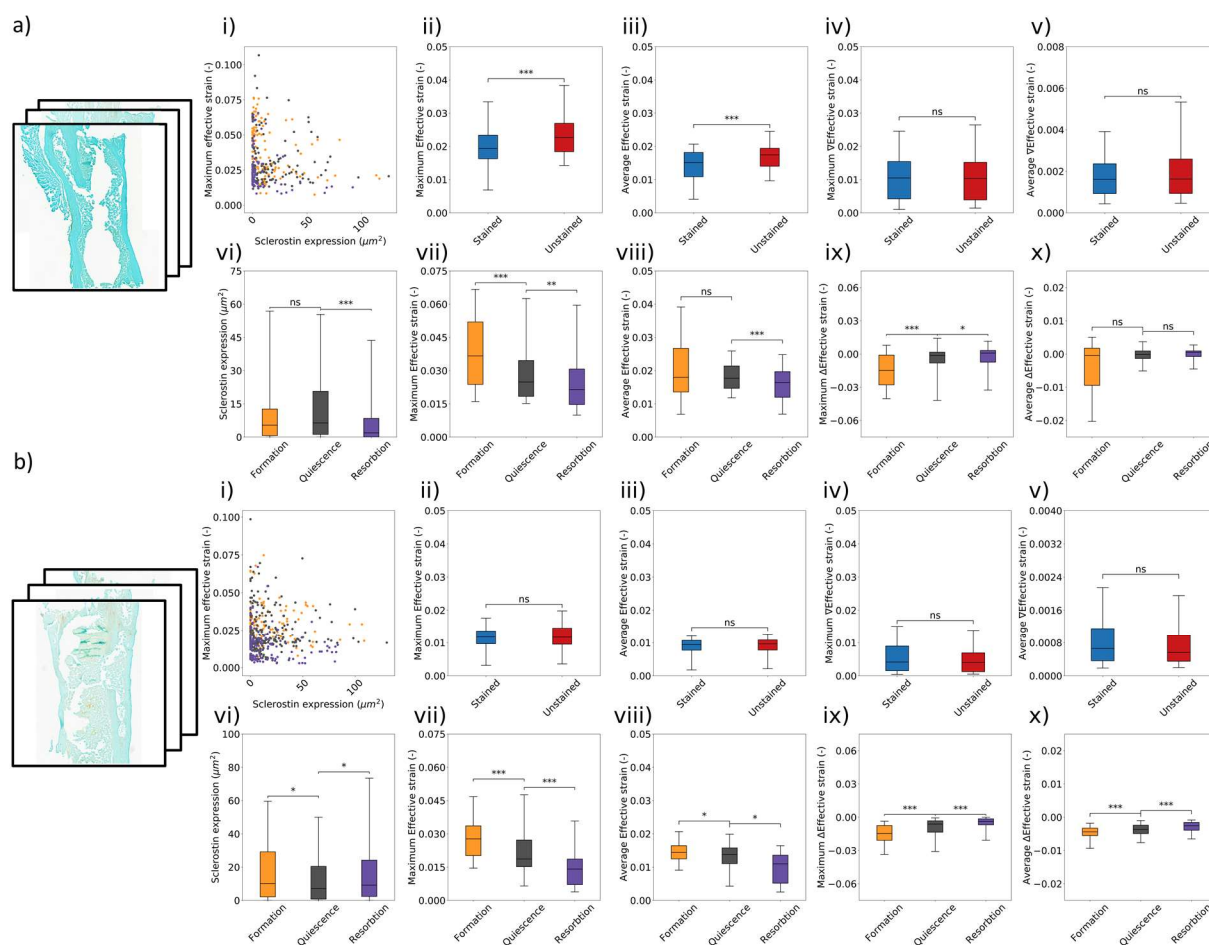


**Figure 4.13:** Results of Sclerostin staining analysis for mouse 09 (a) and mouse 10 (b). i) indicates the Sclerostin expression and maximum effective strain in the Live of each cell. ii) and iii) show the maximum and average effective strain in the Live for each cell categorised via thresholds. iv) and v) show the spatial gradients of maximum and average effective strain in the Live for each categorised cell. vi) groups cells by their nearest region of formation, quiescence and resorption to area of Sclerostin expression. vii), viii), ix) and x) group cells by their nearest region of formation, quiescence and resorption to maximum, average, temporal change in maximum, and temporal change in average effective strain, respectively, within the cell's Live. a) i-x) Mouse 09 displays mechanoregulation of Sclerostin staining without any dependence on formation, quiescence and resorption regions. Cells associated with formation, quiescence and resorption have high, medium and low maximum effective strains at week 6 in their Live in both mouse 09 (a vii, viii) and mouse 10 (b, vii, viii).

In mouse 09, Sclerostin expression showed a clear mechanical stimulation dependency. Cells expressing Sclerostin were significantly more likely to occur in regions of lower mechanical



---

stimulation than cells not expressing Sclerostin over all three sections (total 334 unstained cells, 156 stained cells). For all sections, both average and maximum regional effective strain displayed a significant positive difference between the mechanical environment of strain and unstained cells ( $p < 0.0001$ ). However, effective strain gradient, while often displaying the same directional relationship (i.e. unstained cells had a higher mechanical stimulus), did not display significance. Mouse 10 showed similar, yet non-significant, trends in both maximum and average effective strain. While unstained cells displayed a greater average and maximum mean effective strain, this result was not significant. In addition, neither average nor maximum effective strain gradient showed significance or a positive trend between unstained and stained cells. When grouped together, a strongly significant ( $p < 0.0001$ ) relationship was observed between the maximum effective strain in the *LiveE* of the cells and their staining. That is, unstained cells experienced a significantly higher mechanical stimulus in their immediate environment. This was also seen for the average effective strain in the environment ( $p < 0.0001$ ), but not for the maximum or average effective strain gradient.

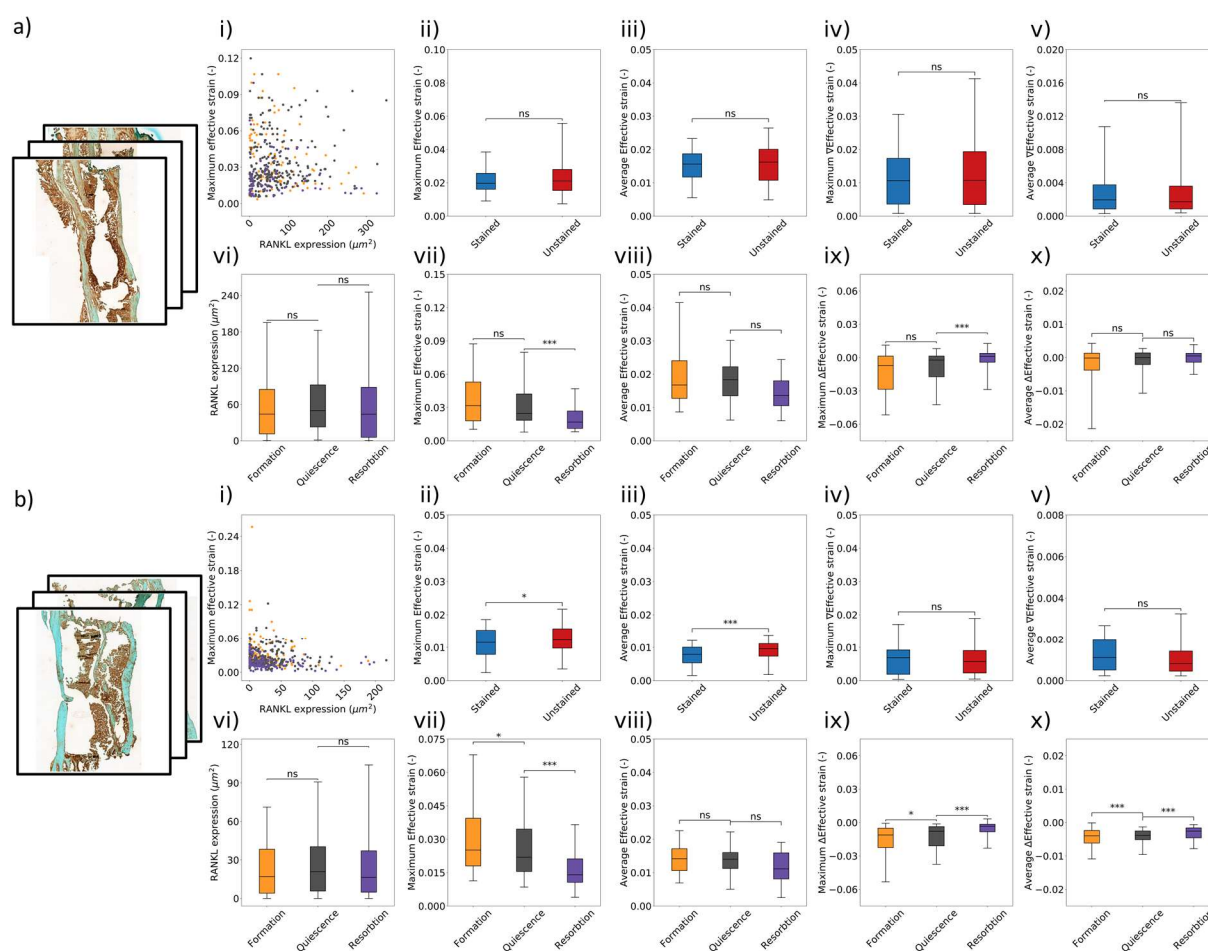


**Figure 4.14:** Results of RANKL staining analysis for mouse 09 (a) and mouse 10 (b). i) indicates the RANKL expression and maximum effective strain in the LivE of each cell. ii) and iii) show the maximum and average effective strain in the LivE of each cell categorised via thresholds. iv) and v) show the spatial gradient of maximum and average effective strain in the LivE of each categorised cell. vi) groups cells by their nearest region of formation, quiescence and resorption to area of RANKL expression. vii), viii), ix) and x) group cells by their nearest region of formation, quiescence and resorption to maximum, average, temporal change in maximum, and temporal change in average effective strain, respectively, within the cell's LivE.

In individual analysis of each bone (**Figure 4.14**), RANKL expression showed a limited relationship between the maximum effective strain in the LivE and the presence of staining. Mouse 10 showed a significant relationship ( $p < 0.05$ ) between maximum effective strain in the LivE, as well as the average mechanical environment. However, mouse 09 showed a trend without significance (i.e. higher mean for unstained cells than stained cells for both maximum and average effective strain in the LivE). No relationship was seen for the gradient of the effective strain in either bone.



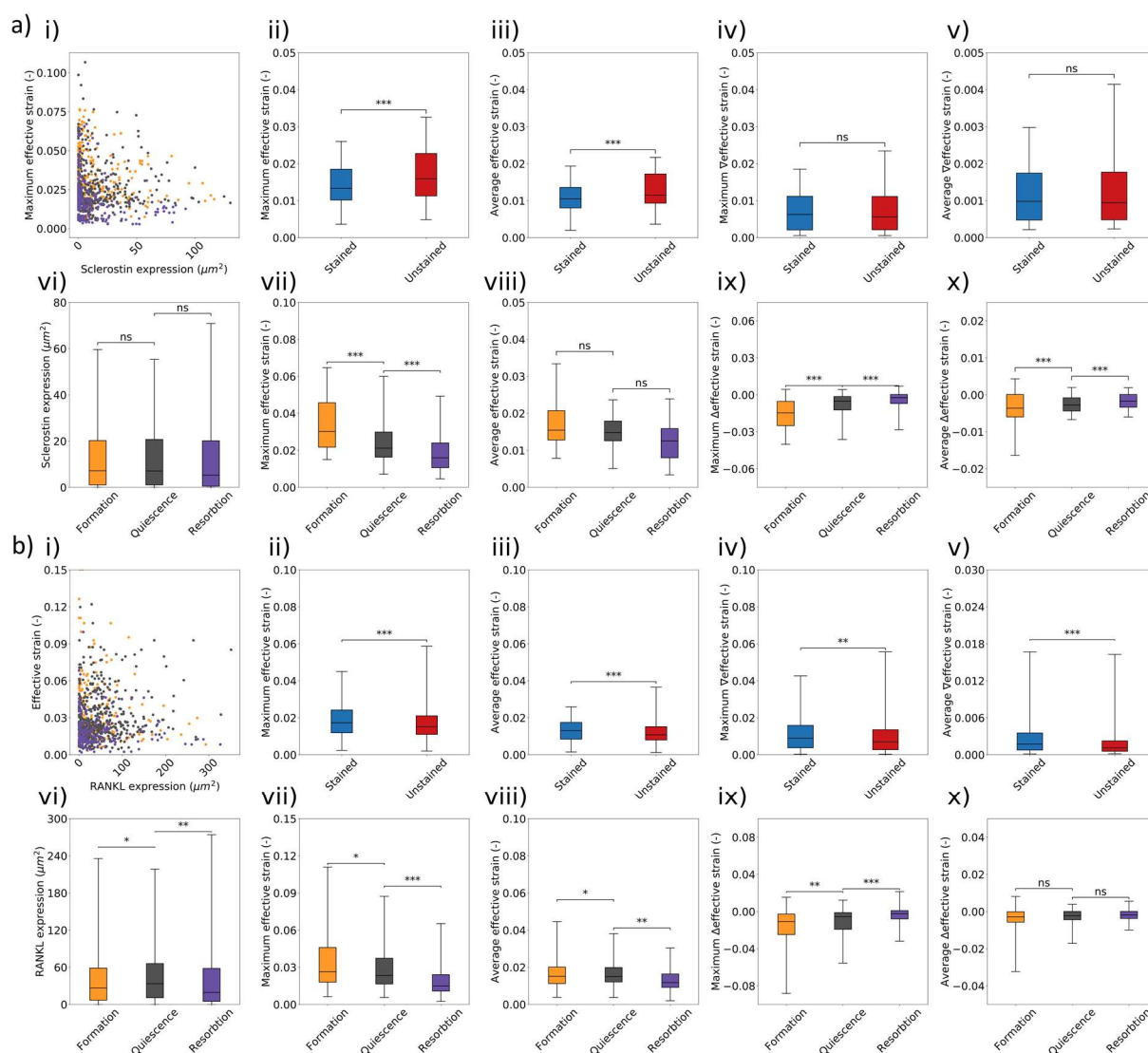


**Figure 4.15:** Combined results of mouse 09 and 10 for a) Sclerostin expression and b) RANKL expression. i) indicates the Sclerostin/RANKL expression and maximum effective strain in the *LivE* of each cell. ii) and iii) show the maximum and average effective strain in the *LivE* of each cell categorised via thresholds. iv) and v) show the spatial gradient of maximum and average effective strain in the *LivE* of each categorised cell. vi) groups cells by their nearest region of formation, quiescence and resorption to area of Sclerostin/RANKL expression. vii), viii), ix) and x) group cells by their nearest region of formation, quiescence and resorption to maximum, average, temporal change in maximum, and temporal change in average effective strain, respectively, within the cell's *LivE*.

However, when analysed together, both the maximum and average effective strain in the *LivE* of unstained and stained cells was significantly different ( $p < 0.001$ ). The mean of unstained cells was lower in both maximum and average cases, but due to outliers, unstained cells

experienced a greater degree of mechanical stimulation in their mechanical environment than stained cells. This relationship was also observed in the effective strain gradient.

*Cell-scale formation, quiescence and resorption associations of cells*

Cells associated with regions of formation showed significantly ( $p < 0.0001$ ) greater levels of maximum effective strain in the *LivE* at the previous time points (week 6) than regions of quiescence or resorption in both mouse 09 and 10. In turn, regions of resorption showed the lowest (significance;  $p < 0.0001$ ) maximum *LivE* strain at week 6. Similar patterns were seen when assessing the average mechanical strain within the *LivE*, yet for mouse 09 the formation-quiescence difference was not significant, and for mouse 10 the significance values were lower ( $p < 0.05$ ). When assessing the relation between cells and the decrease in mechanical stimulation between weeks 6 and 7, cells associated with formation displayed a significant decrease in the maximum strain of the *LivE*. Cells associated with quiescence and resorption showed limited change in their mechanical environments between week 6 and week 7.

Analysis of Sclerostin expression and association of cells with formation, quiescence or resorption showed no significant relationships or obvious trends. Cells associated with formation ( $p < 0.05$ ) and resorption ( $p < 0.01$ ) expressed significantly less RANKL than cells associated with quiescence.

## Discussion

In this study we linked organ-scale loading with tissue-scale changes and cell-scale responses via the reconciliation of spatial and temporal imaging modalities and mechanical simulations. Tissue-scale mechanical strain displayed a greater than random prediction capacity of the formation, resorption or quiescence of bone tissue, with high strains predicting bone formation and low strains better predicting bone resorption. On a cell scale, cells associated with sites of formation displayed higher strains than cells associated with sites of quiescence or resorption. Cells associated with resorption displayed the lowest level of effective strain within the *LivE*. Immunohistochemistry staining for Sclerostin showed that cells with high mechanical signal within their *LivE* showed reduced expression of Sclerostin, while cells under low mechanical strain expressed more Sclerostin. Similar, yet more complicated, results were seen for RANKL expression. On an individualised basis, cells in both mice displayed a trend towards reduced RANKL expression under high strains.

Both mice displayed similar tissue-scale patterns, with the formation of lowly mineralised tissue preceding that of highly mineralised tissue. Formation peaked at week 3, followed by an uptick in resorption. This echoes results seen by Wehrle et al<sup>52</sup> and Tourolle et al<sup>41</sup> in a similar model of fracture healing. However, our mechanical environment contrasts the results seen by Tourolle et al<sup>41</sup> at later time points. Tourolle et al<sup>41</sup> observed decreasing effective strains in the later weeks of their study, while we observed increasing strains towards the end. This demonstrates that non-individualised loading leads to underreporting of the mechanical environment, particularly in the remodelling period, as mice start loading their legs to a greater degree. It is important to note, however, that our boundary conditions and our effective strain values are roughly one tenth of those applied by Tourolle et al. It further appears that the increase in mechanical environment happens sooner and at a higher rate in mice that display the best organ-scale healing progression (see **Figure 3.5** in Chapter 3.1), while the inverse is also true. This can be clearly seen by the juxtaposition of mouse 07, with the best healing outcome, and mouse 12, with the worse healing outcome. Mouse 07 established higher levels of strain within the bone tissue before mouse 12.

In our study, two mice formed non-union fractures. Our analysis showed low rates of bone formation, and earlier peaks and high rates of bone resorption. This led to no bridging occurring in these two mice, as well as an atrophic non-union developing in one mouse. Upon analysis of the mechanical environment, we observed that the strains in the bone tissue were substantially

lower than in mice which displayed good healing, for all time points. However, the mechanoregulatory relationship within the non-union mice were comparable to union mice. The CCR was greater than 45% for weeks 1 to 6 in both non-union mice. This indicates that formation and resorption are under mechanical control, and demonstrates that the lack of a union did not derive from absence of mechanoregulation, but from insufficient levels of mechanical stimulation in general, as theorised by several authors<sup>53-55</sup>. As only two mice formed non-union fractures, our ability to generalise these results is limited. However, since both mice exhibited patterns which align well with the literature, we believe that our approaches are well-suited to investigating the mechanoregulatory patterns occurring in non-union mice. Expanding our model into a non-union model would enhance understanding of the formation of non-union fractures.

Sclerostin is an osteocyte-specific inhibitor of bone formation, and its expression has been linked more often to remodelling than to mechanical stimuli in previous studies<sup>47</sup>. Contrasting this, our work does not explicitly support a greater remodelling dependence than mechanical dependence. We notice no significant difference between Sclerostin expression and cells associated with formation, quiescence or resorption. Though the means of cells associated with formation, quiescence and resorption appear statistically equivalent in **Figure 4.15**, the range of Sclerostin expression for formation-associated cells is smaller than for cells associated with resorption. Since both slide numbers and animal numbers are low, expansion to greater sample sizes may be necessary to properly establish the *in vivo* relationship between Sclerostin expression and remodelling behaviour. We did, however, observe a strongly significant relationship between Sclerostin expression and mechanical stimulation, a result shared by Trüssel et al.<sup>44</sup> in a remodelling study on mouse vertebrae, but not by other authors<sup>47</sup>. While this relationship has not been consistently observed in remodelling experiments, such as those performed by Scheuren et al.<sup>45</sup> and Trüssel et al.<sup>44</sup>, we suspect that this stems from the higher rates of deformation due to the presence of less mineralised bone within our healing model.

RANKL displayed a less clear relationship than Sclerostin. One mouse displayed a significant relationship between high strains and low RANKL expression and low strains and high RANKL expression. The other mouse displayed a similar trend with no significance. However, when the data from both mice was combined, we observed a significant inverse relationship between mechanical stimulation and RANKL expression. In general, the staining of RANKL slices was of poor quality (due to the presence of overstaining). This could account for inconsistent

identification of stained or unstained osteocytes between sections, as thresholds would be inconsistent for the level of staining in each section. In **Figure 4.15a i)**, the vast majority of osteocytes occupy the bottom left quadrant, with some outlier cells in the upper left and bottom right. From this, it appears that the relationship between RANKL expression and mechanical stimulation is regulated as theorised, i.e. high strain led to downregulated expression. However, this cannot be conclusively stated from our data. Better quality staining and a greater sample size are needed to accurately conclude if mechanoregulation of RANKL expression is observable *in vivo*.

For all histological slices, a strongly significant relationship was observed between mechanical strain and associations of formation, quiescence and resorption. That is, cells associated with formation experienced significantly higher levels of mechanical stimulation (both maximum effective strain and average effective strain within the *LivE*) than cells associated with quiescence or resorption. This aligns with observations made at the tissue scale by many authors<sup>11,12,22,23,41,56</sup>, but establishes this link at cell scale. In agreement with this observation, cells associated with formation experience a greater decrease in maximum effective strain within their *LivE* than cells associated with quiescence and resorption. These observations integrate cell-scale associations with tissue-scale changes and the mechanical environment displaying that formation is linked to greater mechanical stimulation, while resorption is linked to lower mechanical stimulation.

Two primary limitations of this work are the lack of inclusion of network effects and the lack of mapping the cellular network. In our study, we assume that each cell is not connected to any other cell. This is not the case, as osteocytes are connected via an extensive lacuna canaliculi network and communicate with each other via dendrites and gap junctions. Network effects might account for the outlier-dominated behaviour observed in both Sclerostin and RANKL expression. If outlier cells, which express large amounts of either Sclerostin or RANKL, are able to transport these cytokines to other cells, we should see lower degrees of expression, but not necessarily changes in activation levels, in neighbouring cells. A benefit of our measured boundary condition approach is that we observe the “background” protein expression within the environment. This is in contrast with approaches where extra-physiological mechanical loading is applied at certain intervals. If extra-physiological loading was applied, the time of sacrifice and post-processing would be important, as currently optimum timelines for protein expression analysis are not known. Our analysis of RANKL and its effect on formation,

quiescence and resorption is limited, as we did not assess the full RANKL/osteoprotegerin (OPG) ratio. Including OPG, and assessing the RANKL/OPG ratio, may explain atypical results seen within our RANKL analysis. Additionally, the two mice that were selected for sectioning and immunohistochemistry staining were chosen because their formation and resorption rates were nearly equal. This indicates that the bone approaches balanced remodelling and that the reparative phase is over. The aim of this selection was to allow comparison of results between these mice. Future studies should investigate cell formation, quiescence and resorption and the mechanical signal-Sclerostin/RANKL relationship in mice that are in the reparative phase and do not exhibit balanced remodelling, in order to understand the roles of these cytokines in the reparative phase.

In our study, we demonstrate mechanical control of bone (re)modelling from organ to tissue scale, and from tissue to cell scale. Mechanical stimulation drove changes at both tissue and cell scales. Effective strain was a predictor of formation, quiescence and resorption at tissue scale, displaying mechanoregulation of tissue-scale changes. Similar relationships were seen at cell scale, where cells under high levels of mechanical strain were more strongly associated with regions of formation, while cells under low levels of mechanical strain were more strongly associated with regions of resorption. Sclerostin and RANKL, proteins commonly associated with formation and resorption, displayed mechanical dependency. In particular, Sclerostin expression displayed a clear mechanodependant relationship, with downregulation of expression being associated with greater mechanical stimulation within the *LivE*. RANKL displayed a more complicated mechanodependant relationship. In one mouse, cells expressing RANKL were significantly more likely to be under lower levels of effective strain than cells not expressing RANKL. The other mouse displayed a similar, non-significant, trend. However, when the results of both mice were combined, downregulated cells displayed a significantly lower mean than stained cells, but a far greater range of maximum strain within the *LivE*. To further unravel this relationship, and to investigate whether outliers drive the RANKL-osteocyte-osteoclast relationship, more studies and a greater sample size are required. Inclusion of network effects and accurate mapping of the relationships between osteocytes would be a potential starting point for such an outlier-driven investigation.

## **Acknowledgements**

The authors would like to acknowledge support from the European Union (ERC Advanced MechAGE, ERC-2016-ADG-741883).

## **Competing Interests**

The authors declare no competing interests

---

## References

- 1 Reznikov, N., Shahar, R. & Weiner, S. Bone hierarchical structure in three dimensions. *Acta Biomater* **10**, 3815-3826, doi:10.1016/j.actbio.2014.05.024 (2014).
- 2 Rho, J. Y., Kuhn-Spearing, L. & Zioupos, P. Mechanical properties and the hierarchical structure of bone. *Med Eng Phys* **20**, 92-102, doi:Doi 10.1016/S1350-4533(98)00007-1 (1998).
- 3 Paul, G. R., Malhotra, A. & Muller, R. Mechanical Stimuli in the Local In Vivo Environment in Bone: Computational Approaches Linking Organ-Scale Loads to Cellular Signals. *Curr Osteoporos Rep* **16**, 395-403, doi:10.1007/s11914-018-0448-6 (2018).
- 4 Clarke, K. A., Smart, L. & Still, J. Ground reaction force and spatiotemporal measurements of the gait of the mouse. *Behav Res Meth Ins C* **33**, 422-426, doi:Doi 10.3758/Bf03195396 (2001).
- 5 Clarke, K. A. & Still, J. Gait analysis in the mouse. *Physiol Behav* **66**, 723-729, doi:Doi 10.1016/S0031-9384(98)00343-6 (1999).
- 6 Charles, J. P., Cappellari, O. & Hutchinson, J. R. A Dynamic Simulation of Musculoskeletal Function in the Mouse Hindlimb During Trotting Locomotion. *Front Bioeng Biotech* **6**, doi:10.3389/fbioe.2018.00061 (2018).
- 7 Charles, J. P., Cappellari, O., Spence, A. J., Wells, D. J. & Hutchinson, J. R. Muscle moment arms and sensitivity analysis of a mouse hindlimb musculoskeletal model. *J Anat* **229**, 514-535, doi:10.1111/joa.12461 (2016).
- 8 Meakin, L. B., Price, J. S. & Lanyon, L. E. The contribution of experimental in vivo models to understanding the mechanisms of adaptation to mechanical loading in bone. *Front Endocrinol* **5**, doi:10.3389/fendo.2014.00154 (2014).
- 9 Klosterhoff, B. S. *et al.* Wireless sensor enables longitudinal monitoring of regenerative niche mechanics during rehabilitation that enhance bone repair. *Bone* **135**, doi:10.1016/j.bone.2020.115311 (2020).
- 10 Wehner, T. *et al.* Temporal Delimitation of the Healing Phases Via Monitoring of Fracture Callus Stiffness in Rats. *J Orthop Res* **32**, 1589-1595, doi:10.1002/jor.22721 (2014).
- 11 Lambers, F. M. *et al.* Trabecular bone adapts to long-term cyclic loading by increasing stiffness and normalization of dynamic morphometric rates. *Bone* **55**, 325-334, doi:10.1016/j.bone.2013.04.016 (2013).



- 12 Lambers, F. M. *et al.* Bone adaptation to cyclic loading in murine caudal vertebrae is maintained with age and directly correlated to the local micromechanical environment. *J Biomech* **48**, 1179-1187, doi:10.1016/j.jbiomech.2014.11.020 (2015).
- 13 Webster, D., Schulte, F., Lambers, F., Kuhn, G. & Muller, R. The mechanical environment in bone marrow predicts osteoblast and osteoclast activities. *Bone* **50**, S73-S73, doi:10.1016/j.bone.2012.02.208 (2012).
- 14 Webster, D., Schulte, F. A., Lambers, F. M., Kuhn, G. & Muller, R. Strain energy density gradients in bone marrow predict osteoblast and osteoclast activity: A finite element study. *J Biomech* **48**, 866-874, doi:10.1016/j.jbiomech.2014.12.009 (2015).
- 15 Gardner, M. J. *et al.* In vivo cyclic axial compression affects bone healing in the mouse tibia. *J Orthop Res* **24**, 1679-1686, doi:10.1002/jor.20230 (2006).
- 16 Wolf, S. *et al.* Effects of high-frequency, low-magnitude mechanical stimulus on bone healing. *Clin Orthop Relat R*, 192-198 (2001).
- 17 Wehrle, E. *et al.* The impact of low-magnitude high-frequency vibration on fracture healing is profoundly influenced by the oestrogen status in mice. *Dis Model Mech* **8**, 93-104, doi:10.1242/dmm.018622 (2015).
- 18 Wehrle, E. *et al.* Distinct Frequency Dependent Effects of Whole-Body Vibration on Non-Fractured Bone and Fracture Healing in Mice. *J Orthop Res* **32**, 1006-1013, doi:10.1002/jor.22629 (2014).
- 19 Blanchard, R., Dejacó, A., Bongaers, E. & Hellmich, C. Intravoxel bone micromechanics for microCT-based finite element simulations. *J Biomech* **46**, 2710-2721, doi:10.1016/j.jbiomech.2013.06.036 (2013).
- 20 Carriero, A., Abela, L., Pitsillides, A. A. & Shefelbine, S. J. Ex vivo determination of bone tissue strains for an in vivo mouse tibial loading model. *J Biomech* **47**, 2490-2497, doi:10.1016/j.jbiomech.2014.03.035 (2014).
- 21 Karali, A. *et al.* Full-field strain of regenerated bone tissue in a femoral fracture model. *J Microsc*, doi:10.1111/jmi.12937 (2020).
- 22 Schulte, F. A., Lambers, F. M., Kuhn, G. & Muller, R. In vivo micro-computed tomography allows direct three-dimensional quantification of both bone formation and bone resorption parameters using time-lapsed imaging. *Bone* **48**, 433-442, doi:10.1016/j.bone.2010.10.007 (2011).

- 23 Schulte, F. A. *et al.* Local Mechanical Stimuli Regulate Bone Formation and Resorption in Mice at the Tissue Level. *Plos One* **8**, doi:ARTN e62172 10.1371/journal.pone.0062172 (2013).
- 24 Wolff, J. <<Das>> *Gesetz der Transformation der Knochen*. (A. Hirschwald, 1892).
- 25 Capulli, M., Paone, R. & Rucci, N. Osteoblast and osteocyte: Games without frontiers. *Arch Biochem Biophys* **561**, 3-12, doi:10.1016/j.abb.2014.05.003 (2014).
- 26 Rucci, N. Molecular biology of bone remodelling. *Clin Cases Miner Bon* **5**, 49-56 (2008).
- 27 Franz-Odenaal, T. A., Hall, B. K. & Witten, P. E. Buried alive: How osteoblasts become osteocytes. *Dev Dynam* **235**, 176-190, doi:10.1002/dvdy.20603 (2006).
- 28 Verbruggen, S. W., Vaughan, T. J. & McNamara, L. M. Strain amplification in bone mechanobiology: a computational investigation of the in vivo mechanics of osteocytes. *J R Soc Interface* **9**, 2735-2744, doi:10.1098/rsif.2012.0286 (2012).
- 29 Vaughan, T. J., Verbruggen, S. W. & McNamara, L. M. Are all osteocytes equal? Multiscale modelling of cortical bone to characterise the mechanical stimulation of osteocytes. *Int J Numer Meth Bio* **29**, 1361-1372, doi:10.1002/cnm.2578 (2013).
- 30 Verbruggen, S. W., Vaughan, T. J. & McNamara, L. M. Mechanisms of osteocyte stimulation in osteoporosis. *J Mech Behav Biomed* **62**, 158-168, doi:10.1016/j.jmbbm.2016.05.004 (2016).
- 31 Vaughan, T. J., Mullen, C. A., Verbruggen, S. W. & McNamara, L. M. Bone cell mechanosensation of fluid flow stimulation: a fluid-structure interaction model characterising the role integrin attachments and primary cilia. *Biomech Model Mechan* **14**, 703-718, doi:10.1007/s10237-014-0631-3 (2015).
- 32 Verbruggen, S. W., Vaughan, T. J. & McNamara, L. M. Fluid flow in the osteocyte mechanical environment: a fluid-structure interaction approach. *Biomech Model Mechan* **13**, 85-97, doi:10.1007/s10237-013-0487-y (2014).
- 33 Boerckel, J. D. *et al.* Effects of in vivo mechanical loading on large bone defect regeneration. *J Orthop Res* **30**, 1067-1075, doi:10.1002/jor.22042 (2012).
- 34 Carter, D. R. Mechanical Loading History and Skeletal Biology. *J Biomech* **20**, 1095-1109, doi:Doi 10.1016/0021-9290(87)90027-3 (1987).
- 35 Carter, D. R., Beaupre, G. S., Giori, N. J. & Helms, J. A. Mechanobiology of skeletal regeneration. *Clin Orthop Relat R*, S41-S55 (1998).

- 36 Claes, L., Augat, P., Suger, G. & Wilke, H. J. Influence of size and stability of the osteotomy gap on the success of fracture healing. *J Orthop Res* **15**, 577-584, doi:DOI 10.1002/jor.1100150414 (1997).
- 37 Huiskes, R., Ruimerman, R., van Lenthe, G. H. & Janssen, J. D. Effects of mechanical forces on maintenance and adaptation of form in trabecular bone. *Nature* **405**, 704-706, doi:Doi 10.1038/35015116 (2000).
- 38 Isaksson, H. *et al.* Remodeling of Fracture Callus in Mice Is Consistent with Mechanical Loading and Bone Remodeling Theory. *J Orthop Res* **27**, 664-672, doi:10.1002/jor.20725 (2009).
- 39 Morgan, E. F., Gleason, R. E., Hayward, L. N. M., Leong, P. L. & Palomares, K. T. S. Mechanotransduction and fracture repair. *J Bone Joint Surg Am* **90a**, 25-30, doi:10.2106/Jbjs.G.01164 (2008).
- 40 Morgan, E. F. *et al.* Correlations between local strains and tissue phenotypes in an experimental model of skeletal healing. *J Biomech* **43**, 2418-2424, doi:10.1016/j.jbiomech.2010.04.019 (2010).
- 41 Tourolle né Betts, D. C. *et al.* The association between mineralised tissue formation and the mechanical local *in vivo* environment: Time-lapsed quantification of a mouse defect healing model. *Sci Rep-Uk* **10**, 1-10, doi:10.1038/s41598-020-57461-5 (2020).
- 42 Taylor C, S. A., Trüssel A, Müller R. Local *in vivo* Environment (LivE) imaging for single cell protein analysis of bone tissue. *CDBME* **2**, 449-453.
- 43 Trüssel, A. J., Dittrich, P. S. & Müller, R. *Spatial mapping and high throughput microfluidic gene expression analysis of osteocytes in mechanically controlled bone remodeling.*
- 44 Scheuren, A. C., Müller, R. & Bellantuono, I. *Longitudinal assessment of frailty and osteosarcopenia in an in vivo model of premature aging.*
- 45 Morse, A. *et al.* Sclerostin Antibody Increases Callus Size and Strength but does not Improve Fracture Union in a Challenged Open Rat Fracture Model. *Calcified Tissue Int* **101**, 217-228, doi:10.1007/s00223-017-0275-2 (2017).
- 46 Moustafa, A. *et al.* Mechanical loading-related changes in osteocyte sclerostin expression in mice are more closely associated with the subsequent osteogenic response than the peak strains engendered. *Osteoporosis Int* **23**, 1225-1234, doi:10.1007/s00198-011-1656-4 (2012).

- 
- 47 Robling, A. G. *et al.* Mechanical stimulation of bone in vivo reduces osteocyte expression of Sost/sclerostin. *J Biol Chem* **283**, 5866-5875, doi:10.1074/jbc.M705092200 (2008).
- 48 Tu, X. L. *et al.* Sost downregulation and local Wnt signaling are required for the osteogenic response to mechanical loading. *Bone* **50**, 209-217, doi:10.1016/j.bone.2011.10.025 (2012).
- 49 Pistoia, W. *et al.* Estimation of distal radius failure load with micro-finite element analysis models based on three-dimensional peripheral quantitative computed tomography images. *Bone* **30**, 842-848, doi:Doi 10.1016/S8756-3282(02)00736-6 (2002).
- 50 Virtanen, P. *et al.* SciPy 1.0: fundamental algorithms for scientific computing in Python. *Nat Methods* **17**, 261-272, doi:10.1038/s41592-019-0686-2 (2020).
- 51 Wehrle, E. *et al.* Evaluation of longitudinal time-lapsed in vivo micro-CT for monitoring fracture healing in mouse femur defect models. *Sci Rep* **9**, 17445, doi:10.1038/s41598-019-53822-x (2019).
- 52 Andrzejowski, P. & Giannoudis, P. V. The 'diamond concept' for long bone non-union management. *J Orthop Traumatol* **20**, doi:10.1186/s10195-019-0528-0 (2019).
- 53 Claes, L., Recknagel, S. & Ignatius, A. Fracture healing under healthy and inflammatory conditions. *Nat Rev Rheumatol* **8**, 133-143, doi:10.1038/nrrheum.2012.1 (2012).
- 54 Giannoudis, P. V. *et al.* Subtrochanteric fracture non-unions with implant failure managed with the "Diamond" concept. *Injury* **44**, S76-S81, doi:Doi 10.1016/S0020-1383(13)70017-2 (2013).
- 55 Palomares, K. T. S. *et al.* Mechanical Stimulation Alters Tissue Differentiation and Molecular Expression during Bone Healing. *J Orthop Res* **27**, 1123-1132, doi:10.1002/jor.20863 (2009).

# Tissue level regeneration and remodelling dynamics are driven by local mechanical stimuli in a post-bridging loaded femur defect healing model in mice

Graeme R Paul<sup>1</sup>, Paul Vallaster<sup>1</sup>, Michelle Rüegg<sup>1</sup>, Ariane C. Scheuren<sup>1</sup>, Duncan C. Tourolle<sup>1</sup>, Gisela A. Kuhn<sup>1</sup>, Esther Wehrle<sup>1</sup>, Ralph Müller<sup>1</sup>

1. Institute for Biomechanics, ETH Zurich, Zurich, Switzerland

## Abstract

Bone healing and remodelling are mechanically driven processes. While the tissue-scale response to mechanical stimulation is well understood, much less is known about the tissue-scale regulation of bone formation and resorption during the various phases of fracture healing. In this study, we used a loaded femoral defect model in mice to investigate the role of mechanical stimulation at the tissue scale with regard to formation, quiescence (no change in bone presence between time points) and resorption dynamics in the late reparative and remodelling phases (post bridging). This was done by combining longitudinal micro-computed tomography to observe temporal changes in bone at different densities, with micro-finite element analysis to map the mechanics of the local *in vivo* environment to those changes. Increasing levels of strain led to increasing conditional probability of bone formation, while decreasing levels of strain led to increasing probability of bone resorption. Additionally, analysis of mineralisation dynamics showed both a temporal and strain level dependent behaviour. Our results indicate that the post-bridging phases of fracture healing show very similar mechanoregulatory behaviour to bone remodelling. A logarithmic-like response was displayed, where the conditional probability of bone formation or resorption rose rapidly and plateaued or fell rapidly and plateaued respectively as mechanical strain increased.

## Keywords:

Bone, defect healing, fracture healing, adaptive loading, rtFE, multi-density analysis

## Introduction

The association between bone healing<sup>1-7</sup>, bone remodelling<sup>8-12</sup> and mechanical stimulation is well established. Many authors have shown mechanoregulatory behaviour at organ and tissue scale in bone remodelling models<sup>10,11,13-15</sup>. However, in bone healing, the influence of mechanical stimulation throughout all three stages of fracture healing lacks a thorough understanding at tissue scale<sup>1</sup>. An improved understanding of the effects of mechanics in the local *in vivo* environment (*LivE*) on all phases of fracture healing will allow better understanding of fixation methods, biomaterial application and pharmacological effects on mechanosensitive cells.

Fracture healing displays three overlapping stages: inflammation, repair and remodelling<sup>16</sup>. During the inflammation and early reparative phase of healing, a haematoma forms, recruiting a wide range of cells and resources to initiate healing. Following the development of a haematoma, lowly mineralised tissue starts forming. The fracture bridges in the reparative phase, and the lowly mineralised tissue begins to mineralise, overshooting the required amount of bone needed for the mechanical environment. This excess bone is removed in the remodelling stage<sup>17</sup>. Similar to studies on bone remodelling, micro-computed tomography (micro-CT) has allowed the longitudinal quantification of this process<sup>18,19</sup>. More recently, micro-finite element analysis (micro-FE) has also been used to link mechanical stimuli to patterns of formation, resorption and quiescence during the fracture healing process<sup>1,7</sup>; indicating that soft- and bone-tissue strains allow improved prediction of where bone will form. This echoes what is seen in bone remodelling studies, where several authors have coupled micro-CT, micro-FE and cyclic mechanical loading to show that tissue-scale changes are correlated with the mechanical environment<sup>10,11,13,20</sup>. More specifically, high local strains within the mature and mineralised bone tissue have been shown to increase the likelihood of site-specific bone formation, whereas sites of resorption correlated with low local strains<sup>5,10,11,13,21,22</sup>. Building on investigations in mature bone, Tourolle et al.<sup>1</sup> developed a multi-density approach, whereby a range of densities was analysed to investigate the link between mechanics and mineralisation dynamics in lowly mineralised woven bone. While the initial periods of the inflammation and reparative phases show limited similarities between fracture healing and bone remodelling, the late reparative and the remodelling phases that occur after bridging should have much in common<sup>23</sup>.

While both micro-CT and micro-FE are well established tools for investigating bone adaptation<sup>11,13-15,20,24-26</sup>, many different approaches have been taken to describe the mechanical environment. Currently, the main mechanism driving cell response to mechanical stimuli is debated, with direct cellular strain and indirect fluid shear stresses being supported by several studies<sup>27-29</sup>. To combine these mechanisms, SED is often used<sup>10-12,14</sup>, as it combines volumetric and deviatoric strains (which drive fluid movement and direct strain, respectively). However, SED scales linearly with material stiffness, and hence, while it is an appropriate metric for mature bone, it has limitations for rapidly mineralising tissue found in bone healing<sup>1</sup>. Hence, effective strain has been used by several authors<sup>1,30</sup>. Since effective strain combines volumetric and deviatoric strains, it allows for better comparison of bone remodelling and bone healing<sup>1</sup> than SED.

*In silico* models can aid understanding of bone remodelling and bone healing<sup>31</sup>. In particular, they allow rapid parameter investigation<sup>32</sup>, forming the foundation for more targeted experimental investigations. Often these models use simplified or mathematically derived relationships<sup>33</sup> to describe the mechanoregulation of bone healing. There exists a lack of accurate, experimentally derived data to quantify the exact relationship between the *LivE* and tissue-scale changes in the late reparative and remodelling phases of fracture healing<sup>34</sup>. This limits the accuracy of the mechanoregulatory aspect of *in silico* modelling in fracture healing. Quantification of this relationship will allow improved mechanoregulatory descriptions in *in silico* models of bone healing.

In this paper, we analyse sites of formation, resorption and quiescence determined via longitudinal *in vivo* micro-CT and couple them with micro-FE analysis to investigate the role played by local strains in the late reparative and remodelling phases of a loaded femur defect healing model. We incorporate a multi-density approach to allow analysis of bone tissue formation and mineralisation under mechanical stimulation. We hypothesise that late stages of fracture healing display similar mechanoregulatory behaviour to bone remodelling. More specifically, we hypothesise that mechanoresponsivity will be greater in the mechanically loaded model and that both the physiological (sham-loaded/control) group and the extra-physiologically loaded group will have greater probability of site-specific formation and resorption in regions of higher and lower strain, respectively. Determining these relationships will provide a foundation for realistic rules for *in silico* investigations of bone during the post-

bridging phases of fracture healing, and improve our understanding of mechanoregulation in fracture healing.

## Materials and Methods

### *In vivo experiments*

All animal procedures were approved by the relevant authorities (license number: 36/2014, Kantonales Veterinäramt Zürich, Zurich, Switzerland). All methods were carried out in accordance with the ARRIVE guidelines and the Swiss Animal Welfare Act and Ordinance. All mice (20, female, C57BL/6J) were acquired from Janvier (Saint Berthevin Cedex, France) at an age of 12 weeks and were housed in the ETH Phonemics Centre animal facility under a 12h:12h light-dark cycle, maintenance feed (3437, KLIBA NAFAG, Kaiseraugst, Switzerland), 5 animals/cage for 8 weeks until surgery. All animals underwent osteotomies on the right femur with a 0.66mm Gigli wire by the same veterinarian at 20 weeks of age. Details can be found elsewhere<sup>19</sup>. Mice were divided into two groups: control/sham loading group (n=10) and a loaded group (n=10). Post surgery, they were housed with 2 to 3 animals per cage. For all surgeries and micro-CT scans, the animals were anaesthetized with 5% isoflurane/oxygen for induction and maintained at 1-2% isoflurane/handling.

Mechanical loading was performed thrice weekly, (10 Hz loading frequency, 300 s loading time, 3000 cycles) from week 3 onwards. Real time finite element analysis (see Chapter 3.2) was used to determine the loading parameters, which are contained in Table 1 in the supplementary material.

Further surgical details can be found in Chapter 3.1.

### *Imaging, pre-processing, masking and multi-density finite element analysis*

Imaging was performed on a (Scanco Medical, Brüttisellen, Switzerland) reconstructed micro-CT image at a nominal resolution of 10.5  $\mu\text{m}$ . The scanned region required two stacks of 105 voxels each (totalling a region 2 mm long) and had an imaging time of 15 minutes. All animals were scanned weekly from week 0 (post operation) until week 7 (post operation). All images for each time point of each mouse were registered to the baseline image (week 0) of that particular mouse. Pre-processing entailed the extraction of the relevant subvolume (reducing the image size to 300x300x180 voxels), Gaussian filtering ( $\sigma=1.2$ , support=1) and binning grey values using a multi-density approach proposed by Tourolle et al<sup>1</sup>.



Masks were generated with a ray tracer approach, as performed by Tourolle et al.<sup>1</sup>, from each baseline image. The original cortices were extracted by thresholding all tissue above 645 mg HA/cm<sup>3</sup>, while the medullary region (marrow cavity) and the peripheral region (everything else) were extracted from the remaining regions.

For mechanical simulations, the binned greyscale values were converted from density (mg HA/cm<sup>3</sup>) to Young's moduli (GPa), on a per voxel basis, from 395 mg HA/cm<sup>3</sup> to 720 mg HA/cm<sup>3</sup> in steps of 25 mg HA/cm<sup>3</sup>, corresponding to 4.045 GPa to 12.170 GPa, respectively, with steps of 0.626 GPa. Regions of soft tissue were set to a Young's modulus of 0.003 GPa<sup>22</sup> and the marrow cavity of the femur was capped with a plate of 20 GPa, preventing edge effects due to the soft tissue found lying on the top slice of the finite element mesh. A linear micro-finite element (micro-FE) solver, ParOSol<sup>35</sup>, was then used to solve the finite element mesh. For the uniaxial loading case, 1% compressive displacement was applied to the top slice in the axial direction and the bottom-most slice was fixed. For the bending case, the centre of bending was determined<sup>36</sup>, and the bending load was centred around the axis of loading from the loading machine and deformed by 1% at the furthest edges of the mesh. The Swiss National Supercomputing Centre (CSCS) was used to solve each finite element simulation, requiring roughly 2 minutes per image. The multi-density ranges (395 mg HA/cm<sup>3</sup> to 720 mg HA/cm<sup>3</sup>) in steps of 25 mg HA/cm<sup>3</sup> were used as masks to specify the level of mineralisation in all further analyses. Further description can be found in Chapter 4.1 and Tourolle et al.<sup>1</sup>.

#### *Estimation of mechanical stimulation*

The local *in vivo* mechanical environment was described using effective strain, calculated as described by<sup>30</sup>. The results of the simulations were appropriately scaled based on the assumed loading parameters using the following ratios:

$$\varepsilon_{axial\_actual} = \frac{F_{axial\_applied}}{F_{axial\_resultant}} \varepsilon_{axial\_simulation}$$

or for a bending moment:

$$\varepsilon_{bending\_actual} = \frac{F_{bending\_applied}}{F_{bending\_resultant}} \varepsilon_{bending\_simulation}$$

where  $\varepsilon_{simulation}$  is the effective strain result of the simulation (based on the 1% displacement),  $F_{resultant}$  is the sum of reaction forces of all the nodes of the upper most surface,  $F_{applied}$  is the selected force (i.e. a force provided by a mechanical stimulation machine) and  $\varepsilon_{actual}$  is the

strain under the applied force. Bending moments were determined using length of the implant pins as the moment (10 mm) and the loading force from the machine (described in supplementary materials, ranging from 8 N to 16 N). Axial forces were taken as the loading force, and the bending and axial loads were superimposed upon one another. All control mice were assumed to have a uniaxial load of 10 N as described previously<sup>1</sup>.

#### *Analysis of bone volume and formation, quiescence and resorption rates*

Bone volume was calculated by counting the number of voxels above the aforementioned density thresholds (395 mg HA/cm<sup>3</sup> to 720 mg HA/cm<sup>3</sup>). Regions of formation, quiescence and resorption were calculated by the binary difference between an image at a given time point and image at a preceding time point to establish their respective rates of change. Voxels present in both images were labelled quiescent, those present in the most current time point were labelled formation, and those only present in the preceding time point, resorption. Masks were then formed to describe these regions.

#### *Analysis of local mechanoregulation*

The scaled results of the micro-FE simulation in terms of effective strain were used as a measure of mechanical stimuli. The mechanical stimuli as calculated above were mapped to each voxel. The mean strain at each time point was calculated on a per group basis. Mean effective strain for each density band was calculated. The conditional probabilities for formation, quiescence and resorption were calculated for a given value of effective strain (as in Schulte et al.<sup>11</sup>) at a given bone tissue density. The surface effective strain values were normalised to the 99<sup>th</sup> percentile effective strain in the whole simulation region to ensure that simulation artefacts did not affect the analysis.

The area under the curve (AUC) of a receiver operating characteristic (ROC) curve was used to assess the performance of the particular effective strain value as a predictor of formation or resorption. As this is a binary classifier, formation and resorption surfaces were analysed separately. An AUC greater than 0.5 implies that the change in voxel (either formation or resorption) is associated with mechanical stimulation. An AUC of 0.5 indicates no relationship between the mechanical stimuli and the voxel, while an AUC below 0.5 indicates an inverse relationship between mechanical stimuli and the voxel's behaviour.

## Results

We combined micro-CT imaging and micro-FE (**Figure 4.16a** and **c**) to determine the *LivE* in 20 animals (10 loaded, 10 control) in a femoral defect loading study. The control group was sham loaded (0 N) for 5 minutes thrice weekly, and the loaded group was loaded according to the real time finite element (rtFE) protocol described in Chapter 3.2, resulting in the loads indicated in the supplementary material.

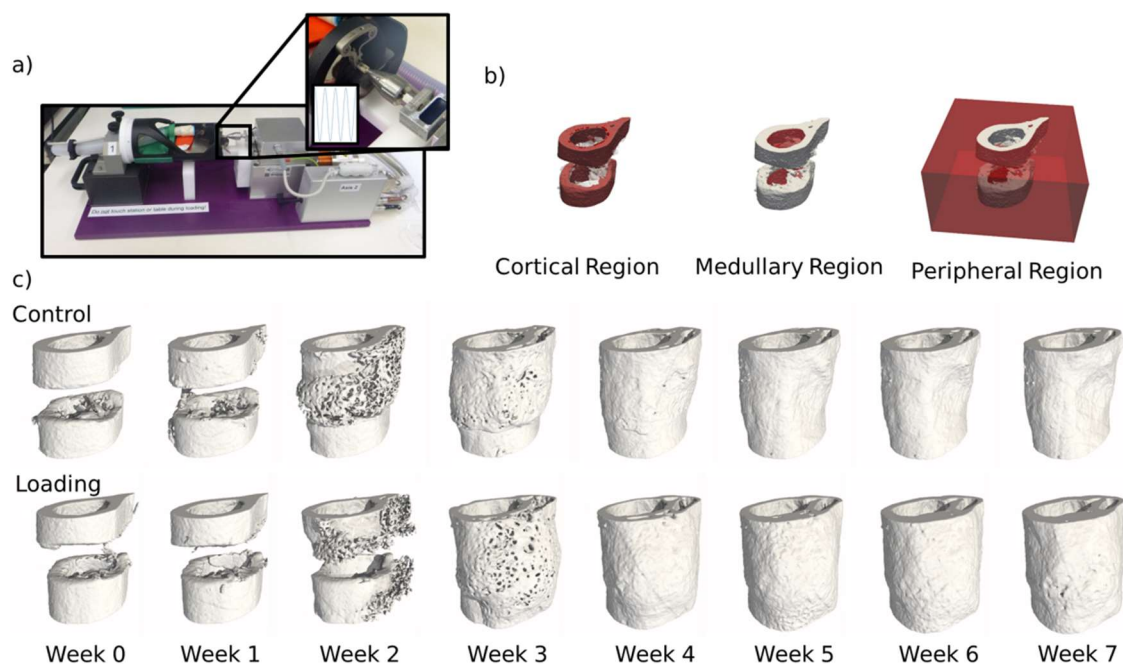


**Figure 4.16:** a) Femur defect loading was achieved using an electromagnetic actuator, a specially designed holder and an external fixator. b) Three mask regions at week 0 of the femur defect regions. c) A temporal progression of femur defect healing of both a control and a loaded mouse.

We assessed the changes in bone volume, rates of bone formation and resorption (**Figure 4.17**) and the mechanical environment in four regions: the cortical region, medullary region, peripheral region, and the combination of all three regions (termed ‘all’ or ‘global’) (**Figure 4.16b**). Mechanoregulation was assessed using two methods. The first entailed a conditional probability approach, whereby the conditional probability of a surface voxel forming, resorbing or remaining quiescent was calculated as a function of percentage of maximum strain in the region. Secondly, the AUC of the ROC was used to indicate the level of mechanoregulation, where the correct classification rate of each voxel at the following time point (a formation or a resorption voxel) for a given strain was determined.

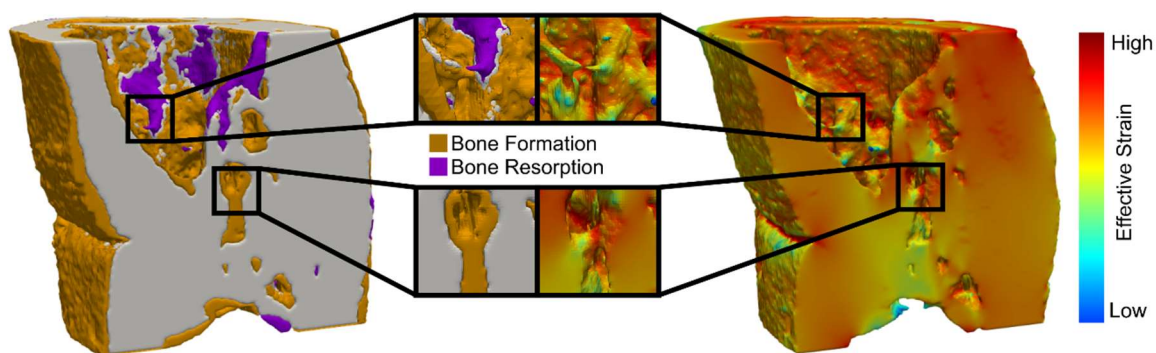


**Figure 4.17:** Regions of high strains have a greater probability of new bone formation, while regions of low strains lead to bone being resorbed in all femur defect regions.

#### Longitudinal bone changes during fracture healing

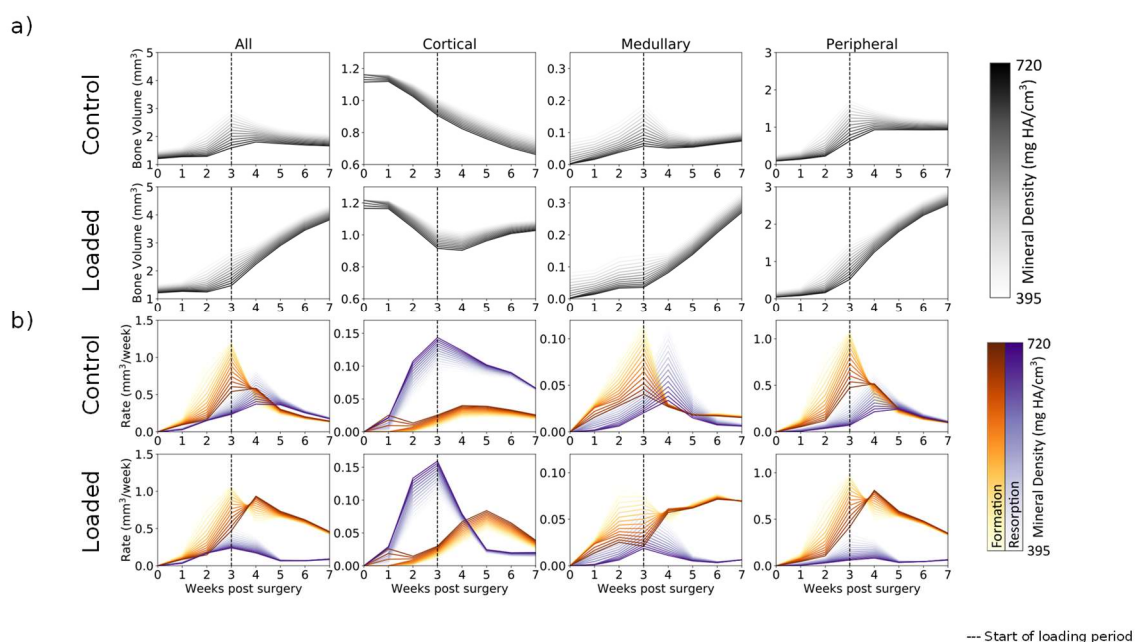


**Figure 4.18:** a) Bone volume over time in femur defect regions. In both loaded and control groups, lowly mineralised tissue starts to form at week 1. After week 3, mineralisation occurs and the control group remodels away excess tissue, while the loaded group continues to form both lowly mineralised and mineralised tissue. A similar pattern is seen in the medullary and peripheral regions, while the cortical region sees substantial bone resorption, a process which is arrested by loading. B) Formation and resorption rates over time. In all regions peak formation occurs at week 3, while loading increases the amount of mineralised tissue forming

*at week 4. Similar patterns are seen in the medullary and peripheral regions, while resorption dominates the cortical region for the control group. Loading increases the rate of formation and decreases the rate of resorption in the loaded group's cortical region.*

Defect healing was observed to follow a typical pattern (**Figure 4.18a**) of bone formation, consolidation and remodelling. Lowly mineralised bone tissue begins to form at week 1 and accelerates until week 3. By week 3 sufficient amounts of bone tissue had formed for both the loaded and the control group to bridge the osteotomy gap for all mice but one in the control group (which bridged at week 4). At week 3 the control group began to display consolidation, whereby lowly mineralised bone tissue was mineralised and the excess callus was remodelled away, approaching an equilibrium by week 7. Contrastingly, from the start of loading in week 3, far greater bone formation was seen in the loaded group. By week 7 twice as much bone tissue was present in the loaded group compared to the control group. Lowly mineralised tissue kept forming, albeit at a decaying rate, but consolidation occurred, leading to far more bone tissue of all levels of mineralisation in comparison to the control group. These patterns were mimicked in the bone formation and resorption rates (**Figure 4.18b**), where high rates of lowly mineralised tissue formation (up to  $\sim 1 \text{ mm}^2$  per week at week 3) preceded rates of highly mineralised tissue formation (up to  $\sim 0.75 \text{ mm}^2$  at week 4). In contrast with the control group, the loaded group expressed a higher peak formation rate of mineralised tissue (loaded group:  $\sim 0.8 \text{ mm}^2$  versus control group:  $\sim 0.5 \text{ mm}^2$ ) at week 4, as well as suppressed resorption rates for all mineralisation levels. Additionally, the control group's peak resorption rate occurred one week later than that of the loaded group.

When separated into the three regions, several interesting patterns emerged. The original cortical region underwent significant resorption during the first 3 weeks of the healing period in both the loaded and control groups. Upon the application of load, bone resorption was arrested in the loaded group, despite the original cortical wall not being restored upon completion of the study. In both the medullary and peripheral regions similar behaviour to the global behaviour was observed.

### The mechanical environment during fracture healing

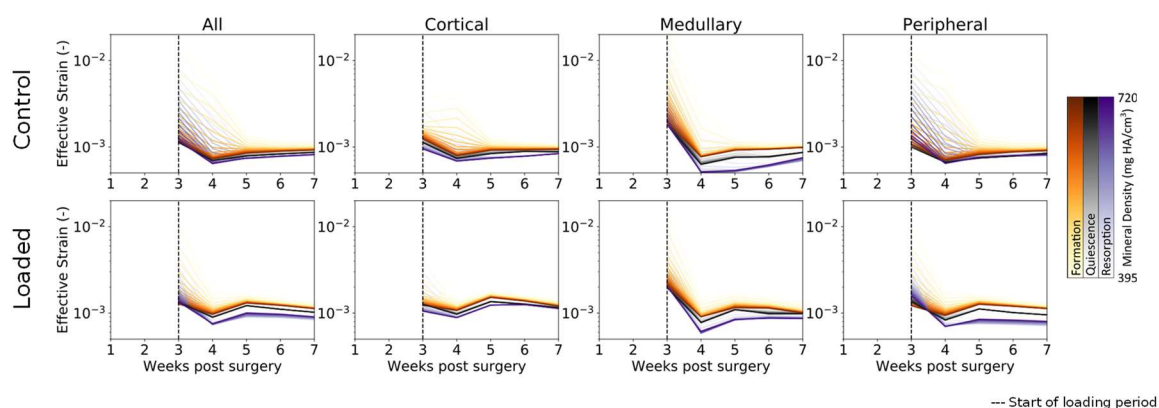


**Figure 4.19:** The longitudinal mechanical environment in femur defect regions. As lowly mineralised tissue further mineralised, the mechanical environment became more homogenous between bone of differing densities in both the control group and loaded groups. For all densities of formation, the average effective strain was higher than for quiescent or resorption voxels, while resorption voxels displayed the lowest effective strain on average out of the three possible changes.

As bridging occurred, strains consolidate within the range of mineralised tissues (**Figure 4.19**), which was seen by reduction in the broad initial range of effective strain across the multiple densities. This is due to the formation of a complete callus and the mineralisation of lowly mineralised tissue. As more tissue forms and mineralises, the organ-scale load is more evenly distributed throughout the tissues, such that extreme deformations of the lowly mineralised tissue can be avoided. Strains in the control group increased slightly throughout the observation period. However, for all time points, strains found in voxels of formation were higher than in quiescent voxels, which in turn were higher than strains in resorption voxels. For the loaded group, the rtFE method led to strains increasing until all mice had reached the maximum load. Hence strains peaked at week 5, and decreased to week 7, as the bone volume approached an equilibrium, while the applied load remained constant. Separation of formation, quiescence and resorption strains were also observed, with greater degrees of separation particularly in the peripheral region.

In all regions, formation voxels of lower levels of mineralisation were more likely to have higher strains than those of greater levels of mineralisation. For the peripheral region, resorbed voxels of lower mineralisation displayed lower levels of strain compared to those of greater mineralisation. Quiescent voxels displayed no mineralisation dependency of strain.



### Mechanoregulation during the post-bridging phase

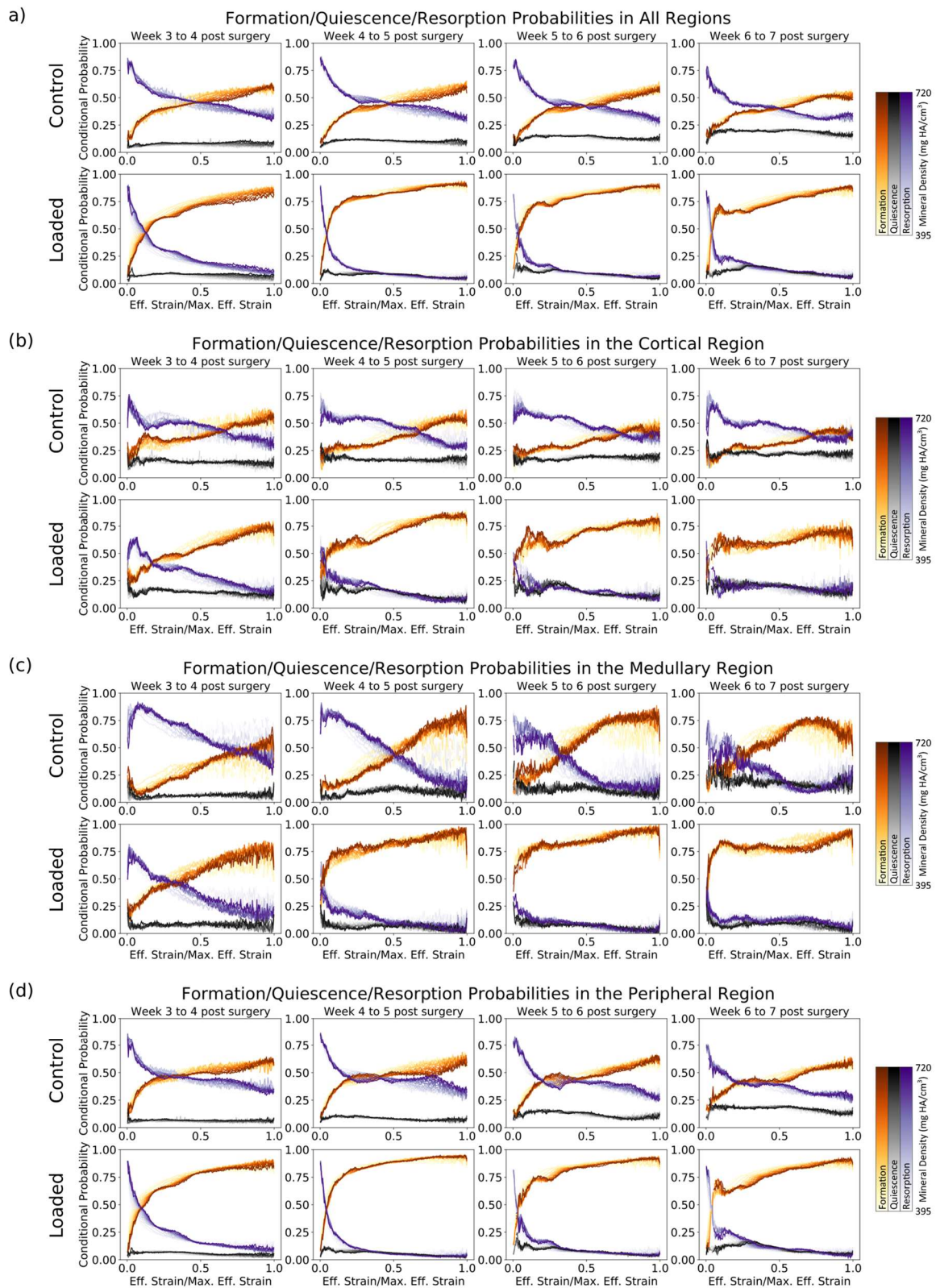


**Figure 4.20:** Conditional probability of formation/quiescence/resorption based on effective strain in femur defect regions. a) Formation and resorption show clear mechanoregulation for

*all time points. b) The cortical regions show less mechanosensitivity at early time points in the loaded group, while the control group shows that very high strains are required before formation is most likely to occur. c) Similar to the cortical region, the loaded group shows increasing mechanosensitivity towards week 7. d) In the peripheral region in both loaded and control groups, it is clear that during the earlier time points lowly mineralised tissue is more likely to form for all strains than highly mineralised tissue.*

Formation and resorption displayed clear mechanoregulatory behaviour in both the loaded and control groups. The conditional probabilities of bone formation and resorption display a logarithmic-like behaviour. High strains increased the conditional probability of formation, which occurred rapidly at first, and then gradually as strain increased further. For resorption, the conditional probability decreased quickly at first, and then gradually as strains increased further.

As seen in **Figure 4.20a**, both the loaded and (to a lesser extent) the control group showed a clear relationship between strain level and tissue mineral density throughout the post-bridging period. For formation voxels at week 3, voxels of lower mineralisation were more likely to be formed for all effective strain values, while by week 7 higher strain values were more likely to lead to the formation of more highly mineralised voxels. Mid-strain values appeared to lead to lower probabilities of resorption in lowly mineralised tissue in comparison to tissue of greater mineralisation, while for very high strains this pattern was reversed. This general pattern was seen in all regions. However in the cortical regions (**Figure 4.20b**), where the original cortex was remodelled away, the mechanosensitivity of the control group decreased substantially over time. Initially, the formation probability at maximum strains was 60% and decreased to 40% by week 7. A similar, but less drastic, decrease was seen in the loaded group from week 4 to week 7, where the probability for formation to occur decreased from 80% to roughly 65%. An additional change in mechanosensitivity was seen in the peripheral region for the final time point (week 6 to week 7). For voxels of mid to lower strains, a lower conditional probability was observed in comparison with earlier time points. The medullary region displayed an increase in mechanosensitivity from week 3 until week 6 for both the control and the loaded groups. This large degree of mechanosensitivity decreased from week 6 to week 7 in the control group, particularly for higher strains. In contrast, the loaded group maintained a high degree of mechanosensitivity until week 7.



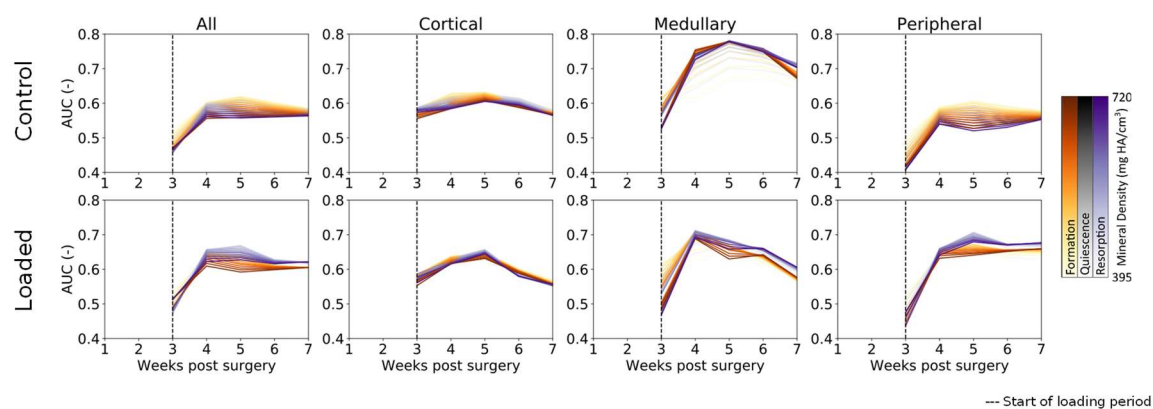


**Figure 4.21:** Area under the curve (AUC) for classification of regions of formation/resorption based on effective strain values in femur defect regions. All regions displayed effective strain as a better than random predictor of formation and resorption. The loaded group displayed effective strain as a better predictor for resorption (in comparison to formation) for all regions except the cortical region.

The AUC results indicate mechanoresponsive behaviour from week 3 onwards (**Figure 4.21**), with an AUC of greater than 0.5 for formation and remodelling in both control and loaded groups. For the loaded group, in the medullary and peripheral regions, the AUC value from week 3 onwards is higher for all resorption voxels (regardless of density) in comparison to formation voxels. This indicates that resorption, in the loaded group, is mechanoregulated to a greater degree than formation.

The conditional probability of quiescence (**Figure 4.20a-d**) displays independence from strain both locally (i.e., for all regions) and globally, demonstrating that quiescence is not mechanoregulated. This observation holds true for all mineralisation levels of the tissue.

## Discussion

The purpose of this study was to investigate the relationship between strain in the Local *in vivo* Environment (LivE) and the formation and resorption behaviour of a loaded femoral defect model in mice. We combined longitudinal micro-CT scanning with micro-FE simulation to calculate tissue-scale strains and changes within the bone and determine mechanoregulatory relationships of bone remodelling and healing. High strains strongly increased the likelihood of bone formation, while low strains increased the likelihood of bone resorption. Our results align with results seen within bone adaptation models, providing support for the idea that the late reparative phase and remodelling phase exhibit similar behaviour to conventional bone remodelling<sup>37</sup>.

Similar to Schulte et al.<sup>11</sup>, in a loaded vertebrae model of bone adaptation in mice, we observed an exponential relationship for formation and resorption. However, while this relationship was generally observed in all regions, the cortical and medullary regions did not display such a clear-cut relationship, appearing somewhat linear at earlier time points. It is worth noting that the steepness of the initial exponential response increased as the study progressed. This indicates that the exponential response of formation and resorption to mechanical stimuli is a dominant function of remodelling behaviour, not reparative behaviour. Given that this exponential response developed earlier in the loaded group than in the control group, mechanical loading may increase the rate of transition from the reparative phase to the remodelling phase. This is also reflected in **Figure 4.18b**, where the resorption peaks of the loaded group occur earlier than in the control group. Furthermore, the rate of mineralisation, as well as the formation peaks, are higher in the loaded group than in the control group at week 4.

Our approach shows that the mineralisation dynamics are tightly interwoven with the formation and resorption of new packets of bone. Lowly mineralised bone displays a greater conditional probability to precede highly mineralised bone, particularly in the reparative phase. Assessing the AUC results (**Figure 4.21**) indicates that the effect of mechanical strains on resorption is greater than that of formation for the loaded group. Extra-physiological loading leads to a greater resorption mechanosensitivity. This is contradictory to some studies in mice that investigated the effect of loading on bone changes<sup>8,11</sup>, where formation displayed a greater mechanosensitivity to mechanical stimulation. However, in a model of frequency-dependent bone remodelling, Scheuren et al.<sup>10</sup> showed similar AUC values for both formation and resorption, with resorption displaying a greater mechanosensitivity. Formation results mimic

those in an equivalent non-loaded femur defect model, as shown by Tourolle et al.<sup>1</sup>, with higher AUC for formation of lower mineralised tissue. Compared to the results of Tourolle et al.<sup>1</sup>, the range of AUC values was more consistent in our data, which is most likely a result of better control of the mechanical environment due to extra-physiological loading. Mechanical loading increased formation and resorption AUC values more for the peripheral region than for the cortical region, while the medullary region showed a greater degree of mechanosensitivity in comparison to all the other regions. This increase in mechanosensitivity has been noted in previous studies. Webster et al.<sup>14</sup>, using a similar combination of micro-CT and micro-FE, demonstrated that strains in the marrow region were an effective predictor of bone formation. Additionally, they observed that marrow strains displayed an even greater correlation with resorption sites, echoing the different mechanoregulatory patterns we see between resorption and formation. However, extra-physiological loading did not increase the AUC values in the medullary or cortical regions, indicating that the mere addition of extra load does not necessarily lead to increased mechanosensitivity. This ties in to the concept of Frost et al.'s mechanostat<sup>38</sup>, where once a specific strain set point has been exceeded, additional mechanical stimulation does not further increase mechanoregulation.

The mapping of the response between local effective strain and the conditional probability for formation, quiescence and resorption has great potential to aid *in silico* simulations. Many authors have built models for the prediction of defect healing<sup>34,37,39</sup>. However, these models most often use theoretical or mathematical descriptions for the likelihood of voxels being remodelled under a particular load. These approaches, while built on global experimental observations and theories, do not use a locally derived relationship such as those observed in our study. Therefore, our results can be used as a “mechanostat” curve to provide experimentally supported probabilities to improve real-world legitimacy of healing simulations.

This work contains several limitations. Partial volume effects affect voxels on the boundary of bone and soft tissue, leading to artificially low greyscale values, hence affecting formation and resorption values for the lowest level of mineralisation within the multi-density analysis. However, this limitation is largely addressed by the multi-density method, where shifts in greyscale values are captured within the binning approach. Another limitation is the description of the boundary conditions. Here, we made use of a simple superposition of a uniaxial load and a bending load derived from geometries and loading parameters of the external fixator. While the fixator-bone arrangement is under a dynamic load, and hence the mechanical response is

dynamic, the range of mechanical stimuli reflects that within the literature<sup>9,40-42</sup>. We therefore consider this static analysis sufficient for this study. As the bone's stiffness increases with the progression of healing, the PEEK fixator's stiffness becomes relatively smaller, leading to an increase in pin rotation. This compliance of the external fixator could lead to a larger bending load than the one we have used here. Capturing such large deformations would require extensive modelling and validation but could decrease error in this dataset.

In summary, we investigated the mechanoregulation of the post-bridging stages in a femoral defect mouse model. Results show that increases in strains lead to increased probability of formation and decreased probability of resorption. The inverse is also true; low strains increase the probability of resorption, while simultaneously decreasing the probability of formation. In addition to this, quiescence is not mechanoregulated, displaying independence from the level of strains. We were able to confirm our hypothesis that high strains would lead to bone formation, while lower strains would lead to resorption. Additionally, we were able to demonstrate that the mineralisation process of the lowly mineralised bone is mechanoregulated and that this relationship is temporally dependent. This means that the mechanosensitivity of different densities of bone changes over time. At certain time points lower levels of mineralised bone are more likely to form, while high levels of mineralised bone are more likely to be resorbed. This work sets the stage for three future investigations. Firstly, extension of mechanical loading protocols and mechanoregulatory analysis into the pre-bridging phase will elucidate the early stages of fracture healing, potentially giving rise to improved interventions. Secondly, the established conditional probability relationship can act as a key input into *in silico* models, allowing accurate mechanoregulatory relationships within bone healing and remodelling simulations. Finally, the translation of this mechanoregulatory behaviour down to cell scale, via the incorporation of either high resolution scanning or histological approaches, would improve our ability to link organ-scale loading to cell-scale responses, allowing further understanding of the osteocyte-osteoblast-osteoclast relationship.

## **Acknowledgements**

The authors would like to acknowledge support from the European Union (ERC Advanced MechAGE, ERC-2016-ADG-741883). E. Wehrle received funding from the ETH Postdoctoral Fellowship Program (MSCA-COFUND, FEL-25\_15-1).

## **Competing Interests**

The authors declare no competing interests.

## Supplementary Material

Table 4: Loading Parameters for the loaded group (in N)

Mouse	Week 3	Week 4	Week 5	Week 6	Week 7
1	8	14	16	16	16
2	8	12	16	16	16
3	12	16	16	16	16
4	8	14	16	16	16
5	12	16	16	16	16
6	10	12	16	16	16
7	8	16	16	16	16
8	10	16	16	16	16
9	10	16	16	16	16
10	12	16	16	16	16

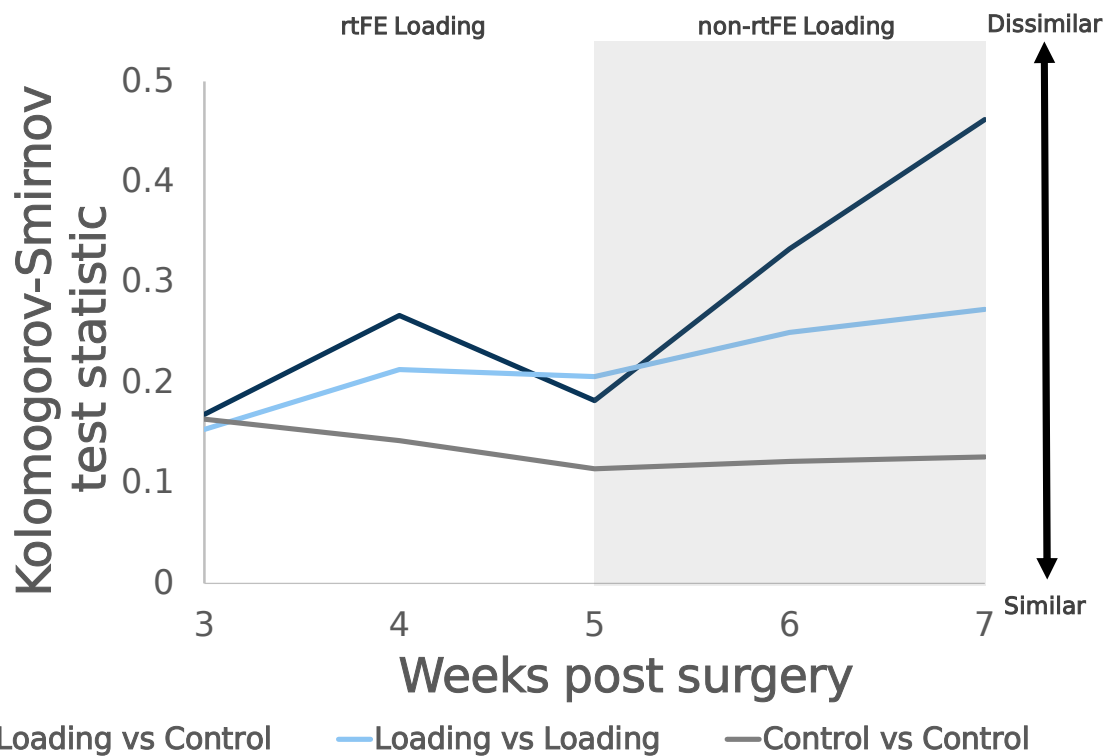


Figure 4.22: Kolmogorov-Smirnov comparison between loaded mice under rtFE and control mice over loading duration

---

## References

- 1     Tourolle né Betts, D. C. *et al.* The association between mineralised tissue formation and the mechanical local *in vivo* environment: Time-lapsed quantification of a mouse defect healing model. *Sci Rep-Uk* **10**, 1-10, doi:10.1038/s41598-020-57461-5 (2020).
- 2     Augat, P. *et al.* Local tissue properties in bone healing: Influence of size and stability of the osteotomy gap. *J Orthop Res* **16**, 475-481, doi:DOI 10.1002/jor.1100160413 (1998).
- 3     Augat, P., Simon, U., Liedert, A. & Claes, L. Mechanics and mechano-biology of fracture healing in normal and osteoporotic bone. *Osteoporosis Int* **16**, S36-S43, doi:10.1007/s00198-004-1728-9 (2005).
- 4     Bailon-Plaza, A. & van der Meulen, M. C. H. Beneficial effects of moderate, early loading and adverse effects of delayed or excessive loading on bone healing. *J Biomech* **36**, 1069-1077, doi:10.1016/S0021-9290(03)00117-9 (2003).
- 5     Carter, D. R., Beaupre, G. S., Giori, N. J. & Helms, J. A. Mechanobiology of skeletal regeneration. *Clin Orthop Relat R*, S41-S55 (1998).
- 6     Morgan, E. F., Gleason, R. E., Hayward, L. N. M., Leong, P. L. & Palomares, K. T. S. Mechanotransduction and fracture repair. *J Bone Joint Surg Am* **90a**, 25-30, doi:10.2106/Jbjs.G.01164 (2008).
- 7     Morgan, E. F. *et al.* Correlations between local strains and tissue phenotypes in an experimental model of skeletal healing. *J Biomech* **43**, 2418-2424, doi:10.1016/j.jbiomech.2010.04.019 (2010).
- 8     Birkhold, A. I. *et al.* Mineralizing surface is the main target of mechanical stimulation independent of age: 3D dynamic *in vivo* morphometry. *Bone* **66**, 15-25, doi:10.1016/j.bone.2014.05.013 (2014).
- 9     Meakin, L. B., Price, J. S. & Lanyon, L. E. The contribution of experimental *in vivo* models to understanding the mechanisms of adaptation to mechanical loading in bone. *Front Endocrinol* **5**, doi:10.3389/fendo.2014.00154 (2014).
- 10    Scheuren, A. C. *et al.* Mechano-regulation of bone adaptation is controlled by the local *in vivo* environment and logarithmically dependent on loading frequency. *bioRxiv* (2020).
- 11    Schulte, F. A. *et al.* Local Mechanical Stimuli Regulate Bone Formation and Resorption in Mice at the Tissue Level. *Plos One* **8**, doi:ARTN e62172 10.1371/journal.pone.0062172 (2013).

- 12 Webster, D., Schulte, F., Lambers, F., Kuhn, G. & Muller, R. The mechanical environment in bone marrow predicts osteoblast and osteoclast activities. *Bone* **50**, S73-S73, doi:10.1016/j.bone.2012.02.208 (2012).
- 13 Lambers, F. M. *et al.* Bone adaptation to cyclic loading in murine caudal vertebrae is maintained with age and directly correlated to the local micromechanical environment. *J Biomech* **48**, 1179-1187, doi:10.1016/j.jbiomech.2014.11.020 (2015).
- 14 Webster, D., Schulte, F. A., Lambers, F. M., Kuhn, G. & Muller, R. Strain energy density gradients in bone marrow predict osteoblast and osteoclast activity: A finite element study. *J Biomech* **48**, 866-874, doi:10.1016/j.jbiomech.2014.12.009 (2015).
- 15 Webster, D. J., Morley, P. L., van Lenthe, G. H. & Muller, R. A novel in vivo mouse model for mechanically stimulated bone adaptation - a combined experimental and computational validation study. *Comput Method Biomec* **11**, 435-441, doi:10.1080/10255840802078014 (2008).
- 16 Marsell, R. & Einhorn, T. A. The biology of fracture healing. *Injury* **42**, 551-555, doi:10.1016/j.injury.2011.03.031 (2011).
- 17 Ghiasi, M. S., Chen, J., Vaziri, A., Rodriguez, E. K. & Nazarian, A. Bone fracture healing in mechanobiological modeling: A review of principles and methods. *Bone Rep* **6**, 87-100, doi:10.1016/j.bonr.2017.03.002 (2017).
- 18 Morgan, E. F. *et al.* Micro-computed tomography assessment of fracture healing: Relationships among callus structure, composition, and mechanical function. *Bone* **44**, 335-344, doi:10.1016/j.bone.2008.10.039 (2009).
- 19 Wehrle, E. *et al.* Evaluation of longitudinal time-lapsed in vivo micro-CT for monitoring fracture healing in mouse femur defect models. *Sci Rep* **9**, 17445, doi:10.1038/s41598-019-53822-x (2019).
- 20 Lambers, F. M. *et al.* Trabecular bone adapts to long-term cyclic loading by increasing stiffness and normalization of dynamic morphometric rates. *Bone* **55**, 325-334, doi:10.1016/j.bone.2013.04.016 (2013).
- 21 Claes, L. E. *et al.* Effects of mechanical factors on the fracture healing process. *Clin Orthop Relat R*, S132-S147 (1998).
- 22 Claes, L. E. & Heigele, C. A. Magnitudes of local stress and strain along bony surfaces predict the course and type of fracture healing. *J Biomech* **32**, 255-266, doi:10.1016/S0021-9290(98)00153-5 (1999).



- 23 Huiskes, R., Ruimerman, R., van Lenthe, G. H. & Janssen, J. D. Effects of mechanical forces on maintenance and adaptation of form in trabecular bone. *Nature* **405**, 704-706, doi:Doi 10.1038/35015116 (2000).
- 24 Schulte, F. A., Lambers, F. M., Kuhn, G. & Muller, R. In vivo micro-computed tomography allows direct three-dimensional quantification of both bone formation and bone resorption parameters using time-lapsed imaging. *Bone* **48**, 433-442, doi:10.1016/j.bone.2010.10.007 (2011).
- 25 Bouxsein, M. L. *et al.* Guidelines for Assessment of Bone Microstructure in Rodents Using Micro-Computed Tomography. *J Bone Miner Res* **25**, 1468-1486, doi:10.1002/jbmr.141 (2010).
- 26 Paul, G. R., Malhotra, A. & Muller, R. Mechanical Stimuli in the Local In Vivo Environment in Bone: Computational Approaches Linking Organ-Scale Loads to Cellular Signals. *Curr Osteoporos Rep* **16**, 395-403, doi:10.1007/s11914-018-0448-6 (2018).
- 27 Fritton, S. P. & Weinbaum, S. Fluid and Solute Transport in Bone: Flow-Induced Mechanotransduction. *Annu Rev Fluid Mech* **41**, 347-374, doi:10.1146/annurev.fluid.010908.165136 (2009).
- 28 Klein-Nulend, J., Bakker, A. D., Bacabac, R. G., Vatsa, A. & Weinbaum, S. Mechanosensation and transduction in osteocytes. *Bone* **54**, 182-190, doi:10.1016/j.bone.2012.10.013 (2013).
- 29 Weinbaum, S., Duan, Y., Thi, M. M. & You, L. D. An Integrative Review of Mechanotransduction in Endothelial, Epithelial (Renal) and Dendritic Cells (Osteocytes). *Cell Mol Bioeng* **4**, 510-537, doi:10.1007/s12195-011-0179-6 (2011).
- 30 Pistoia, W. *et al.* Estimation of distal radius failure load with micro-finite element analysis models based on three-dimensional peripheral quantitative computed tomography images. *Bone* **30**, 842-848, doi:Doi 10.1016/S8756-3282(02)00736-6 (2002).
- 31 Ghiasi, M. S., Chen, J. E., Rodriguez, E. K., Vaziri, A. & Nazarian, A. Computational modeling of human bone fracture healing affected by different conditions of initial healing stage. *Bmc Musculoskel Dis* **20**, doi:10.1186/s12891-019-2854-z (2019).
- 32 Lacroix, D. & Prendergast, P. J. A mechano-regulation model for tissue differentiation during fracture healing: analysis of gap size and loading. *J Biomech* **35**, 1163-1171, doi:10.1016/S0021-9290(02)00086-6 (2002).

- 
- 33 Isaksson, H. *et al.* Bone regeneration during distraction osteogenesis: Mechano-regulation by shear strain and fluid velocity. *J Biomech* **40**, 2002-2011, doi:10.1016/j.jbiomech.2006.09.028 (2007).
- 34 Geris, L., Sloten, J. V. & Van Oosterwyck, H. In silico biology of bone modelling and remodelling: regeneration. *Philos T R Soc A* **367**, 2031-2053, doi:10.1098/rsta.2008.0293 (2009).
- 35 Flaig, C. & Arbenz, P. A scalable memory efficient multigrid solver for micro-finite element analyses based on CT images. *Parallel Comput* **37**, 846-854, doi:10.1016/j.parco.2011.08.001 (2011).
- 36 Virtanen, P. *et al.* SciPy 1.0: fundamental algorithms for scientific computing in Python. *Nat Methods* **17**, 261-272, doi:10.1038/s41592-019-0686-2 (2020).
- 37 Isaksson, H. *et al.* Remodeling of Fracture Callus in Mice Is Consistent with Mechanical Loading and Bone Remodeling Theory. *J Orthop Res* **27**, 664-672, doi:10.1002/jor.20725 (2009).
- 38 Frost, H. M. Bone Mass and the Mechanostat - a Proposal. *Anat Record* **219**, 1-9, doi:DOI 10.1002/ar.1092190104 (1987).
- 39 Isaksson, H., Wilson, W., van Donkelaar, C. C., Huiskes, R. & Ito, K. Comparison of biophysical stimuli for mechano-regulation of tissue differentiation during fracture healing. *J Biomech* **39**, 1507-1516, doi:10.1016/j.jbiomech.2005.01.037 (2006).
- 40 Liu, C. *et al.* Effects of mechanical loading on cortical defect repair using a novel mechanobiological model of bone healing. *Bone* **108**, 145-155, doi:10.1016/j.bone.2017.12.027 (2018).
- 41 Duda, G. N. *et al.* Influence of muscle forces on femoral strain distribution. *J Biomech* **31**, 841-846, doi:Doi 10.1016/S0021-9290(98)00080-3 (1998).
- 42 Razi, H. *et al.* Skeletal maturity leads to a reduction in the strain magnitudes induced within the bone: A murine tibia study. *Acta Biomater* **13**, 301-310, doi:10.1016/j.actbio.2014.11.021 (2015).

# **Chapter 5 :**

## **Synthesis**

## Background

Diseases affecting bone, such as osteoporosis, and traumatic events, such as hip fractures, have a significant impact on the health and well-being of aging populations worldwide<sup>1,2</sup>. Bone is a multiscale and hierarchical material providing structural support and a range of essential physiological functions within the human body<sup>3,4</sup>. It is a dynamic material, constantly adapting and renewing itself<sup>5</sup> in a process known as bone remodeling, and upon injury, is able to repair itself completely<sup>6</sup>. It is well understood that mechanical loading is essential for both remodeling and healing in bone<sup>7-15</sup>. Therefore, a deeper understanding of the physiological processes behind bone has the potential to aid the development of pharmacological or mechanical interventions aimed at correcting physiological function, preventing fractures, and optimising healing.

Over the past several decades, mouse models have become commonly used to investigate bone remodeling and healing<sup>16</sup>. This is due to specific advantages they possess over other models, such as the availability of gene targeted animals<sup>17</sup> and the ability to use mice to investigate bone healing or remodeling at organ<sup>18-20</sup>, tissue<sup>21</sup>, cell<sup>22,23</sup> or molecular<sup>24,25</sup> scales. Micro-CT imaging has proved an important tool in the longitudinal monitoring of tissue scale changes in both fracture healing and bone remodelling<sup>26-30</sup>. This has facilitated investigations into mechanoregulatory relationships via the use of micro-FE, derived from micro-CT images, to simulate the mechanical environment at the tissue scale<sup>27,31</sup>. However, a limiting factor is the specification of boundary conditions for these models when linking organ scale loading to tissue scale strains. Strain gauging of bone has been performed with some success<sup>32,33</sup>, however it is invasive and limited to measuring surface strains. Algorithmic methods have also been developed for back calculating the boundary conditions theoretically necessary to generate a given bone microstructure<sup>27,34</sup>. However, these methods are not well suited to rapidly changing structures, such as the callus in bone healing. To overcome these limitations, two approaches have emerged. The first uses instrumented fixators, which are able to measure direct deformation brought about by locomotion<sup>35-37</sup> while the second uses extra-physiological loading models<sup>31</sup>. Extra-physiological loading models allow greater loads than would be habitually applied by the animal while also allowing better stipulation of boundary conditions for mechanical environment simulations.

Developing quantitative links between the strains at the tissue scale and the cell scale has also proved challenging. Micro-CT imaging alone is unable to identify neither cell locations, nor gene regulation or protein expression and hence is insufficient to link organ scale loading with cell level mechanoregulation. Scheuren et al.<sup>38</sup> and Trüssel et al.<sup>39</sup> have attempted to overcome these

limitations by incorporating immunohistochemistry and by spatially relating cells with their mechanical signal in a mouse vertebrae model of bone adaptation. The application of such multimodal techniques, combined with an improved assessment of the boundary conditions, enables a more complete understanding of *in vivo* bone mechanobiology by linking mechanical loading at organ scale to cell specific regulation, fate, and behaviour.

Therefore, this thesis aimed to 1) develop approaches to link organ scale loading to both tissue scale and cell scale mechanical stimulation and 2) investigate the mechanoregulation of these signals at each scale, in both physiological loading and extra-physiological loading in a femur defect model. To achieve these aims, measurement techniques for organ scale loading were developed to track the longitudinal progression of physiological loading. This employed strain gauges to longitudinally measure deformation on the external fixation of the defect. These measurements were subsequently analysed to establish relationships between organ scale habitual loading and the organ scale outcome of fracture healing. Furthermore, these measurements were used as simulation parameters for longitudinal micro-FE simulations derived from time-lapsed micro-CT images. From these mechanical simulations, mechanical stimulation was linked to protein expression in the immediate region around the cell, i.e. the Local *in vivo* Environment (LivE), by localising cell locations with immunohistochemistry and histology, building on the work done by Trüssel et al.<sup>39</sup> and Scheuren et al.<sup>38</sup>. This combination of 3D structural information from longitudinal micro-CT, mechanical information from micro-FE simulations, and molecular information from immunohistochemistry allowed us to quantify mechanoregulatory relationships between organ scale loading, tissue scale bone changes, and cell scale protein expression in a femur defect model of bone healing in mice.

## **Novel findings**

The studies described in this thesis have established relationships from loading measured at the organ scale, to outcomes at organ, tissue, and cell scales on an individualised basis within a defect-healing model. Firstly, at the organ scale, individualised habitual loading prior to bridging was found to predict the outcome of the fracture healing progression. While this result has not been observed in mice prior to our study, it aligns with results seen in rats by Klosterhoff et al.<sup>37</sup> and confirms general observations that sufficient mechanical loading prior to bridging is essential for successful fracture healing<sup>7-9,11,15,40-42</sup>.

The next achievement was the development and application of the real time finite element (rtFE) approach. Observation of the effects and risks of non-individualised loading motivated the development of an approach to homogenise tissue scale strains and target a particular median tissue strain in a group of mice by determining individualised extra-physiological loading parameters. This approach enables control of mechanical environments to either develop individualised interventions or reduce mechanical environment variation within mouse groups. rtFE thus enabled the application of individualised loading across a group of mice to investigate the effects of extra-physiological loading on longitudinal changes in bone tissue, post bridging. Using micro-CT imaging and micro-FE simulations, with boundary conditions determined from the rtFE derived loading parameters, relationships were established between regions of high mechanical stimulation and increased probability of bone formation, as well as regions of low mechanical stimulation and increased probability of bone resorption. These results are aligned with previous fracture healing studies<sup>27</sup>, as well as bone adaptation studies<sup>22,23,28,31</sup>. These results suggest that the late reparative phase and the remodelling phase in fracture healing share similar mechanoregulatory relationships to those in bone adaptation, further supporting the theory that these processes are governed by similar mechanisms<sup>14,19</sup>. Regional analysis of cortical, medullary and peripheral regions indicated that the medullary region was more mechanosensitive than the other regions in the unloaded mice, which initially suggested that the endo-cortical region is more mechanosensitive than the periosteal region. However, upon the application of extra-physiological loading, the mechanosensitivity of the peripheral region increased to parity with the medullary region.

Building on work done by Trüssel et al.<sup>39</sup> and Scheuren et al.<sup>38</sup> on bone adaptation in mouse tail vertebrae models, measured deformation boundary conditions were applied to micro-CT-based micro-FE models in order to approximate the mechanical stimulation occurring at cell scale. 2D immunohistochemistry sections were registered to micro-CT images and protein expression was measured at cell locations with respect to the mechanical stimulation in the *LivE*. This approach overcomes both the resolution limits of micro-CT scanning and the temporal limits of immunohistochemistry. Relationships were observed between increased mechanical signal in the *LivE* and decreased expression of both Sclerostin and RANKL. Our results align with the expression of both these proteins reported in previous *in vitro* studies<sup>43,44</sup>, as well as other generalised *in vivo* observations from bones loaded at organ scale<sup>45</sup>. We were also able to link cells associated with regions of formation, quiescence and resorptions with levels of high, moderate and low mechanical signal respectively. Contrasting *in vitro* studies<sup>24,43,44</sup> and previous observations<sup>45</sup>, no link was observed between area of Sclerostin expression within the sections, to cells associated

with formation, quiescent, or resorption regions. However, RANKL expression was significantly different in cells associated with resorption when compared with cells associated with quiescence. Even though the resorption-associated cells had a lower mean RANKL expression area than quiescent-associated cells, the resorption-associated cells exhibited a greater range, with many highly stained outliers. This approach linking organ scale loading to individual cell protein expression lays the groundwork for holistic multiscale mechanoregulatory investigation and can be expanded to investigate such multiscale relationships *in vivo* for any other appropriate protein. This could potentially enable the understanding of *in vivo* bone mechanobiology in its entirety, by directly linking mechanical stimulation at cell scale to cell regulation, behaviour and fate. In particular, our results show that mechanical stimulation in the surrounding region of a cell is a driver of downregulation of Sclerostin and RANKL expression, confirming that organ scale loading drives cell scale expression of molecules key to bone formation and resorption.

## **Limitations and future research**

The primary limitation of the technique used to measure the longitudinal boundary conditions in chapter 3.1 is their discontinuous nature. This approach only captured a small section of the animal's movement at limited time-periods. Ideally, this can be improved upon by a wireless and, potentially, continuous monitoring approach. However, an advantage of the direct measurement approach presented in this thesis involves the high sampling rate, which allowed the measurement of habitual loading amplitude in the femur over the full duration of the gait cycle. This is clearly an advantage compared to indirect measurement techniques such as force plates<sup>46</sup>. Furthermore, these simulations present new research potential to analyse additional metrics beyond amplitude, such as total energy contained within each foot strike or habitual loading frequency. Incorporation of such parameters into further analysis or dynamic simulations would provide a more robust measurement of habitual loading and its effect on fracture progression.

A limitation of the rtFE method is the absence of a robust study to compare with conventional loading approaches, such as group loading. As seen in the supplementary material of chapter 3.2, a brief Kolmogorov–Smirnov analysis indicated that the strain distributions between mice under rtFE become similar while the method is being applied, in comparison to group loading. The individualised results of the rtFE approach over the first two week of loading were compared with the response once the 16 N loading limit was reached, which acts as a non-individualised loading regime comparison. However, this is insufficient to justify superiority over conventional approaches as it compared different time points. The design of a thorough comparison study poses

several challenges. To apply non-adaptive loading as soon as possible, post-bridging, could lead to refracture or other injury to the animal. This makes the design of such a study difficult, because either the mechanical loading needs to be limited to a low enough magnitude to prevent animal harm, which would result in sub-threshold stimulus at the tissue level and thus would not be an appropriate loading regime for comparison. Alternatively, confirmation of the ability of rtFE to reduce variance and homogenise tissue strains may be easier in a non-defect model. If the rtFE approach was used to target specific strain distributions in a vertebrae model of bone adaption, such as the one investigated by Lambers et al.<sup>47,48</sup>, the risk to animal welfare could be mitigated and longitudinal comparisons to non-individualised loading approaches could be made.

With respect to Chapter 4.1, the linking of organ scale loading to protein scale expression contains many time intensive manual steps. During decalcification, embedding, sectioning, and staining the sections undergo changes in their morphology, and potentially differ greatly from the micro-CT images. Hence, past attempts at non-deformable automatic registration of the 2D micrograph to the 3D micro-CT image have been unsuccessful and registration is instead performed manually. Manual registration is time intensive and induces inter-operator variability that an automatic approach could prevent, thus the development and validation of an automatic registration tool using deformable registration would reduce error and improve data analysis throughput. Such a tool would also help address another limitation of our study, the small sample size. We analysed three slices per bone for two bones for both RANKL and Sclerostin expression. Previous studies utilizing these methods used similar sample sizes<sup>38,39,49</sup> and scaling this study design remains challenging. However, to find clear evidence linking organ scale loading patterns, cell scale mechanical stimulation, and mechanoregulation of protein expression requires more animals, more bone locations, and more bone samples. A multi-staining immunohistochemistry approach would improve studies where small sample sizes are unavoidable. Dymant et al.<sup>50</sup> have developed protocols, which allow single sections to be stained for multiple proteins and cell nuclei location. This would allow improved identification of cell location and association of several proteins to a particular location, in contrast to the current approach, which allows just a single protein. Future research could also apply *LivE* techniques to link the mechanical environment to genetic regulation within a cell, as well as the cells fate. The combination of emerging approaches such as laser micro-dissection and transcriptomic<sup>51,52</sup> or proteomic<sup>53</sup> profiling with mechanical simulations would provide additional insight into direct gene regulation instead of only measuring the proteins present in the surrounding tissue.



## Conclusion

In conclusion, the measurement of individualised boundary conditions and their multiscale translation from organ to cell in a mouse model of defect healing was successful. We incorporated multi-modal techniques of strain gauge measurement, micro-CT, micro-FE and immunohistochemistry to reconcile the temporal and spatial differences across the organ, tissue, cell, and molecular scales. At the organ scale, habitual loading prior to bridging predicts the outcome of the fracture healing process. Post bridging, the loading at organ scale translates to heterogeneous strain fields at tissue scale. We demonstrated that within these strain fields regions of high strain led to bone formation, while regions of low strain led to bone resorption, both in habitually and extra-physiologically loaded mice. Investigations down to cell and molecular scales demonstrated a clear relationship between cells associated with formation and resorption, and the occurrence of high and low strains, respectively, in their *LivE*. We observed that the increased mechanical signal within the *LivE* was linked to the decreased expression of two proteins, namely Sclerostin, a bone formation inhibitor, and RANKL, an osteoclast differentiator and resorption promotor.

The combination of strain gauge measurement, micro-CT imaging, micro-FE simulation and immunohistochemistry allows the comprehensive investigation of mechanoregulation within bone. The biologically relevant results presented in this thesis indicate that these technologies enable investigation into many open questions regarding the multiscale mechanoregulation of bone during fracture healing. In the future, expansion of such studies to include cell-scale observations during the pre-bridging period would allow a full unravelling of the fracture healing process.

---

## References

- 1 Burge, R. *et al.* Incidence and economic burden of osteoporosis-related fractures in the United States, 2005-2025. *J Bone Miner Res* **22**, 465-475, doi:10.1359/jbmr.061113 (2007).
- 2 Stafford, R. S., Drieling, R. L. & Hersh, A. L. National trends in osteoporosis visits and osteoporosis treatment, 1988-2003. *Arch Intern Med* **164**, 1525-1530, doi:DOI 10.1001/archinte.164.14.1525 (2004).
- 3 Rho, J. Y., Kuhn-Spearing, L. & Zioupos, P. Mechanical properties and the hierarchical structure of bone. *Med Eng Phys* **20**, 92-102, doi:Doi 10.1016/S1350-4533(98)00007-1 (1998).
- 4 Fukumoto, S. & Martin, T. J. Bone as an endocrine organ. *Trends Endocrin Met* **20**, 230-236, doi:10.1016/j.tem.2009.02.001 (2009).
- 5 Hill, P. A. Bone remodelling. *Br J Orthod* **25**, 101-107, doi:10.1093/ortho/25.2.101 (1998).
- 6 Claes, L., Recknagel, S. & Ignatius, A. Fracture healing under healthy and inflammatory conditions. *Nat Rev Rheumatol* **8**, 133-143, doi:10.1038/nrrheum.2012.1 (2012).
- 7 Augat, P. *et al.* Early, full weightbearing with flexible fixation delays fracture healing. *Clin Orthop Relat R*, 194-202 (1996).
- 8 Augat, P., Simon, U., Liedert, A. & Claes, L. Mechanics and mechano-biology of fracture healing in normal and osteoporotic bone. *Osteoporosis Int* **16**, S36-S43, doi:10.1007/s00198-004-1728-9 (2005).
- 9 Boerckel, J. D. *et al.* Effects of in vivo mechanical loading on large bone defect regeneration. *J Orthop Res* **30**, 1067-1075, doi:10.1002/jor.22042 (2012).
- 10 Carter, D. R. Mechanical Loading History and Skeletal Biology. *J Biomech* **20**, 1095-1109, doi:Doi 10.1016/0021-9290(87)90027-3 (1987).
- 11 Carter, D. R., Beaupre, G. S., Giori, N. J. & Helms, J. A. Mechanobiology of skeletal regeneration. *Clin Orthop Relat R*, S41-S55 (1998).
- 12 Claes, L. E. *et al.* Effects of mechanical factors on the fracture healing process. *Clin Orthop Relat R*, S132-S147 (1998).
- 13 Giannoudis, P. V., Einhorn, T. A. & Marsh, D. Fracture healing: The diamond concept. *Injury* **38**, S3-S6, doi:Doi 10.1016/S0020-1383(08)70003-2 (2007).
- 14 Huiskes, R., Ruimerman, R., van Lenthe, G. H. & Janssen, J. D. Effects of mechanical forces on maintenance and adaptation of form in trabecular bone. *Nature* **405**, 704-706, doi:Doi 10.1038/35015116 (2000).

- 15 Klein, P. *et al.* The initial phase of fracture healing is specifically sensitive to mechanical conditions. *J Orthop Res* **21**, 662-669, doi:10.1016/S0736-0266(02)00259-0 (2003).
- 16 Histing, T. *et al.* Small animal bone healing models: Standards, tips, and pitfalls results of a consensus meeting. *Bone* **49**, 591-599, doi:10.1016/j.bone.2011.07.007 (2011).
- 17 Manigrasso, M. B. & O'Connor, J. P. Comparison of fracture healing among different inbred mouse strains. *Calcified Tissue Int* **82**, 465-474, doi:10.1007/s00223-008-9144-3 (2008).
- 18 Gardner, M. J. *et al.* In vivo cyclic axial compression affects bone healing in the mouse tibia. *J Orthop Res* **24**, 1679-1686, doi:10.1002/jor.20230 (2006).
- 19 Isaksson, H. *et al.* Remodeling of Fracture Callus in Mice Is Consistent with Mechanical Loading and Bone Remodeling Theory. *J Orthop Res* **27**, 664-672, doi:10.1002/jor.20725 (2009).
- 20 Rontgen, V. *et al.* Fracture Healing in Mice under Controlled Rigid and Flexible Conditions Using an Adjustable External Fixator. *J Orthop Res* **28**, 1456-1462, doi:10.1002/jor.21148 (2010).
- 21 Webster, D. J., Morley, P. L., van Lenthe, G. H. & Muller, R. A novel in vivo mouse model for mechanically stimulated bone adaptation - a combined experimental and computational validation study. *Comput Method Biomec* **11**, 435-441, doi:10.1080/10255840802078014 (2008).
- 22 Webster, D., Schulte, F., Lambers, F., Kuhn, G. & Muller, R. The mechanical environment in bone marrow predicts osteoblast and osteoclast activities. *Bone* **50**, S73-S73, doi:10.1016/j.bone.2012.02.208 (2012).
- 23 Webster, D., Schulte, F. A., Lambers, F. M., Kuhn, G. & Muller, R. Strain energy density gradients in bone marrow predict osteoblast and osteoclast activity: A finite element study. *J Biomech* **48**, 866-874, doi:10.1016/j.jbiomech.2014.12.009 (2015).
- 24 Moustafa, A. *et al.* Mechanical loading-related changes in osteocyte sclerostin expression in mice are more closely associated with the subsequent osteogenic response than the peak strains engendered. *Osteoporosis Int* **23**, 1225-1234, doi:10.1007/s00198-011-1656-4 (2012).
- 25 Robling, A. G. & Turner, C. H. Mechanical Signaling for Bone Modeling and Remodeling. *Crit Rev Eukar Gene* **19**, 319-338, doi:DOI 10.1615/CritRevEukarGeneExpr.v19.i4.50 (2009).

- 
- 26 Wehrle, E. *et al.* Evaluation of longitudinal time-lapsed in vivo micro-CT for monitoring fracture healing in mouse femur defect models. *Sci Rep* **9**, 17445, doi:10.1038/s41598-019-53822-x (2019).
- 27 Tourolle né Betts, D. C. *et al.* The association between mineralised tissue formation and the mechanical local *in vivo* environment: Time-lapsed quantification of a mouse defect healing model. *Sci Rep-Uk* **10**, 1-10, doi:10.1038/s41598-020-57461-5 (2020).
- 28 Schulte, F. A., Lambers, F. M., Kuhn, G. & Muller, R. In vivo micro-computed tomography allows direct three-dimensional quantification of both bone formation and bone resorption parameters using time-lapsed imaging. *Bone* **48**, 433-442, doi:10.1016/j.bone.2010.10.007 (2011).
- 29 Bouxsein, M. L. *et al.* Guidelines for Assessment of Bone Microstructure in Rodents Using Micro-Computed Tomography. *J Bone Miner Res* **25**, 1468-1486, doi:10.1002/jbmr.141 (2010).
- 30 Morgan, E. F. *et al.* Micro-computed tomography assessment of fracture healing: Relationships among callus structure, composition, and mechanical function. *Bone* **44**, 335-344, doi:10.1016/j.bone.2008.10.039 (2009).
- 31 Schulte, F. A. *et al.* Local Mechanical Stimuli Regulate Bone Formation and Resorption in Mice at the Tissue Level. *Plos One* **8**, doi:ARTN e62172 10.1371/journal.pone.0062172 (2013).
- 32 Razi, H. *et al.* Skeletal maturity leads to a reduction in the strain magnitudes induced within the bone: A murine tibia study. *Acta Biomater* **13**, 301-310, doi:10.1016/j.actbio.2014.11.021 (2015).
- 33 Willie, B. M. *et al.* Diminished response to in vivo mechanical loading in trabecular and not cortical bone in adulthood of female C57Bl/6 mice coincides with a reduction in deformation to load. *Bone* **55**, 335-346, doi:10.1016/j.bone.2013.04.023 (2013).
- 34 Christen, P., van Rietbergen, B., Lambers, F. M., Muller, R. & Ito, K. Bone morphology allows estimation of loading history in a murine model of bone adaptation. *Biomech Model Mechan* **11**, 483-492, doi:10.1007/s10237-011-0327-x (2012).
- 35 Grasa, J. *et al.* Monitoring In Vivo Load Transmission Through an External Fixator. *Ann Biomed Eng* **38**, 605-612, doi:10.1007/s10439-009-9889-5 (2010).
- 36 Wehner, T. *et al.* Temporal Delimitation of the Healing Phases Via Monitoring of Fracture Callus Stiffness in Rats. *J Orthop Res* **32**, 1589-1595, doi:10.1002/jor.22721 (2014).

- 37 Klosterhoff, B. S. *et al.* Wireless sensor enables longitudinal monitoring of regenerative niche mechanics during rehabilitation that enhance bone repair. *Bone* **135**, doi:10.1016/j.bone.2020.115311 (2020).
- 38 Scheuren, A. C., Müller, R. & Bellantuono, I. *Longitudinal assessment of frailty and osteosarcopenia in an in vivo model of premature aging.*
- 39 Trüssel, A. J., Dittrich, P. S. & Müller, R. *Spatial mapping and high throughput microfluidic gene expression analysis of osteocytes in mechanically controlled bone remodeling.*
- 40 Bailon-Plaza, A. & van der Meulen, M. C. H. Beneficial effects of moderate, early loading and adverse effects of delayed or excessive loading on bone healing. *J Biomech* **36**, 1069-1077, doi:10.1016/S0021-9290(03)00117-9 (2003).
- 41 Kolar, P. *et al.* The Early Fracture Hematoma and Its Potential Role in Fracture Healing. *Tissue Eng Part B-Re* **16**, 427-434, doi:10.1089/ten.teb.2009.0687 (2010).
- 42 Schell, H. *et al.* The haematoma and its role in bone healing. *J Exp Orthop* **4**, 5, doi:10.1186/s40634-017-0079-3 (2017).
- 43 Rubin, J., Murphy, T., Nanes, M. S. & Fan, X. Mechanical strain inhibits expression of osteoclast differentiation factor by murine stromal cells. *Am J Physiol-Cell Ph* **278**, C1126-C1132 (2000).
- 44 Kim, C. H., Kim, K. H. & Jacobs, C. R. Effects of high frequency loading on RANKL and OPG mRNA expression in ST-2 murine stromal cells. *Bmc Musculoskel Dis* **10**, doi:Artn 10910.1186/1471-2474-10-109 (2009).
- 45 Tu, X. L. *et al.* Sost downregulation and local Wnt signaling are required for the osteogenic response to mechanical loading. *Bone* **50**, 209-217, doi:10.1016/j.bone.2011.10.025 (2012).
- 46 Clarke, K. A., Smart, L. & Still, J. Ground reaction force and spatiotemporal measurements of the gait of the mouse. *Behav Res Meth Ins C* **33**, 422-426, doi:Doi 10.3758/Bf03195396 (2001).
- 47 Lambers, F. M. *et al.* Trabecular bone adapts to long-term cyclic loading by increasing stiffness and normalization of dynamic morphometric rates. *Bone* **55**, 325-334, doi:10.1016/j.bone.2013.04.016 (2013).
- 48 Lambers, F. M. *et al.* Bone adaptation to cyclic loading in murine caudal vertebrae is maintained with age and directly correlated to the local micromechanical environment. *J Biomech* **48**, 1179-1187, doi:10.1016/j.jbiomech.2014.11.020 (2015).

- 
- 49 Taylor C, S. A., Trüssel A, Müller R. Local in vivo Environment (LivE) imaging for single cell protein analysis of bone tissue. *CDBME* **2**, 449-453.
- 50 Dymont, N. A. *et al.* High-Throughput, Multi-Image Cryohistology of Mineralized Tissues. *Jove-J Vis Exp*, doi:ARTN e5446810.3791/54468 (2016).
- 51 Nichterwitz, S. *et al.* Laser capture microscopy coupled with Smart-seq2 for precise spatial transcriptomic profiling. *Nat Commun* **7**, doi:ARTN 1213910.1038/ncomms12139 (2016).
- 52 Chen, J. *et al.* Spatial transcriptomic analysis of cryosectioned tissue samples with Geo-seq. *Nat Protoc* **12**, 566-580, doi:10.1038/nprot.2017.003 (2017).
- 53 MacDonald, M. L. *et al.* Laser capture microdissection-targeted mass spectrometry: a method for multiplexed protein quantification within individual layers of the cerebral cortex. *Neuropsychopharmacol* **44**, 743-748, doi:10.1038/s41386-018-0260-0 (2019).